Advanced Control Strategies for Modular Multilevel Converters

Wang, Songda

Publication date:
2020

Document Version
Publisher's PDF, also known as Version of record

ADVANCED CONTROL STRATEGIES FOR MODULAR MULTILEVEL CONVERTERS

BY
SONGDA WANG

DISSERTATION SUBMITTED 2020

AALBORG UNIVERSITY
DENMARK

Advanced Control Strategies for Modular Multilevel Converters

Ph.D. Dissertation

Songda Wang

Aalborg University
Department of Energy Technology
Pontoppidanstræde 101
DK-9220 Aalborg

Dissertation submitted: October 2020

PhD supervisors: Professor Remus Teodorescu
Aalborg University

Associate Professor Sanjay Chaudhary
Aalborg University

PhD committee: Professor Frede Blaabjerg (chairman)
Aalborg University

Prof. Dr. Ing. Marco Liserre
Christian-Albrechts-Universität of Kiel

Principal Scientist Kalle Ilves
ABB Power Grids Research

PhD Series: Faculty of Engineering and Science, Aalborg University

Department: Department of Energy Technology

ISSN (online): 2446-1636
ISBN (online): 978-87-7210-828-5

Published by:
Aalborg University Press
Kroghstræde 3
DK – 9220 Aalborg Ø
Phone: +45 99407140
aauf@forlag.aau.dk
forlag.aau.dk

Printed in Denmark by Rosendahls, 2020

Abstract

Voltage source converter (VSC) based high voltage direct current (HVDC) transmission systems have many merits including the flexibility to control the active/reactive power transmission of the system and to connect two power systems of different frequencies, etc. In the VSC-HVDC system, the converters are the most important part. The Modular Multilevel Converter (MMC) is the most popular converter topology for the VSC-HVDC system. With the help of the MMC, the HVDC system will have high scalability, low harmonics, and good fault tolerance. However, Because of the numerous submodules in the MMC, this can pose some challenges for MMC-HVDC systems. In this thesis, two following challenges of the MMC-HVDC system are researched: (1). The submodule capacitor voltage ripple problem under unbalanced grid conditions; (2). The high computation burden problem of the model predictive control of MMC.

To address those problems, this Ph.D. project proposes analytical models, necessary grid conditions to analyze the submodule capacitor voltage ripple of MMC under unbalanced grid conditions. The analytical equations of the submodule capacitor voltage under an unbalanced grid fault are derived to help to understand the behavior of the submodule capacitors under unbalanced grid conditions. Then, two capacitor voltage balancing methods are proposed to maintain the submodule-capacitor voltages balanced and within the desired limits, avoiding the tripping of the converter due to overvoltages. Then, a machine learning based capacitor ripple reducing method is proposed. With the machine learning network approach, the complicated non-linear capacitor voltage ripple model is replaced by neural networks based on deep learning method with a low computational burden. What is more, the circulating current reference is determined by the machine learning network to reduce and balance the ripple.

A machine learning based model predictive (MPC) control emulation for MMCs is proposed in this Ph.D. project to achieve fast dynamic response with a low computational burden. Two machine learning networks are applied to replace the traditional proportional–integral (PI)/ proportional-resonant (PR) controller to control the MMC systems, then the complicated control parameter design is avoided. The machine learn-

ing based controller can achieve the same dynamic response as the MPC, thus the proposed machine learning based controller could be suitable for the applications which need high response speed. What is more, the high computation burden problem of the MPC controller is also addressed by the proposed machine learning based method. The computation-light machine learning networks emulate the behavior of the MPC controller to control the MMC with a lower computational burden.

Danish Resumé

Voltage source converter (VSC) baseret high voltage direct current (HVDC) tramissions systemer har mange fordele, blandt andet fleksibiliteten til at kontrollere den aktive/reaktive strøm transmission af systemet og at forbinde to strøm systemer med forskellige frekvenser, ect. I VSC-HVDC systemet, er konverteren den vigtigste del. Modular Multilevel Converter (MMC) er den mest populære konvertortopologi til VSC-HVDC-systemet. Ved hjælp af MMC vil HVDC-systemet have høj skalerbarhed, lav harmonik og god fejltolerance. Men, på grund af de mange undermoduler i MMCer kan dette skabe nogle udfordringer for MMC-HVDC-systemer. I denne afhandling undersøges de to følgende udfordringer af MMC-HVDC-systemet: (1). Undermodulet kondensator spændings krusning problem under ubalancerede netforhold; (2). Problemet med den høje beregningsbyrde ved modelprædiktiv kontrol af MMC.

For at løse disse problemer foreslår dette ph.d. projekt analytiske modeller, nødvendige netforhold for at analysere MMC's submodul kondensator spændingsring under ubalancerede netforhold. De analytiske ligninger af submodulkondensatorspændingen under en ubalanceret netfejl er afledt for at hjælpe med at forstå opførelsen af submodulkondensatorerne under ubalancerede netforhold.Derefter foreslås to kondensatorspændingsbalanceringsmetoder til at opretholde submodul-kondensatorspændingerne afbalanceret og inden for de ønskede grænser, idet man undgår udløsning af konverteren på grund af overspændinger. Derefter foreslås en metode til maskinlæring baseret kondensator-krusningsreduktion. Med maskinindlærings netværksmetoden erstattes den komplicerede ikke-lineære kondensator spændingsrippelmodel med neurale netværk baseret på dyb læringsmetode med en lav beregningsbyrde.

En maskinlærings baseret kontrolemulering forudsigelses model for MMC'er bliver præsenteret i dette ph.d. projekt for at opnå en hurtig dynamisk respons med lav beregningsbyrde. To maskinlæringsnetværker anvendes til at erstatte den traditionelle proportional-integrale (PI) / proportional-resonant (PR) controller til at styre MMC-systemerne, så det komplicerede design af kontrolparametre undgås. Den maskinindlæringsbaserede controller kan opnå den samme dynamiske respons som Model Predic-

tive Control (MPC), og derfor kan den foreslåede maskinlærings-baserede controller være egnet til applikationer, der har brug for høj responshastighed. Udover det, behandles det høje beregningsbyrdeproblem for MPC-controlleren også af den foreslåede metode til maskinindlæring. Computation-light beregningsmaskinindlæringsnetværkerne efterligner MPC-controllerens opførsel til at kontrollere MMC.

Contents

Thesis Details

Thesis Title:	Advanced Control Strategies for Modular Multilevel Converters
Ph.D. Student:	Songda Wang
Supervisors:	Prof. Remus Teodorescu, Aalborg University
	Assoc. Prof. Sanjay K Chaudhary, Aalborg University

This thesis has been submitted for assessment in partial fulfillment of the PhD degree. The thesis is based on the submitted or on a collection of papers published or under review. As part of the assessment, co-author statements have been made available to the assessment committee and are also available at the Faculty. The thesis is not in its present form acceptable for open publication but only in limited and closed circulation as copyright may not be ensured.

Preface

The content of this PhD dissertation is a summary of the results obtained from the Ph.D. project: *Advanced Control Strategies of Modular Multilevel Converters* which is carried out by Department of Energy Technology, Aalborg University, Denmark. The author would like to express their deepest gratitude to Aalborg University for providing such an advanced research environment.

First of all, I would like to express my most sincere gratitude to my supervisor, Professor Remus Teodorescu for his precious guidance, sharp advice, and patience during my Ph.D. period. Because of his precise and instructive advice, I was able to realize my potential and complete my Ph.D. project. I would like also thank to Associate Professor Sanjay Chaudhary, the co-supervisor of my Ph.D. project. It's been a pleasure to do our work under your guidance. Special thanks to the Professor Tomislav Dragicevic for his insightful advice and detailed help for our papers.

I am also want to be grateful to Haofeng Bai, Yuhei Okazaki for giving me an opportunity to work in Hitachi ABB Power Grids, Sweden as a Ph.D. student researcher. The project in Hitachi ABB helped me to widen my knowledge about stability of the grid-connected systems. I would also like to thank my colleagues at ABB for the friendly help and reassuring companionship I received.

Lastly, I would like to extend my gratitude to my parents and brother for their love and support. It is your support that gives me the motivation to work hard during the pandemic. And also thanks to my girlfriend, Jiawei. It is your company that gives me the motivation to our life.

Songda Wang
Aalborg University, October 17, 2020

Part I

Report

1 Introduction

1.1 Background

1.1.1 MMC-HVDC System

With the economic development of modern society, both industrial production and residents' lives require more electricity. Moreover, the development of renewable power generation can also help reduce carbon dioxide emissions globally, thereby achieving the goals of the Paris Agreement: to limit the global average temperature rise below 2C (3.6F) higher than the pre-industrial level [1]. Despite the world was hit by the COVID-19 pandemic in 2020 because of the lockdown policy of the government, the share of renewable energy power generation has risen because the output of renewable energy is largely unaffected by demand. In the first quarter of 2020, global power generation decreased by 2.6% compared with the same period in 2019, but renewable energy power generation increased by 3%, and the wind power generation increase by 3%, and also the share of renewable energy in electricity supply increased from 26% in the first quarter of 2019 to nearly 28% [2].

Although the worldwide demand for electricity has declined in the short term due to the impact of the pandemic, in the long run, the demand for electricity will still increase significantly because countries around the world are working to increase the proportion of electricity [3]. According to the forecast of the International Energy Agency, under conservative prediction, wind and solar power generation will account for more than half of the new power generation in 2040. Under optimistic prediction, almost all growth in power generation will come from wind and solar power [3]. The electricity will reach 31% of the overall energy consumption and takeover the position of oil by 2040.

Offshore wind power is a promising technical solution to meet the development of renewable energy power generation.With the development of technology, the capacity of wind power turbines is getting higher. Moreover, in the sea farther away from the shore, the wind speed is higher. Therefore, offshore wind power can generate more renewable electricity. According to IEA prediction, offshore wind power projects will attract a trillion dollars investment in 2040 [2].

In order to transfer the large amount of energy from offshore wind farm to the onshore load center, a high-efficiency power transmission solution is needed. High voltage direct current (HVDC) transmission technology has many advantages against the traditional high voltage alternating current (HVAC) transmission for the offshore electricity transmission:

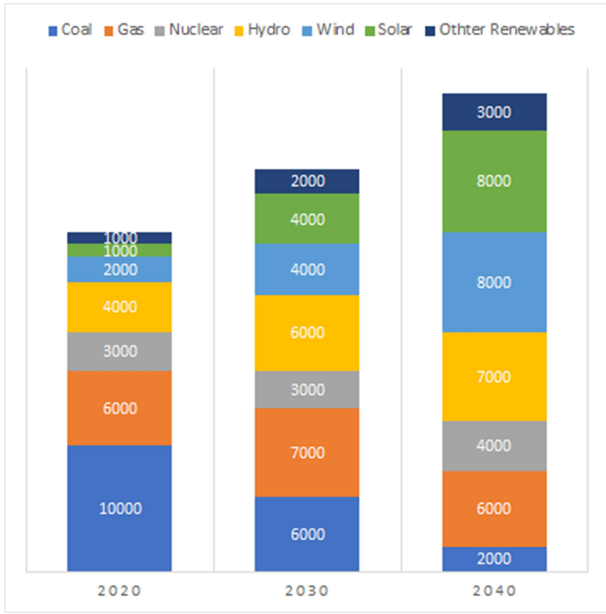

Fig. 1: Electricity generation, 2020 - 2040 (TWh) [3]

(1) Long-distance, large-scale power transfer;

(2) The ability to connect two AC systems with different frequencies;

(3) The ability of fast control the power transmassion direction [4].

There are two technologies for HVDC transmission, current source converter (CSC) and voltage source converter (VSC). Compared to the CSC systems, VSC systems have some typical advantages:

(1) Independent active and reactive power control, can support the AC systems with no cost;

(2) Low grid harmonics, no strict filter requirements;

(3) The low cost extruded polyethylene (XLPE) cables can be used;

(4) Fast AC fault handling capability;

(5) Suitable for future multi-terminal direct current(MTDC) transmission network [4].

In 2003, professor R. Marquardt from University of Bundeswehr proposed an advanced modular topology for HVDC system [5], modular multilevel converter (MMC). The advantages of the MMC is, compared to other converters, the modular structure allows MMC to be easily scaled up into a large scale converter. What is more, MMC has low grid-side current harmonics, low filter cost, and low converter losses [6] [7] [8]. These merits made MMC the solution of choice candidate for offshore high voltage direct current (HVDC) applications.

However, several challenges of the MMC still need to be addressed. In the following sections, those challenges are introduced.

1.1.2 Capacitor Voltage Ripple Problem under Unbalanced Grid Conditions

MMC has a unique structure, it has a large number of series-connected submodules. Each submodule has one submodule capacitor. This submodule capacitor is inserted or bypassed by the submodule switches. In each phase, the series-connected capacitors withstand the DC line voltage evenly. Due to the large number of submodules, the reliability of each submodule needs to be paid attention, otherwise it will endanger the stable operation of the entire system. The capacitors need to be controlled and analyzed carefully.

The submodule capacitors contain the voltage ripple when the MMC is running. Under balanced grid conditions, the capacitor voltages in three phases are three-phase balanced voltages. The ripple contains both fundamental and double fundamental frequency components because the fundamental component is from the power difference between the upper and lower arms, and the double fundamental components is from the power sum between the upper and lower arms [9]. Normally, this ripple will not exceed the safe limit of the capacitor voltage due to the careful design. However, when the MMC is under an asymmetric grid fault, the capacitor voltages will not only become higher than the normal conditions but will be unbalanced [10]. The reason is, the unbalanced three-phase power flow caused by fault grid further changes the extra internal circulating currents components of MMC systems. Then the extra circulating current components will charge the capacitors in an unbalanced way. Therefore, careful control of capacitor voltages is required to prevent overvoltage fault under unbalanced grid conditions.

The high capacitor voltage can cause serious failures in MMC systems. The MMC systems will trip to protect the submodule capacitor if the submodule capacitor voltages

exceed the safe limit. What is more, even if the high capacitor voltage does not exceed the safe voltage limit, it still could be dangerous. The reason is, the MMC capacitance will gradually reduce while aging due to the overvoltage vaporization [11]. Then, the capacitor voltage will be higher when the capacitor charging current is the same due to the reduced capacitance. When the submodule capacitor voltage exceeds its breakdown limit, the capacitor will be short circuit. That means the total submodule number will be reduced by one. The remaining submodules will withstand the same DC line voltage, then each capacitor voltage needs to withstand a higher DC voltage. This can cause the remaining sub-modules to break down one by one due to the higher capacitor voltage. Therefore, careful control of capacitor voltages is required to prevent overvoltage fault under unbalanced grid conditions.

Several literatures have been discussed the submodule voltage problems under various grid situations. Regarding balanced grid, three main methods are proposed to reduce the submodule capacitor voltages as follows:

(1) Circulating current injection method

In [12], Ilves et al. have presented the analytical equations of submodule voltages under symmetrical grid conditions are first derived. Then based on the equations, the injected double fundamental frequency circulating currents are calculated to reduce the capacitor voltage. In [13], an instantaneous circulating current based method is proposed to change the arm equivalent capacitance. Both methods can significantly reduce submodule capacitor voltage ripple under a asymmetrical grid. However, those methods do not give a solution to reduce and balance the submodule voltage ripple under asymmetrical grid faults.

(2) Offset pulse width modulation and zero-sequence voltage injection method

In [14], the 3rd harmonic voltage is injected to reduce the submodule voltage ripple. The submodule capacitance can be reduced by 24% based on this paper. In [15], an offset PWM method is proposed to reduce the capacitor voltage ripple. The capacitor voltage ripple is reduced especially when the inserted number is low. However, when the inserted number is high, those methods have the limit to reduce the submodule capacitor ripple.

(3) Hardware solution

In [16], the chains of dual half-bridge (DHB) modules are used to to enable active sharing of the three-phase power. Then the capacitor ripple is reduced a lot under

balanced grid conditions. However, the hardware solution will increase the cost of the MMC system a lot so it is not a practical solution for the HVDC systems.

Regarding the unbalanced grid conditions, there are also some methods to reduce the submodule capacitor voltage ripple as follows:

(1) Circulating current based methods

In [17] and [18], different circulating current components under unbalanced grid conditions are derived. Then the AC circulating currents are eliminated to reduce the capacitor voltages. However, this method cannot achieve an obvious capacitor voltage reduction performance. In [19], the double fundamental circulating currents are injected to reduce the submodule capacitor voltage ripple under asymmetrical grid condition. However, those methods do not give a clear analytical equation of the submodule capacitor voltage ripple and cannot make the three-phase submodule voltages balanced again under analytical grid conditions.

(2) Offset pulse width modulation (OPWM) and zero-sequence voltage (ZSV) injection method

In [20], the OPWM and ZSV injection method are used to reduce the three-phase capacitor voltages. However, this paper cannot make the three-phase voltages balanced.

Although some articles propose strategies to reduce submodule capacitor voltage ripple when the grid is symmetrical, they fail to take into account some important points. First, there are no analytical equations of the capacitor voltages under asymmetrical grid conditions. So the direct effect of the unbalanced grid on the capacitor voltage has not been clearly represented. Second, most of the papers analyze the three-phase MMC capacitor voltage independently, there is no paper treat the unbalanced capacitor voltages as a three-phase system.

1.1.3 Machine Learning Emulation of Model Predictive Controller for MMCs

Although MMC has many superior features, the control of MMC is still a challenging problem due to the MMC's complicated structure. Several control methods are proposed to control the MMC system such as linear proportional-integral control (PI) [18] and proportional-resonant (PR) control [21], non-linear sliding mode control [22], and model predictive control [23] [24].

In some specific scenarios, the controller dynamic performance should be very fast, then the model predictive control is used to control the MMC in those applications due

to MPC's fast dynamic response [24], [25]. MPC is a discrete mathematical model based control method for multi-input-multi-output (MIMO) systems. For MMC, the control targets can be output current, circulating current, and capacitor voltages, etc [26], [27]. The MPC algorithms predict all the possible controlled variables' values in the next control period based on MMC's discrete model. Then the optimized control signals are selected based on the cost function [28]. However, the biggest disadvantage of MMC MPC is that the heavy computational burden. The MPC algorithms need to finish the prediction, control signal section in every control period. The computational burden gets heavier as the number of submodule increases [23] [29]. Many papers proposed the improved MPC methods to reduce the computational burden [30], [26], [31]. However, the core feature of MPC have not been changed. This feature is, the MPC controller is always fatigued to estimate all possible values online, and calculate the control signal online based on these estimated values. This online characteristic will cause a high computational burden, especially when the number of MMC submodules and the prediction step size increase.

In order to reduce the computational burden of MPC, using machine learning(ML) technology to emulate the MPC is a promising solution. In order words, the ML network can be trained by the data from MPC to achieve the similar performance of MPC, then the computational cost is reduced due to the computation-light characters of ML. The definition of ML based on [32] is: "A computer program learns from past experience to process certain tasks and achieve certain performance, and the performance increase with the increase in experience". ML is mainly divided into two categories: supervised learning and unsupervised learning. Supervised learning technology uses labeled data to train a ML network, and finally uses the trained network for classification or regression. Unsupervised learning uses unlabeled data to train the ML network then let the network itself discover the relationship of the unlabeled data. In power electronics applications, at this stage, we usually use supervised learning because the labeled data is commonly used to train the network.

There are a lot of ML applications in power electronics. From design, control, to maintenance [33], etc. In [34], the reliability design for the power electronics system is accelerated by two artificial neural networks. In [35], the selection of weighting factors for predictive torque control of induction machines fed by three level Neutral Point Clamped converters is accelerated by the help of artificial neural networks, less than 3% error in simulation and less than 10% error in the experiment is achieved with this method. An immune algorithm is applied to achieve the lowest total harmonic distortion (THD) in single-phase full-bridge inverter, the optimal sinusoidal pulse-width modulation (PWM) control sequences of four switches are selected by the proposed method. In [36], the system impedance is monitored by the recurrent neural network (RNN), with this ML-based impedance monitor method. The system impedance can

be measured without interrupting the system operation. However, those methods have been proposed for robotic systems and very simple power converter systems. To the best of our knowledge, no machine learning based MPC emulator has been developed, nor have experimental tests been conducted for MMC converters.

1.2 Project Motivation

As discussed in previous sections, the submodule capacitors are at risk of experiencing high and unbalanced voltages under unbalanced grid faults. This high voltage can lead to a serious HVDC system trip, the loss of the submodule capacitor lifetime, and a high control complexity to balance and reduce the capacitor voltages. In order to improve this, the root cause of the high and unbalanced capacitor voltages under the grid fault needs to be understood and detailed analyzed first. Even though, the capacitor voltage reduction under a balanced grid has been researched comprehensively, but how to understand and analyze the capacitor voltages under unbalanced grid conditions is still a challenge. There are several issues that need to be addressed in this thesis. Those issues contain a deep and precise understanding of the unbalanced mechanism of capacitor voltages under unbalanced grid faults. Moreover, the key difference between capacitor voltages under a balanced and unbalanced grid needs to be addressed precisely to understand the risk of capacitor voltages under fault conditions. And also the controllable variables of the MMC system under grid fault need to be detailed analyzed and selected to reduce and balance the capacitor voltages and avoid the overvoltage trip. Naturally, comprehensive analytical equations to represent the capacitor voltages relationship is needed to balance and control the capacitor voltages. Then based on those equations, the capacitor voltages can be reduced and balanced by selecting the properly controllable variable references. In addition, when the theoretical formula is derived. Some alternative, more intuitive, and concise methods are also needed to reduce and balance the capacitor voltages. These methods can reduce the workload of engineers and avoid complicated theoretical derivation.

Secondly, the demand for new control technologies for MMCs is of crucial importance. By applying the advanced control methods (model predictive control), the dynamic performance of the system is better. Moreover, by applying a new machine learning-based controller to emulate the MPC, the new method further reduces the computational burden on the controller while ensuring a fast dynamic response.

1.3 Project Objectives

1.3.1 Research Question and Objectives

The main target of this Ph.D. thesis is to widen the knowledge on the advanced control strategies of MMC systems, including the balancing of capacitor voltages under grid faults and the machine learning based control of the MMC. The research question of the whole project can be simplified to the following sentence:

"How can the capacitor voltages under unbalanced grid conditions be modeled in an analytically way, and how should the MMC capacitor voltages be reduced and balanced to avoid the overvoltage trip in an easy and intuitive method, and how to control the MMC to achieve a low computational burden as well as a fast dynamic response."

To answer those questions, the modeling of the MMC capacitor voltages including several controllable variables needs to be derived clearly and accurately. This analytical model can help to reveal the unbalanced mechanism and predict the capacitor voltages under unbalanced grid conditions. And also this model can help assess how to reduce and balance the capacitor voltages. What is more, the machine learning technology help to assess how to reduce and balance the capacitor voltage in an easy and non-mathematically derived way. And also, help to find a low computational burden control solution to achieve a good dynamic response. Based on the overall research question, sub research questions are listed in regard to advanced control of MMC systems.

- How can a detailed analytical equation that represents the relationship between circulating current, output current, and unbalanced grid voltages be developed?
- How should the MMC capacitor overvoltage phenomenon be understood, and what is the key reason for it? Which controllable variables can influence the capacitor voltages?
- How can the capacitor voltages be balanced and reduced based on the analytical equations to avoid the overvoltage trip? How complicated is this control method?
- How can mathematically prove control methods be developed to enhance the reliability of the submodule capacitor under unbalanced grid conditions?
- How can model the capacitor voltages without complicated analytical derivation by machine learning technology?
- How can simple, efficient, and easy to understand control method to be developed to balance the capacitor voltages by applying the machine learning technology?
- How can advanced technology like machine learning be adopted to achieve a similar behavior of model predictive controller with a lower computational burden?

Three main objectives of the Ph.D. thesis are listed to answer the research questions:

(1) Analytical Capacitor Voltage Ripple Reduction under Unbalanced Grid Conditions

First, the analytical derivation process of capacitor voltages under a balanced grid are extended to unbalanced grid conditions. A three-phase system is considered in this project instead of a single-phase system, and also the symmetrical component method is applied to analyze the MMC capacitor overvoltage phenomenon. Based on the analytical equations, two capacitor voltage balancing methods are proposed to reduce the capacitor voltage ripple, then the overvoltage trip can be avoided. Simulation verification of the proposed methods is also shown in the thesis.

(2) Machine Learning Based Capacitor Voltage Ripple Reduction under Unbalanced Grid Conditions

In this sub-project, the machine learning based method is used to represent the relationship between the capacitor voltage amplitude, circulating current amplitude, and grid voltages. By this model, the complicated mathematical derivation is avoided. The parallel simulation based data collection method is proposed in this chapter and also the network training procedure is shown. The simulation and experimental results show that the proposed machine learning based method is a simple, efficient, and easy to understand control method to balance and reduce the capacitor voltage ripple under unbalanced grid conditions.

(3) Machine Learning Emulation of Model Predictive Controller for MMCs

In this sub-project, a traditional model predictive controller for MMC is first reproduced. Then the machine learning network is applied to emulate the behavior of the MPC. With the proposed machine learning controller, a lower computational burden and a fast dynamic performance are achieved. What is more, the possibility of using other networks has also been explored, the pattern recognition network is applied to improve the performance when the input variables are not within the training range. All of these contributions will be experimentally verified.

1.4 Thesis Outline

This Ph.D. thesis has two parts: a report part and a collection of Selected Publications done in the Ph.D. study period. The relationship between thesis chapter and selected publications is shown in Fig. 2. The outline of the thesis is as follows: Chapter 1 gives an introduction of the Modular Multilevel Converters, the problem of the high capacitor voltage ripple under unbalanced grid conditions and the problem of the MPC high computational burden are also introduced. And the objectives of thesis are determined.

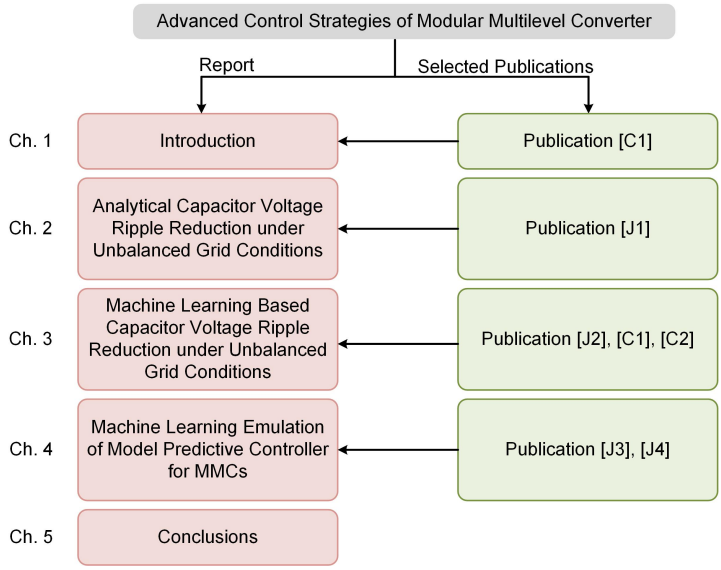

Fig. 2: Report structure and identification of how the selected publications in this thesis fit in regard to the thesis chapter

Chapter 2 proposes an analytical capacitor voltage ripple reduction method under unbalanced grid conditions. This includes a detailed analytical equations of the capacitor voltage ripple, and the components of the three-phase capacitor voltage ripples are analyzed by the symmetrical component method. Then, those equations are used to reduce the capacitor voltage ripple under unbalanced grid conditions. Chapter 3 includes a more easy way to reduce the capacitor voltage ripple under unbalanced grid conditions, a machine learning based capacitor voltage ripple reduction method is proposed. The data collection and network training is introduced in chapter. In chapter 4, a machine learning based emulation of model predictive control is proposed to control the modular multilevel converter with a lower computation burden. The two networks neural network regression and neural network pattern recognition are introduced to emulate the behavior of the MPC. The data collection and the network training are also described. Finally, the contributions are concluded in Chapter 5. And the future works are also planned in Chapter 5.

1.5 List of Publications

The research outcomes during the Ph.D. period have been disseminated in journal papers, conference papers. The following lists show the publications:

J1. **S. Wang,** G. F. Gontijo, S. K. Chaudhary, D. Bao, and R. Teodorescu, “New Modeling and Mitigation Control of Submodule-Capacitor Voltage Ripple of Modular Multilevel Converter Under Unbalanced Grid Conditions. “ under review in *Energies.*

J2. **S. Wang,** T. Dragicevic, Y, Gao, S. K. Chaudhary, and R. Teodorescu, "Machine Learning based Operating Region Extension of Modular Multilevel Converters under Unbalanced Grid Faults." in *IEEE Transactions on Industrial Electronics.*, 2020.

J3. **S. Wang,** T. Dragicevic, Y, Gao, and R. Teodorescu, "Neural Network based Model Predictive Controllers for Modular Multilevel Converters." in *IEEE Transactions on Energy Conversion.*, 2020.

J4. **S. Wang,** G. F. Gontijo, T. Dragicevic, and R. Teodorescu, "Machine Learning Emulation of Model Predictive Control for Modular Multilevel Converters." under review in *IEEE Transactions on Industrial Electronics.*

C1. **S. Wang,** S. K. Chaudhary, and R. Teodorescu, "Capacitor Voltage Ripple Reduction Methods of Modular Multilevel Converter under Unbalanced Fault Conditions: A Comparison." in *Proc IEEE International Power Electronics and Application Conference and Exposition (PEAC).*, Shenzhen, China, 2018.

C2. **S. Wang,** T. Dragicevic, and R. Teodorescu, "Machine Learning Based Current Control of Modular Multilevel Converters under Two Phases to Ground Fault Grid Conditions." in *Proc IEEE 18th International Symposium on Power Electronics for Distributed Generation Systems.*, Dubrovnik, Croatia, 2020.

2 Analytical Capacitor Voltage Ripple Reduction under Unbalanced Grid Conditions

2.1 Background

As a key topology of the VSC-HVDC transmission system, MMCs play an important role in the modern electrical grids. The MMCs help the transmission system to transmit power more efficiently. However, the repeated grid faults can significantly affect the lifetime of submodule capacitors. The submodule overvoltage fault can occur when the submodule capacitor voltages are unbalanced under the unbalanced fault grid. In severe cases, extremely high submodule voltage can even cause the system to trip. One way to overcome this problem would be to design the submodule capacitors with considerably higher capacitances in such a way as to limit the high voltage ripple. Nonetheless, this approach would result in intolerably high costs and, thus, the MMC would no longer be a competitive industrial solution.

A capacitor voltage balancing method is proposed and analyzed in this chapter. First, the analytical equations of the submodule capacitor voltage under unbalanced grid fault will be derived to help to understand behavior of the submodule capacitors under unbalanced grid conditions. Then, two capacitor voltage balancing methods are proposed to maintain the submodule-capacitor voltages balanced and within the desired voltage limits, avoiding the tripping of the converter due to ovevoltages.

2.2 Analytical Capacitor Voltage Ripple Estimation under Unbalanced Grid Conditions

Fig. 3 shows the simplified diagram of a three-phase grid-connected MMC system. The converter consists of three phase units with two arms per phase, known as upper and lower arm [37], [38]. Each arm contains a series connection of N half bridge (HB) submodules and an arm inductor [39]. Each submodule can be either inserted or bypassed, allowing the arm to behave as a controllable voltage source [40], [41]. The grid-connected MMC converter injects the active and reactive power according to the grid code [42].

In Fig. 3, the definition of voltage and current of each part in MMC are shown. The grid voltages are represented by v_{sk}, k means phase number (0 for A, 1 for B, 2 for C). The upper and lower arm voltages are represented by v_{uk} and v_{lk} respectively. Each arm voltage contains two voltages: the voltages of submodule string v_{cuk}, v_{clk} and the voltages of the upper and lower arm inductor v_{zuk} and v_{zlk}. Regarding the currents, the upper and lower arm currents are represented by i_{uk} and i_{lk} respectively. The output current (grid current) is i_{sk}, and the circulating current is i_{ck}.

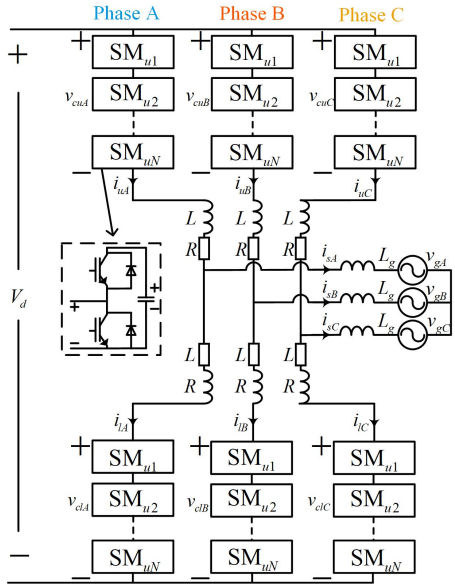

Fig. 3: MMC Topology Block Diagram

The unbalanced grid voltage contains both positive-sequence and negative-sequence components, as described by (1), the zero-sequence of grid voltage is not considered here because the neural point is not grounded [43].

$$v_{sk} = \widehat{V}_{+1}\cos(\omega t - \frac{2}{3}k\pi) + \widehat{V}_{-1}\cos(\omega t - \frac{4}{3}k\pi) \tag{1}$$

Where ω is fundamental angular frequency, $\widehat{V}_{+1}$ and $\widehat{V}_{-1}$ are the positive-sequence and negative-sequence grid voltage amplitudes respectively.

Similarly, grid current is given by:

$$i_{sk} = \widehat{I}_{+1}\cos(\omega t - \frac{2}{3}k\pi + \varphi) + \widehat{I}_{-1}\cos(\omega t - \frac{4}{3}k\pi + \varphi) \tag{2}$$

Where φ is the current angle with respect to voltage, $\widehat{I}_{+1}$ and $\widehat{I}_{-1}$ are the positive-sequence and negative-sequence current amplitudes respectively.

In order to derive the submodules ripple equations, the power of each arm should be calculated first. Then the arm voltages and arm currents are introduced below. Based on the Kirchhoff voltage law and Kirchhoff current law, the sum of capacitor voltages

in the MMC arms and the MMC arm currents are defined in equations (3) and (4), respectively:

$$\begin{bmatrix} v_{cuk} \\ v_{clk} \end{bmatrix} = \begin{bmatrix} \frac{1}{2}V_d - v_{sk} - v_{zuk} \\ \frac{1}{2}V_d + v_{sk} - v_{zlk} \end{bmatrix} \tag{3}$$

$$\begin{bmatrix} i_{uk} \\ i_{lk} \end{bmatrix} = \begin{bmatrix} i_{ck} + \frac{1}{2}i_{sk} \\ i_{ck} - \frac{1}{2}i_{sk} \end{bmatrix} \tag{4}$$

Where V_d is the DC line voltage. Assuming that circulating current only contains DC component $i_{ck} = i_{ckDC}$ by applying proper circulating current controller [44].

The power of upper and lower arm is calculated by multiplying the arm current and arm voltage (neglecting the arm inductance voltage, i.e. $v_{zuk} = 0$):

$$\begin{bmatrix} p_{uk} \\ p_{lk} \end{bmatrix} = \begin{bmatrix} v_{cuk} \cdot i_{uk} \\ v_{clk} \cdot i_{lk} \end{bmatrix} \tag{5}$$

Calculating the submodule voltage ripple becomes easier by introducing the sum power $P_\Sigma = P_u + P_l$ and delta power $P_\Delta = P_u - P_l$, and then equation (5) can be written as::

$$\begin{bmatrix} p_{uk} \\ p_{lk} \end{bmatrix} = \begin{bmatrix} P_{\Sigma k} + P_{\Delta k} \\ P_{\Sigma k} - P_{\Delta k} \end{bmatrix} \tag{6}$$

From (1) to (6), the sum of arm power can be calculated as follows

$$\begin{aligned} \mathrm{P}_{\Sigma k} = {} & i_{ck}V_d - \tfrac{1}{2}\widehat{V}_{+1}\widehat{I}_{+1}\cos\varphi - \tfrac{1}{2}\widehat{V}_{+1}\widehat{I}_{-1}\cos\varphi - \tfrac{1}{2}\widehat{V}_{-1}\widehat{I}_{+1}\cos\varphi - \tfrac{1}{2}\widehat{V}_{-1}\widehat{I}_{-1}\cos\varphi - \\ & \tfrac{1}{2}\widehat{V}_{+1}\widehat{I}_{+1}\cos(2\omega t + \theta_{vk-} + \varphi) - \tfrac{1}{2}\cos\widehat{V}_{-1}\widehat{I}_{-1}(2\omega t + \theta_{vk+} - \varphi) - \tfrac{1}{2}\widehat{V}_{+1}\widehat{I}_{-1}\cos(2\omega t - \varphi) - \\ & \tfrac{1}{2}\widehat{V}_{-1}\widehat{I}_{+1}\cos(2\omega t + \varphi) \end{aligned} \tag{7}$$

Where θ_{vk+} and θ_{vk-} are phase angle of positive-negative and negative-sequence voltage respectively. Similarly, the delta of arm power can be derived:

$$\begin{aligned} \mathrm{P}_{\Delta k} = {} & \tfrac{1}{2}V_d\widehat{I}_{+1}\cos(\omega t + \theta_{vk+} + \varphi) + \tfrac{1}{2}V_d\widehat{I}_{-1}\cos(\omega t + \theta_{vk-} - \varphi) - 2\widehat{V}_{+1}i_{ck}\cos(\omega t + \\ & \theta_{vk+}) - 2\widehat{V}_{-1}I_{ckDC}\cos(\omega t + \theta_{vk-}) \end{aligned} \tag{8}$$

It is important to notice that, under unbalanced grid conditions, the DC circulating currents of the three MMC legs are not equal anymore since the grid voltage becomes

asymmetrical.

Integrating sum power (7) and delta power (8) yields sum energy in (9) and delta energy in (10). The sum energy consists of two parts: sum DC energy $W_{\Sigma kDC}$ and sum AC energy $W_{\Sigma k} = W_{\Sigma k}(1) + W_{\Sigma k}(2)$. In the same way, the delta energy also consists of two parts: delta DC energy $W_{\Delta k}$ and delta AC energy $W_{\Delta k} = W_{\Delta k}(1) + W_{\Delta k}(2)$. The sum and delta energy are described in the equations below.

$$\begin{aligned} W_{\Sigma k} = W_{\Sigma kDC} &- \underbrace{\frac{\widehat{V}_{+1}\widehat{I}_{+1}\sin(2\omega t + \theta_{vk-} + \varphi)}{4\omega} - \frac{\widehat{V}_{-1}\widehat{I}_{+1}\sin(2\omega t + \varphi)}{4\omega}}_{\Delta W_{\Sigma k}(1)} \\ &- \underbrace{\frac{\widehat{V}_{+1}\widehat{I}_{-1}\sin(2\omega t - \varphi)}{4\omega} - \frac{\widehat{V}_{-1}\widehat{I}_{-1}\sin(2\omega t + \theta_{vk+} - \varphi)}{4\omega}}_{\Delta W_{\Sigma k}(2)} \end{aligned} \tag{9}$$

$$\begin{aligned} W_{\Delta k} = W_{\Delta kDC} &+ \underbrace{\frac{V_d\widehat{I}_{+1}\sin(\omega t + \theta_{vk+} - \varphi)}{2\omega} + \frac{V_d\widehat{I}_{-1}\sin(\omega t + \theta_{vk-} - \varphi)}{2\omega}}_{\Delta W_{\Delta k}(1)} \\ &- \underbrace{\frac{2V_{+1}i_{ck}\sin(\omega t + \theta_{vk+})}{\omega} - \frac{2\widehat{V}_{-1}I_{ckDC}\sin(\omega t + \theta_{vk-})}{\omega}}_{\Delta W_{\Delta k}(2)} \end{aligned} \tag{10}$$

Therefore, the submodules voltage can be derived based on (11), which describes the relationship relationship between the energy and submodules voltage:

$$v_{cu,lk}^{\Sigma} = \sqrt{\frac{2N}{C}W_{u,lk}} \tag{11}$$

Based on (11), we can make a further approximation. The following submodules voltage approximations can be made according to [9]:

$$\begin{aligned} v_{cuk} &\approx V_d + \frac{N}{2CV_d}(\mathfrak{N}W_{\Sigma k} + \mathfrak{N}W_{\Delta k}) \\ v_{clk} &\approx V_d + \frac{N}{2CV_d}(\mathfrak{N}W_{\Sigma k} - \mathfrak{N}W_{\Delta k}) \end{aligned} \tag{12}$$

Where $\mathfrak{N}$ represents the operation to extract the AC component of a variable. For example, $\mathfrak{N}W_{\Sigma k}$ means the AC component of sum energy in phase k.

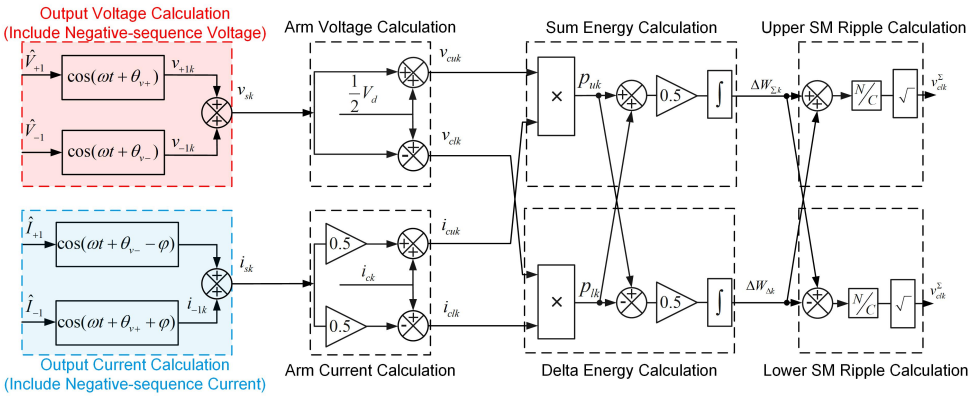

Fig. 4: Submodule capacitor voltage ripple estimator block diagram

The submodules voltage in the upper and lower arm contains three components: DC part, sum submodules ripple component, and delta submodules ripple component. Based on (9), (10), and (12), the sum and delta submodules voltage ripple can be obtained:

$$v_{cuk}^{\Sigma sum} = \frac{N}{2CV_d}\mathfrak{N}W_{\Sigma k},\ v_{cuk}^{\Sigma delta} = \frac{N}{2CV_d}\mathfrak{N}W_{\Delta k} \tag{13}$$

By neglecting the DC energy in (9) and (10) and by substituting (9) and (10) into (13), the sum submodule voltage ripple and the delta submodule voltage ripple are obtained as described in equations (14) and (15), respectively.

$$\begin{aligned}\mathfrak{N}v_{ck}^{\Sigma sum} = \frac{N}{2CV_d}\Bigg[\underbrace{-\frac{\widehat{V}_{+1}\widehat{I}_{+1}\sin(2\omega t+\theta_{vk-}+\varphi)}{4\omega}}_{Negative-sequence\ component}\underbrace{-\frac{\widehat{V}_{-1}\widehat{I}_{-1}\sin(2\omega t+\theta_{vk+}-\varphi)}{4\omega}}_{Positive-sequence\ component}\Bigg]\\ +\frac{N}{2CV_d}\Bigg[\underbrace{-\frac{\widehat{V}_{+1}\widehat{I}_{-1}\sin(2\omega t-\varphi)}{4\omega}-\frac{\widehat{V}_{-1}\widehat{I}_{+1}\sin(2\omega t+\varphi)}{4\omega}}_{Zero-sequence\ component}\Bigg]\end{aligned} \tag{14}$$

$$\mathfrak{N}v_{ck}^{\Sigma del} = \frac{N}{2CV_d}\Bigg[\underbrace{\frac{1}{2\omega}V_d\widehat{I}_{+1}\sin(\omega t+\theta_{vk+}-\varphi)}_{Positive-sequence\ component}+\underbrace{\frac{1}{2\omega}V_d\widehat{I}_{-1}\sin(\omega t+\theta_{vk-}-\varphi)}_{Negative-sequence\ component}\Bigg]$$

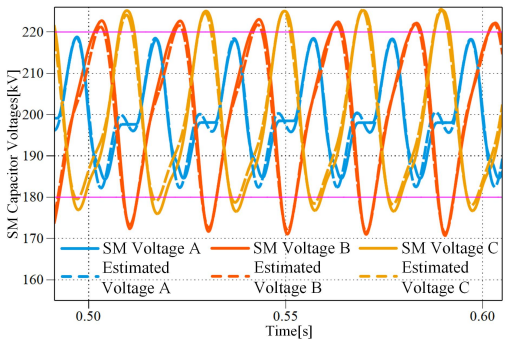

Fig. 5: Estimated and simulated submodules voltage ripple

$$+\frac{N}{2CV_d}\left[\underbrace{-\frac{2}{\omega}\widehat{V}_{+1}i_{ckDC}\sin(\omega t+\theta_{vk+})}_{Delta\ ripple\ part\ 1}+\underbrace{\frac{2}{\omega}\widehat{V}_{-1}i_{ckDC}\sin(\omega t+\theta_{vk-})}_{Delta\ ripple\ part\ 2}\right] \tag{15}$$

To clarify the derivation steps of the submodule capacitor voltage ripple, Fig. 4 shows the structure of unbalanced submodule capacitor ripple estimator.

In order to validate the derived equations, a simulation analysis was carried out and the results obtained through both the analytical equations (based on equations (14) and (15)) and the simulation analysis are depicted in Fig. 5. In both estimation and simulation, the parameters used are the ones shown in Table 1. From Fig. 5 we can conclude that the estimated submodule capacitor ripple is a good reflection of the actually simulated ripple.

For the sake of simplicity, this paper employs the assumptions that AC circulating current components are eliminated by a proper circulating current controller and no negative-sequence current is injected into grid. So the second and third term in (14) are zero. Sum voltage ripple in (14) is transferred to:

$$v_{ck}^{\Sigma sum}=\frac{N}{2CV_d}\left[\underbrace{-\frac{\widehat{V}_{+1}\widehat{I}_{+1}\sin(2\omega t+\theta_{vk-}+\varphi)}{4\omega}}_{Negative-sequence\ component}\underbrace{-\frac{\widehat{V}_{-1}\widehat{I}_{+1}\sin(2\omega t+\varphi)}{4\omega}}_{Zero-sequence\ component}\right] \tag{16}$$

A double-fundamental-frequency zero-sequence components appears in (16) due to the negative-sequence grid voltage. The unbalanced sum submodules voltage ripple is

Table 1: MMC Parameters

	Simulation
Number of submodules per arm (N)	100
Rated DC voltage (V_d)	200 kV
Rated active power	150 MW
Nominal submodule capacitance (C)	3.75 mF
Nominal submodule capacitor voltage (v_c)	2 kV
Rated frequency (f)	50 Hz
Arm inductance (L)	50.9 mH
Sample frequency	10k Hz
Grid voltage amplitude	100 kV
Positive-sequence grid voltage($\widehat{V_{+1}}$)	80 kV
Negative-sequence grid voltage ($\widehat{V_{+1}}$)	40 kV

composed of the negative-sequence and zero-sequence components which is shown in Fig. 6.

In a same reason, there is no negative-sequence current. The second term of (15) is zero. So (15) is also transferred to (17):

$$v_{ck}^{\Sigma del} = \frac{N}{2CV_d}\left[\underbrace{\frac{1}{2\omega}V_d\widehat{I}_{+1}\sin(\omega t+\theta_{vk+}-\varphi)}_{Positive-sequence\ component}\right]$$

$$+\frac{N}{2CV_d}\left[\underbrace{-\frac{2}{\omega}\widehat{V}_{+1}I_{ckDC}\sin(\omega t+\theta_{vk+})}_{Delta\ ripple\ 1}\underbrace{-\frac{2}{\omega}\widehat{V}_{-1}I_{ckDC}\sin(\omega t+\theta_{vk-})}_{Delta\ ripple\ 2}\right] \tag{17}$$

Double fundamental frequency delta ripple part 1 and 2 in (17) cause the unbalance of delta submodules voltage ripple. It is worth noting that delta ripple part 1 and part 2 are not symmetrical components because DC circulating current of each phase are not equal under unbalanced grid conditions. Fig. 6 also shows submodules voltage ripple contains several kinds of unbalanced delta submodules ripple components which make submodules voltage ripple unbalanced.

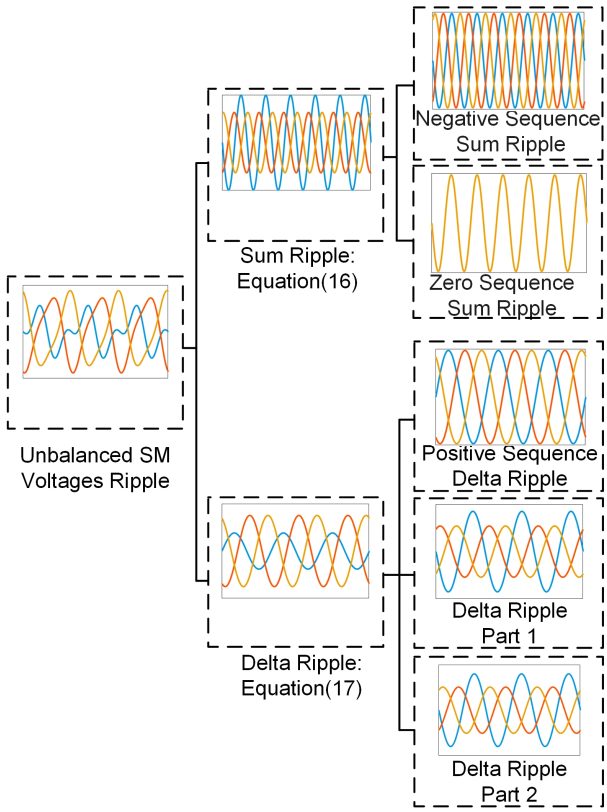

Fig. 6: The components of unbalanced submodules ripple

2.3 Capacitor Voltage Ripple Balancing Methods

After the derivation of submodule capacitor voltage equations in previous section. In this section, the submodule capacitor voltage ripple reduction methods based on the derived equations will be proposed. From equation (16) and (17), we can conclude that following variables affect the submodule capacitor voltage: positive-sequence grid voltage ($\widehat{V}_{+1}$), negative-sequence grid voltage ($\widehat{V}_{-1}$), positive-sequence output current ($\widehat{I}_{+1}$), DC voltage (V_d), and DC component of circulating current (I_{ckDC}). All these variables are fixed by grid code or cannot be changed. In order to optimize the submodule capacitor voltage in (16) and (17), a new variable should be introduced into the MMC system.

Injecting AC circulating current is a suitable choice to reduce the submodule capacitor voltage ripple. Circulating current is a current that circulates inside the MMC, without affecting the output current. It only influences the internal performance of the MMC system. In this paper, we define the circulating current as containing both DC and AC components:

$$i_{ck} = \frac{i_{uk} + i_{lk}}{2} = i_{ckDC} + i_{ckAC} \tag{18}$$

The submodule capacitor voltage ripple will be reduced by injecting AC circulating current under balanced grid conditions. However, these methods are only designed for the balanced grid case, the amplitude of the injected AC circulating current under unbalanced grid conditions is unknown. Since in last section the circulating current was considered to contain only DC component, in the following section, the analytical equations for the submodule capacitor voltage ripple will be further improved by considering AC components of the circulating current. The proper amplitude of the AC components of the circulating current to be injected will be derived, in such a way to reduce the submodule capacitor voltage ripple. Two ripple balancing methods are proposed in this subsection.

2.3.1 Capacitor Voltage Ripple Balancing Method A

The circulating current definition states that this is a current that flows through the upper and lower arms, of a given leg of the MMC, in the same direction. That means circulating current will charge the submodule capacitors in upper and lower arms in an equivalent fashion. So, the circulating current will only affect the sum submodule capacitor voltage ripple as shown in (16). In this paper, we only consider to inject double fundamental frequency negative–sequence circulating current $\widehat{I}_{cAC2}$ and double

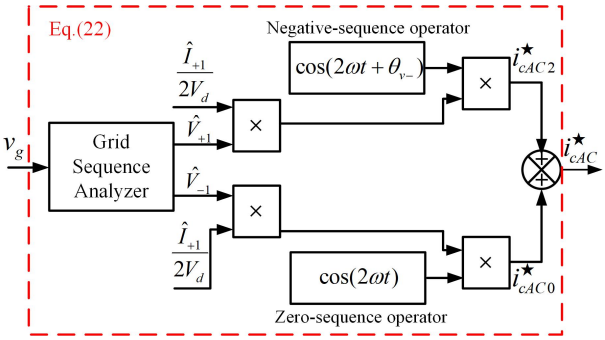

Fig. 7: Block diagram of Method A

fundamental frequency zero-sequence circulating current $\widehat{I}_{cAC0}$ reduce the submodule capacitor components. These circulating current components can offset the sum submodule capacitor component in (16). Then circulating current is now defined as:

$$i_{ck} = I_{ckDC} + \widehat{I}_{cAC2}\cos(2\omega t + \theta_{vk-}) + \widehat{I}_{cAC0}\cos(2\omega t) \tag{19}$$

Repeating the derivation steps in last subsection to get sum submodules ripple equation when circulating current is injected, result in the equation show below, which describes the submodule sum voltage.

$$\Delta v_{cu}^{\Sigma} = \frac{N}{2CV_d}\left[\underbrace{\frac{V_d\widehat{I}_{ckAC2}\sin(2\omega t + \theta_{vk-})}{2\omega} - \frac{\widehat{V}_{+1}\widehat{I}_{+1}\sin(2\omega t + \theta_{vk-} + \varphi)}{4\omega}}_{Negative-sequence\ sum\ ripple}\right]$$
$$+ \frac{N}{2CV_d}\left[\underbrace{\frac{V_d\widehat{I}_{ckAC0}\sin(2\omega t)}{2\omega} - \frac{\widehat{V}_{-1}\widehat{I}_{+1}\sin(2\omega t + \varphi)}{4\omega}}_{Zero-sequence\ sum\ ripple}\right] \tag{20}$$

As previously explained, injecting circulating current can only influence the sum submodules voltage ripple. In order to reduce the sum submodules unbalanced ripple, the value of injected AC circulating currents are derived based on (20) and the block diagram of Method A is shown in Fig. 7.

Compared to (16), the derived submodule capacitor voltage ripple has two more terms, which are caused by injecting negative-sequence and zero-sequence circulating current respectively. Moreover, we set the phase angle to 0 , that means the first two

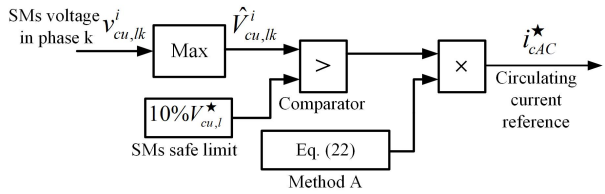

Fig. 8: Block diagram of Method B

terms in (20) have the same frequency and phase angle, and so do the last two terms in (20). Therefore, the submodule capacitor voltage can be reduced or eliminated by injecting circulating current with a proper amplitude. The proper amplitudes of the circulating-current terms to be injected, in order to cancel the voltage ripples in the submodule capacitor during unbalanced grid conditions, are described in (21). Finally, the current reference to be synthesized by the compensation control (Method A) is shown in (22) and the control diagram is depicted in Fig. 7.

$$\widehat{I}_{ckAC2} = \frac{\widehat{V}_{+1}\widehat{I}_{+1}}{2V_d}, \quad \widehat{I}_{ckAC0} = \frac{\widehat{V}_{-1}\widehat{I}_{+1}}{2V_d} \tag{21}$$

$$\widehat{I}^{\bigstar}_{ckAC2} = \widehat{I}_{ckAC2}\cos(2\omega t + \theta_{vk-}) + \widehat{I}_{ckAC0}\cos(2\omega t) \tag{22}$$

Since an arbitrary unbalanced grid can be represented by the combination of positive-sequence and negative-sequence components, this method is a universal approach to reduce capacitor voltage ripple under unbalanced grid conditions.

2.3.2 Capacitor Voltage Ripple Balancing Method B

As Fig. 5 shows, the amplitude of unbalanced submodules voltage ripple in phase B and C exceed its limit, the limit is the 10% of rated submodules capacitor voltage. The submodules voltage ripple in phase A still in rated voltage range. That is to say, the submodules capacitors in phase A still can work safely without any circulating current injection as Method A do.

Intuitively, there is no need to insert circulating current in phase A to reduce the ripple. Only insert circulating current in phase B and C is a good choice. The block diagram of Method B is shown in Fig. 8. When one phase submodules voltage ripple exceed its limit, then this phase will be injected balancing circulating current. The circulating current is derived in (22) which is same as Method A. If the submodule voltage doesn't exceed its limit, no circulating current will be injected in this phase.

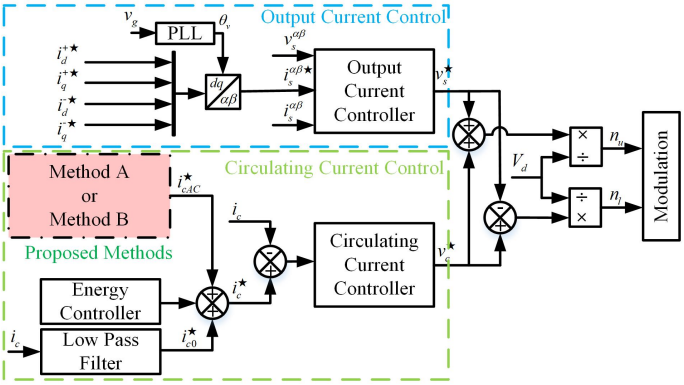

Fig. 9: Block diagram of MMC controller

This technique improves the efficiency of the system since circulating currents are only injected when necessary, to avoid submodule capacitor voltage to exceed its limits, and, thus, conduction losses are reduced.

The control block diagram of the MMC converter is shown in Fig. 9. The MMC controller is divided into two main parts: a) output current controller, b) circulating current controller. The output of current controller and the circulating current controller is used to calculate the insertion index of MMC. Each part of the control system is briefly described in the following subsections.

(1) Output Current Control

In order to achieve the grid-connected control, PR controller in $\alpha\beta$ axis is used to control the output current. Detailed introduction of output current controller can be found in [9], [45].

(2) Circulating Current control

In this paper, the proportional resonant controller is used to suppress the AC circulating current under balanced conditions [21] [46]. And the sum and delta energy controllers keep the sum energy of each phase equal and the delta energy of the upper and lower arm be zero by injecting instantaneous circulating current. The proposed ripple reduction methods balance the submodule voltage ripple by injecting AC circulating current under unbalanced grid conditions.

2.4 Results

The proposed ripple balancing methods are validated by simulating the grid-connected MMC converter. The specification of the simulated converter is listed in Table 1. The simulated submodules model is average arm model which described in [9].

The simulation results of MMC under balanced grid condition are presented in Fig. 10(a1), (a2), and (a3). The grid voltage is a three-phase symmetrical voltage with an amplitude of 100 kV, which is shown in Fig. 10(a1). The number of submodules is 100 and it should be noticed that the rated submodules voltage is this case should be 100 times nominal submodule capacitor voltage because the average arm model is used in the simulation to save simulation time. The Fig. 10(a2) shows submodules voltage ripple is three-phase symmetrical and each phase submodules voltage amplitude does not exceed its limit (10% of rated submodules voltage, 220 kV). Fig. 10(a3) shows that the AC components of the circulating current are practically null due to the circulating-current suppression control. Moreover, the average values (DC component) of the circulating currents of each phase are the same since the grid voltage is balanced and, thus, each grid phase presents an equal power value. Detailed data can be found in Table. 2.

The unbalanced grid fault with the amplitude of 0.8 positive-sequence grid component 0.8 $\widehat{V_g}$ and the amplitude of 0.4 $\widehat{V_g}$ negative grid component is shown in Fig. 10(b1), (c1), and (d1). The submodules voltage ripple is unbalanced due to the effect of the unbalanced grid. Fig. 10(b2) shows the amplitudes of submodules voltage ripple in phase B and C are 222.45 kV and 225.32 kV respectively which exceed its limit (220 kV). Also, the DC value of circulating current in phase A is 275A which higher than phase B (175 A) and C (175 A). The average submodules ripple of three phases in Fig. 10(b2) is 44.96 kV, and the unbalanced degree (UD) of submodules voltage ripple is 3.08%. The unbalanced degree is defined in (23).

$$UD = \frac{max(V_a, V_b, V_c) - min(V_a, V_b, V_c)}{V_{avg}}, \quad V_{avg} = \frac{V_a + V_b + V_c}{3} \tag{23}$$

The simulation results of method A are presented in Fig. 10(c). The double fundamental frequency negative- and zero-sequence circulating current are injected. Fig. 10(c3) shows the circulating currents are injected in three phases. As a result, the submodules voltage ripples which shown in Fig. 10(c2) are reduced considerably, especially on phase A. The average submodules ripple with Method A is 31.65 kV, this average submodules ripple is reduced by 29.6% compared to no injection submodules ripple. The unbalanced degree is 5.41%.

In Fig. 10(d3), circulating currents are injected only in phase B and C because the submodules voltage ripple in phase A does not exceed its limit. A more balanced submodules voltage ripple result compared to Fig. 10(b2) is shown in Fig. 10(d2). The

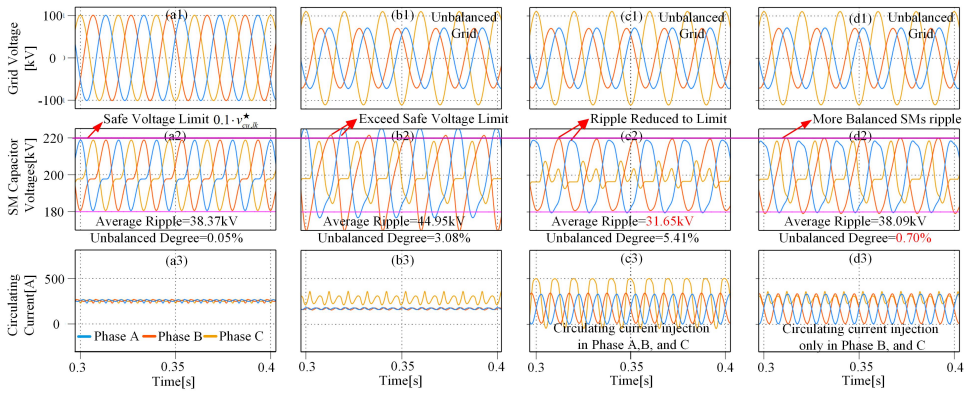

Fig. 10: Simulation results, (a) Normal grid condition, (b) Unbalanced grid condition without submodules balancing method, (c) Unbalanced grid condition with Method A, (d) Unbalanced grid condition with Method B.

Table 2: Simulation Value of Capacitor Voltage Ripple

	Normal Grid	No Injection	Method A	Method B
Average Ripple	38.37 kV	44.96 kV	31.65 kV	38.09 kV
Amplitude A	218.3 kV	218.41 kV	207.9 kV	218.6 kV
Amplitude B	218.2 kV	222.4 kV	219.8 kV	219.9 kV
Amplitude C	218.3 kV	225.3 kV	218.9 kV	218.5 kV
Unbalanced Degree	0.05%	3.08%	5.41%	0.70%

unbalanced degree, in this case, is reduced to 0.7%, and also the average submodules ripple with Method B is 38.09 kV, this average submodules ripple is reduced by 15.3% compared to no injection submodules voltage ripple.

From the simulation results, both Method A and B can reduce the submodules voltage ripple to a safe range. The average submodules ripple with Method A is smallest, however, this big ripple reduction is only on phase A, voltage reduction only in one phase does not increase the safety of the whole system. Method B can get a more compromised result. On the one hand, a more balanced three-phase submodules voltage ripple is achieved, on the other hand, the average submodules voltage ripple is also reduced. What is more, the losses in phase A will be lower because there is no AC circulating current injection in phase A.

2.5 Conclusion

The submodules voltage ripple unbalanced mechanism and two submodules voltage ripple balancing methods are introduced in this paper. Method A injects the double fundamental frequency of negative-sequence and zero- sequence circulating current into MMC system. Method B first detects the three-phase submodules voltage ripple amplitude, the circulating current will be injected in a dangerous high ripple phase to balance the submodules voltage ripple. The main contributions of this paper are summarized as follows. It offers 1). The submodules voltage ripple under unbalanced grid conditions contains double fundamental frequency positive-sequence and zero-sequence components and two fundamental frequency unbalanced components. 2). The double fundamental frequency positive-sequence and zero-sequence components are reduced by injecting three-phase circulating current with Method A, then the average ripple will be reduced. 3). The unbalanced submodules ripple can be balanced by Method B. The circulating current is injected only when one phase submodules voltage ripple exceed its limits. The proposed methods are believed to be competitive methods to improve the availability of MMC during unbalanced grid conditions.

3 Machine Learning Based Capacitor Voltage Fluctuation Reduction under Asymmetrical Grid Conditions

3.1 Background

In Chapter 2, the analytical equations of capacitor voltage fluctuation for asymmetrical grid conditions are derived, then based on the equations, two capacitor voltage fluctuation balancing and reduction methods are proposed. However, the analytical equations are complicated and nonlinear, it is difficult for the engineers to calculate the proper circulating current references quickly. What is more, the derived equations are based on the positive-sequence and negative-sequence asymmetrical grid model. This kind of grid model is not intuitive because the engineers need to convert the specific asymmetrical grid, such as a single line to ground fault, to the positive-sequence and negative-sequence grid.

In this chapter, a new machine learning based capacitor voltage fluctuation reduction method under asymmetrical grid conditions is proposed. The machine learning network is offine trained to represent the nonlinear relationship of the submodule capacitor voltage fluctuation, the output current reference, and the circulating current reference under asymmetrical grids. With this network, the circulating/output current references can be easily calculated to balance the submodule capacitor voltage fluctuation under asymmetrical grid conditions. What is more, this machine learning network can be implemented in the real controller with a very small computational burden. When the grid fault is relatively minor, only circulating current will be inserted into the system. When the grid fault is serious, the output current will be changed to reduce the submodule voltage fluctuation.

The chapter outline is as follows. In section 3.1, the introduction of machine learning will be given. In section 3.2, the proposed methods under different grid dip severity factor are introduced. In section 3.3, the procedures of data extraction and network training are shown. Then the results are presented in 3.4. And the conclusion is presented in 3.5.

3.2 Machine Learning Technology Introduction

The definition of Machine Learning (ML) based on [32] is: "A computer program learns from past experience to process certain tasks and achieve certain performance, and the performance increase with the increase in experience."

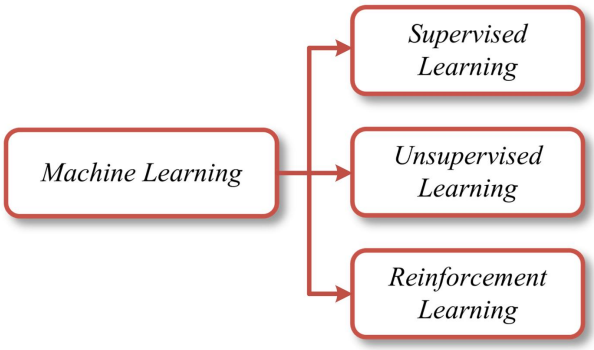

Fig. 11: Machine learning technology classification

Today, machine learning techniques are used in human society on a large scale. Examples include face recognition [47], [48], autonomous cars [49], [50], and natural language processing [51], [52].

ML is mainly divided into three categories: supervised learning, unsupervised learning, and reinforcement learning.

(1) Supervised learning

Supervised learning is an algorithm that can map the relationship between input data (feature) and the labeled output data by learning from the input-output data pairs. Firstly, the engineer/researcher extracts the labeled data of the system for the next training. For example, the animal pictures are labeled as a cat or a dog. And then train the machine learning model such as neural network to represent the input-output relationship. Then the trained network The machine learning network can recognize whether a new input animal picture is a cat or a dog [53].

(2) Unsupervised learning

Unsupervised learning is an algorithm that can automatically discover the relationship of input-output data without the labeled targets [54].

Table 3: Vector Definition of Asymmetrical Grids

Fault	Vector Equations
Double Line to Ground Fault	$\begin{cases} \widehat{V}_{ga\_pu} = 1 \\ \widehat{V}_{gb\_pu} = -\frac{1}{2}D - j\frac{\sqrt{3}}{2}D \\ \widehat{V}_{gc\_pu} = -\frac{1}{2}D + j\frac{\sqrt{3}}{2}D \end{cases}$
Three Phase to Ground Fault	$\begin{cases} \widehat{V}_{ga\_pu} = D \\ \widehat{V}_{gb\_pu} = -\frac{1}{2}D - j\frac{\sqrt{3}}{2}D \\ \widehat{V}_{gc\_pu} = -\frac{1}{2}D + j\frac{\sqrt{3}}{2}D \end{cases}$
Line to Line Short Circuit Fault	$\begin{cases} \widehat{V}_{ga\_pu} = 1 \\ \widehat{V}_{gb\_pu} = -\frac{1}{2} - j\frac{\sqrt{3}}{2}D \\ \widehat{V}_{gc\_pu} = -\frac{1}{2} + j\frac{\sqrt{3}}{2}D \end{cases}$
Single Line to Ground Fault	$\begin{cases} \widehat{V}_{ga\_pu} = D \\ \widehat{V}_{gb\_pu} = -\frac{1}{2} - j\frac{\sqrt{3}}{2} \\ \widehat{V}_{gc\_pu} = -\frac{1}{2} + j\frac{\sqrt{3}}{2} \end{cases}$

(3) Reinforcement learning

Reinforcement learning is an algorithm that can achieve the best task by automatically find a solution without any existed input-output data. With the accumulation of experience, the performance of reinforcement learning will get better and better [55].

3.3 The Asymmetrical Grids

The four typical types of asymmetrical grids are: Double line to ground fault, three phase to ground fault, line to line short circuit fault, single line to ground fault [56]. When the asymmetrical grid faults happen in the grid, the voltages of the three-phase grid will become asymmetrical. The reduced voltage is usually 10% to 90% of the rated value, the fault duration is about from half a cycle to a few seconds. Table 3 shows the vector definition of the four asymmetrical grid faults [57], [58]. The grid voltage vector definition is using grid dip severity factor D. Factor D represents the degree of voltage drop in the faulty grid, factor D varies between 0 and 1, where 1 means the grid is in a faultless condition, 0 means the grid is completely short-circuited and the grid voltage is zero. By this asymmetrical grid definition, all the possible grid conditions can

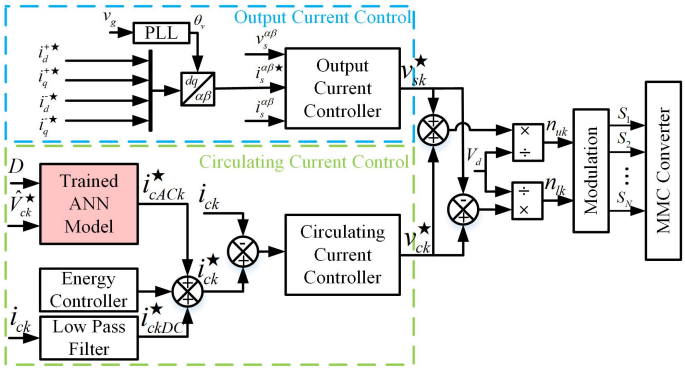

Fig. 12: The control block diagram of proposed capacitor voltage fluctuation reduction algorithm: Low grid dip severity factor condition

be covered by those two factors. First is the type of fault, and the second is the grid severity factor D.

3.4 The Proposed Method

The proposed machine learning based controller can balance and reduce the capacitor voltage fluctuation under the aforementioned asymmetrical grid faults. The proposed method can make a decision to change the circulating currents or the output currents then reduce the submodule capacitor voltage fluctuation of MMCs. Such a control task is achieved by applying the machine learning technology to train a surrogate model of the relationship between circulating currents, output currents, and the grid dip severity dip factor. The proposed controller selects different variables to change depending on the severity of fault in the grid voltage. The AC circulating current will be inserted to balance the submodule capacitor voltage fluctuation under minor grid fault, and the output currents will be changed to reduce the fluctuation under serious grid fault.

3.4.1 Low Grid Dip Severity Factor

Figure. 12 shows the diagram of the ML based submodule capacitor voltage fluctuation reduction method under low grid dip severity factor conditions. The pink block is the proposed controller to determine the three-phase circulating curreng (CC) references. The input variables of this block are the ideal capacitor voltage fluctuation value and the grid dip severity factor. In order to track the AC CC references, the proportional resonant (PR) controller is applied. The energy controller is also used to balance the three-phase energy of MMC. The three-phase sum energy (the sum of the upper and

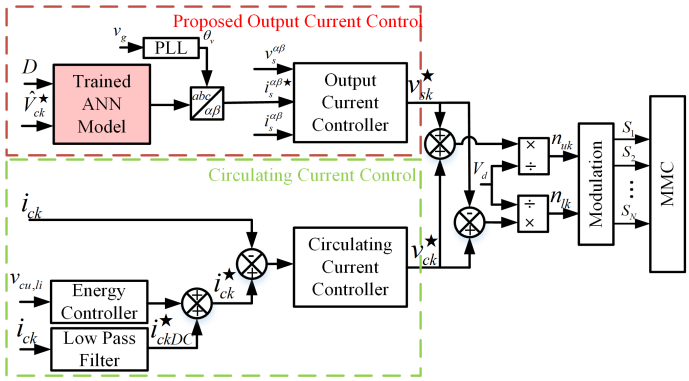

Fig. 13: The proposed machine learning based capacitor voltage fluctuation reduction algorithm: High grid dip severity factor condition

lower arm energy) is regulated to equal and the three-phase delta energy (the difference of the upper and lower arm energy) is controlled to zero [59], [60]. Besides the circulating current, the output current controller is used to control the output current. The proportional resonant (PR) controller is also applied. With circulating current and output current controllers, the inserted number of the MMC can be calculated. The inserted number is sent to the sort&select algorithm block to insert the best submodule to track the references and also balance the capacitor voltages of the MMC system [61], [62].

The trained ANN model represents the relationship between circulating current amplitudes, D, and the capacitor fluctuation amplitudes. ANN structure in this chapter is a three-layer feedforward neural network with 9 neurons. The equation (24) shows this relation particularly.

$$y = F(x) \Leftrightarrow (\widehat{I}_{cACa}, \widehat{I}_{cACb}, \widehat{I}_{cACc}) = F(D, \widehat{V}_{cua}, \widehat{V}_{cub}, \widehat{V}_{cuc}) \tag{24}$$

Where $\widehat{I}_{cACa}, \widehat{I}_{cACb}, \widehat{I}_{cACc}$ are the amplitudes of the three-phase circulating currents in phase A, B, and C respectively. $\widehat{V}_{cua}, \widehat{V}_{cub}, \widehat{V}_{cuc}$ are the amplitudes of the three-phase submodule capacitor voltages in phase A, B, and C respectively.

3.4.2 High Grid Dip Severity Factor

Figure. 13 shows the proposed ML based capacitor voltage fluctuation reduction method under high grid dip severity factor conditions. The proposed method is similar with the controller under low grid dip severity factor conditions, circulating current controller

and output current controller are used. This different part is, the output currents are controlled by the ML based controller.

3.5 Data Extraction and Neural Network Model Training

In order to achieve the goal of the proposed method, the neural network based capacitor voltage fluctuation controller is proposed. Obtaining the necessary data is a prerequisite. In this subsection, we show the data collection steps for the proposed method, and also show the neural network model training steps. We take one particular asymmetrical fault (double line to ground fault) as an example to show the data collection method under low/high grid dip severity factor. The other asymmetrical grid conditions follow the same steps. Then the training steps are presented in the remaining parts of this section.

3.5.1 Data Extraction and Network Training for Low Grid Dip Severity Factor

The vector definition of double line to ground fault is represented in (25)

$$\begin{cases} \widehat{V}_{ga\_pu} = 1 \\ \widehat{V}_{gb\_pu} = -\frac{1}{2}D - j\frac{\sqrt{3}}{2}D \\ \widehat{V}_{gc\_pu} = -\frac{1}{2}D + j\frac{\sqrt{3}}{2}D \end{cases} \tag{25}$$

Where D is the grid dip severity factor. By sweeping D from [0, 1] we can generate every conditions of double line to ground fault. The D will sweep from [0.7, 1] when the grid dip severity factor is low. And the D will sweep from [0, 0.7] when the grid dip severity factor is high.

By the definition in [63], the circulating current is a current that flows through both the upper and lower bridge arms of the MMC at the same direction. This current current has no effect on the external output performance. We define the three-phase circulating currents contain both DC component and AC component as follows:

$$i_{ck} = \frac{i_{uk} + i_{lk}}{2} = I_{ckDC} + \widehat{I}_{ckAC}\cos(2\omega t + \theta_{vk-}) \tag{26}$$

Where k represents different phase (Phase A, B, and C are represent by 0, 1, 2 respectively) , i_{ck} represents circulating currents in three-phase, i_{uk} is the upper arm current and i_{uk} is the lower arm current, I_{ckDC} represents the DC component of circulating current and $\widehat{I}_{ckAC}$ is the amplitude of the AC circulating current, ω is the grid fundamental angular frequency, and θ_{vk-} represents the negative-sequence phase angle

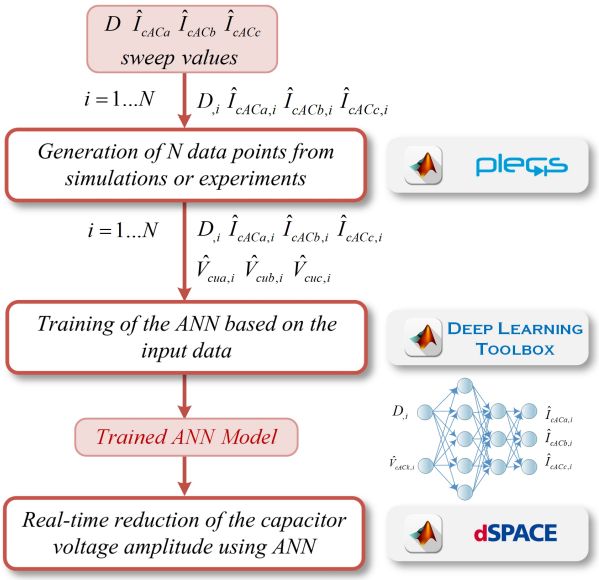

Fig. 14: Training procedures for the proposed ML based capacitor voltage fluctuation reduction method

$\left[0, -\frac{4}{3}\pi, -\frac{2}{3}\pi\right]$.

To clearly show the data collection and training steps, Fig. 14 shows the detailed flow chart of the proposed method. Each steps will be introduced as follows:

(1) Data Collection

In order to train the ANN model, the data should be collected first. The training data can be collected by the experimental setup or a detailed simulation model. With experimental setup, the advantage is the good accuracy of the data. However, it will take a long time to collect the same amount data compared to the simulation data collection. With simulation data collection, a detailed simulation model is applied to achieve the best simulation results as experimental setup has. Then the data collection time can be saved a lot by using the parallel computing technology. In this subsection, we use detailed simulation models to collect data for two cases: high voltage case and low voltage experimental setup case.

The three-phase capacitor voltage data under different grid dip severity factors

Table 4: MMC Parameters

	Simulation	Experiment
Submodule number in one arm(N)	100	4
DC line voltage	200 kV	200 V
Active power	150 MW	1 kW
Submodule capacitance (C)	3.75 mF	2000 uF
Submodule capacitor voltage (Vc)	2 kV	50 V
AC system frequency	50 Hz	50 Hz
Inductance in the arm	50.9 mH	10 mH
Sampling frequency	10k Hz	10k Hz
Amplitude of the grid	100 kV	83 V

and different injected AC circulating currents will be collected. In high voltage case, the grid dip severity factor will sweep from 0.5 to 0.9 with 0.1 resolution: [0.5, 0.6, 0.7, 0.8, 0.9], 5 values in each phase. The injected AC circulating current amplitudes $\widehat{I}_{cACa,b,c}$ sweep from 0 A to 400 A with 50 A resolution: [0, 50, 100, 150, 200, 250, 300, 350, 400], 8 values in each phase. So the total number of different case is 5*8*8*8=2560, that means the simulation model should run 2560 times for collecting the data. Regarding the low voltage experimental setup case, the grid dip severity factor will also sweep from 0.5 to 0.9 with 0.1 resolution: [0.5, 0.6, 0.7, 0.8, 0.9], 5 values. The injected AC circulating current amplitudes $\widehat{I}_{cACa,b,c}$ sweep from 0.3 A to 1.5 A with 0.2 A resolution: [0.3, 0.5, 0.7, 0.9, 1.1, 1.3, 1.5], 7 values in each phase. So the total number of different case is 5*7*7*7=1715. With the help of parallel computing technology, the data collection time for high voltage case is 14 minutes, for low voltage experimental setup case, the collection time is 10 minutes.

(2) Training

After the data is collected, this data can be used to train the ANN model to represent the relationship between three-phase voltage fluctuations, injected AC circulating currents, and the grid dip severity factors. With this trained network, the AC circulating current references can be determined by the model based on the input grid severity factor D and ideal capacitor values. Classic three-layer ANN with is applied, a input layer, a hidden layer, and a output layer . In the hidden layer, there are 9 neurons. The training process is implemented in MATLAB environment with the deep learning toolbox.

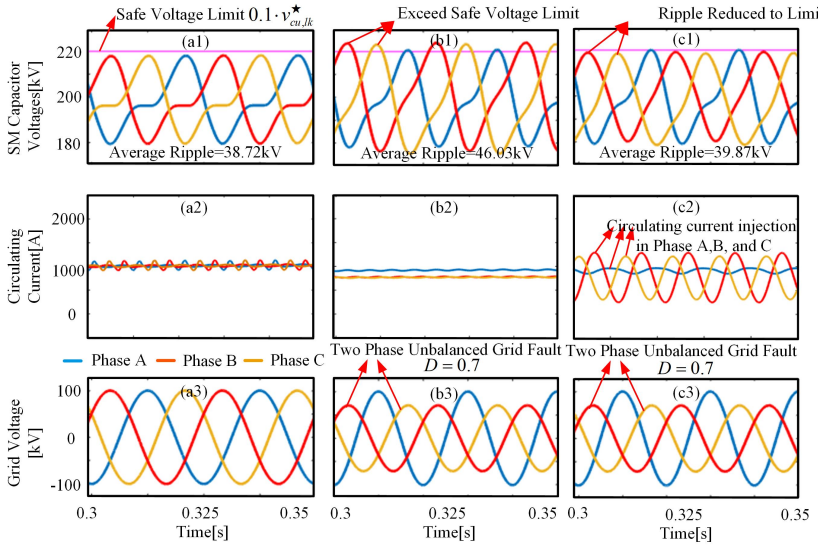

Fig. 15: Simulation: (a) symmetrical grid; (b) asymmetrical grid (no injection); (c) asymmetrical grid with proposed ML strategy.

3.5.2 Data Extraction and Network Training for High Grid Dip Severity Factor

When the grid fault is serious, the grid dip severity factor is high. In this case, only inject AC circulating current is not enough to reduce the capacitor voltage fluctuation to a safe level. So we select the output current to be the controllable variable to reduce the capacitor voltage fluctuation level. Similar as low grid dip severity factor case, we sweep D and three-phase output current amplitude $\widehat{I}_{sa,b,c}$. The grid dip severity factor will sweep from 0 to 0.7 with 0.1 resolution: [0, 0.1, 0.2, 0.3, 0.4, 0.5, 0.6, 0.7], 8 values. The output current amplitudes $\widehat{I}_{sa,b,c}$ sweep from 600A to 1000A with 100A resolution: [600, 700, 800, 900, 1000], 5 values in each phase. So the total number of different case is 8*5*5*5=1000, that means the simulation model should run 1000 times for collecting the data.

3.6 Results

In this subsection, the results of the proposed capacitor fluctuation reduction strategies under different grid conditions are presented. In simulation, the PLECS (blockset version) is used to verify the proposed method. The parameter of the simulation model is present in Table 3. In experiment, a dSPACE based controller is applied to verify the

proposed method. The parameter of the MMC lab prototype is shown in Table 3.

(1) The Results of Double Line to Ground Fault

Fig. 15 shows the simulation results. In Fig. 15(a), the MMC under balanced grid conditions is simulated, the three-phase capacitor voltages are symmetrical and below the capacitor voltage limit (10% of rated DC capacitor voltage). The average voltage fluctuation (maximum voltage minus minimum voltage) here is 38.72 kV. In order to define the unbalance with three-phase, the definition of unbalanced degree (UD) is introduced:

$$UD = [max(V_a, V_b, V_c) - min(V_a, V_b, V_c)]/V_{avg} + (V_a + V_b + V_c)/3 \tag{27}$$

Under balanced grid, the UD of three-phase capacitor voltages is 0.046%. Fig. 15(b) shows the results of proposed method under double line to ground fault without the proposed method. From the results we can see, the asymmetrical grid in Fig. 15(b3) influences the submodule capacitor voltage fluctuation in Fig. 15 (b1), the fluctuation is increased and exceed the safe limit. In this case, the UD of three-phase capacitor voltages is increased to 1.48% and the average voltage fluctuation is increased to 46.03 kV.

Fig. 15(c) shows the results of the proposed method under double line to ground grid fault. From Fig. 15(c2), the three-phase AC circulating currents are injected into the MMC. Then the capacitor voltage fluctuation in Fig. 15(c1) are reduced. The UD here is reduced to 0.64%, and the average capacitor fluctuation is reduced to 39.87 kV. In this case, the operation region is extended by 30% by the ML method.

Fig. 16 shows the experimental results of the proposed method. The three-phase capacitor voltages are balanced and within the safe limit. The average voltage fluctuation here is 6.5V, and the UD is 0.18%.

Fig. 16(b) shows the results of MMC under double line to ground fault without the proposed method. From the results we can see, the asymmetrical grid in Fig. 16(b3) influences the capacitor voltage fluctuation in Fig. 16(b1), the fluctuation is increased and higher than the capacitor voltage limit. In this case, the UD is increased to 1.112% and the average voltage fluctuation is increased to 7.3V.

Fig. 16(c) shows the results of the proposed method under double line to ground grid fault. From Fig. 16(c2), the three-phase AC circulating currents are injected into the MMC system. Then the capacitor voltage fluctuation in Fig. 16(c1) are reduced.

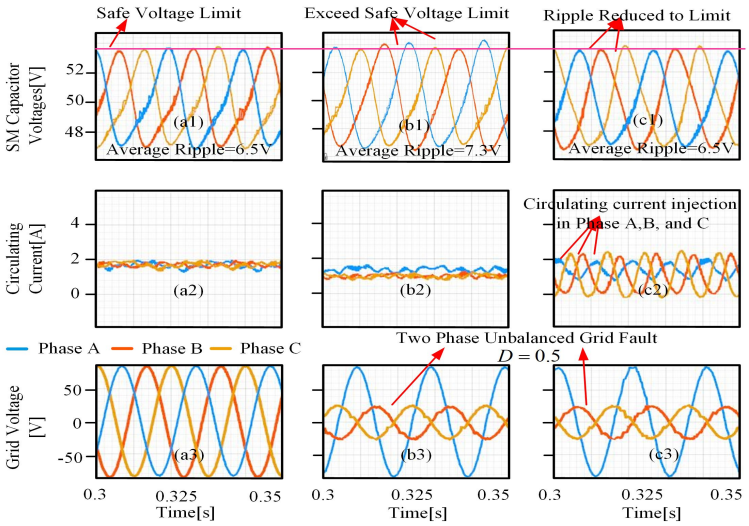

Fig. 16: Experiment: (a) symmetrical grid; (b) asymmetrical grid (no injection); (c) asymmetrical grid with proposed ML strategy.

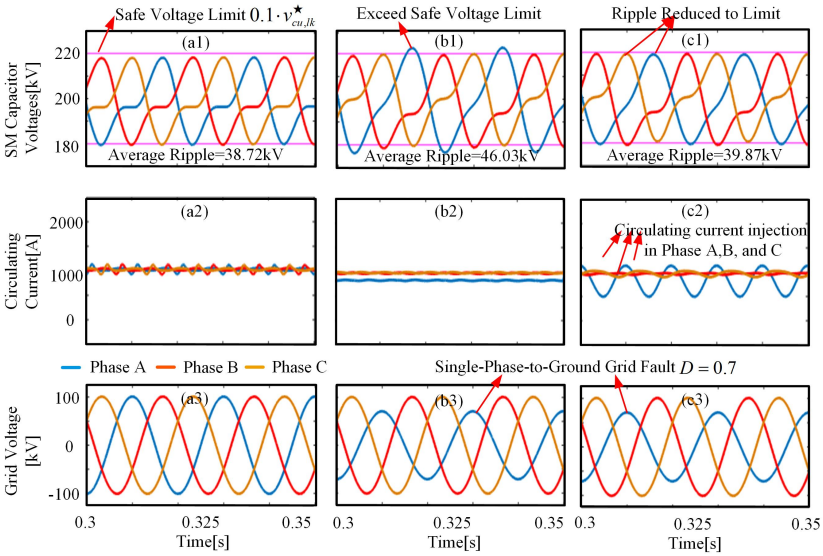

Fig. 17: Single line to ground grid results (a) asymmetrical grid; (b) asymmetrical grid (no injection); (c) asymmetrical grid with proposed ML strategy.

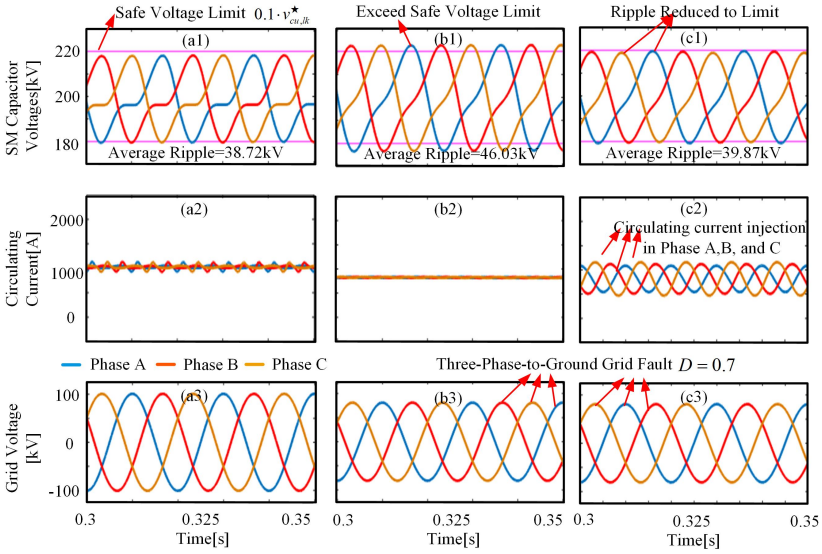

Fig. 18: Three-phase-to-ground grid results (a) asymmetrical grid; (b) asymmetrical grid (no injection); (c) asymmetrical grid with proposed ML strategy.

The UD here is reduced to 0.18%, and the average capacitor fluctuation is reduced to 6.5V. In experiment, the operation region is extended by 50% by the proposed ML method.

(2) The Results of Single Line to Ground Fault

To further illustrate our point, we have extended our proposed method to two new asymmetrical grid conditions in simulation: Single line to ground grid and three phase to ground grid. The simulation results of MMC under single line to ground fault are shown in Fig. 17.

In Fig. 17(b) and (c), the grid is under single line to ground fault with a 0.7 grid dip severity factor. The grid voltage in the fault phase A is 70% of the rated grid voltage, 70 kV. This fault voltage influences the charging of the capacitor voltage, then the capacitor voltage fluctuation is increased. The capacitor voltage is higher than the safe voltage limit (220 kV), which is shown in Fig. 17(b2). After enabling the proposed method, the capacitor voltage in phase A is reduced to the safe limit by injected the circulating current, this can be seen from Fig. 17(c1) and (c2).

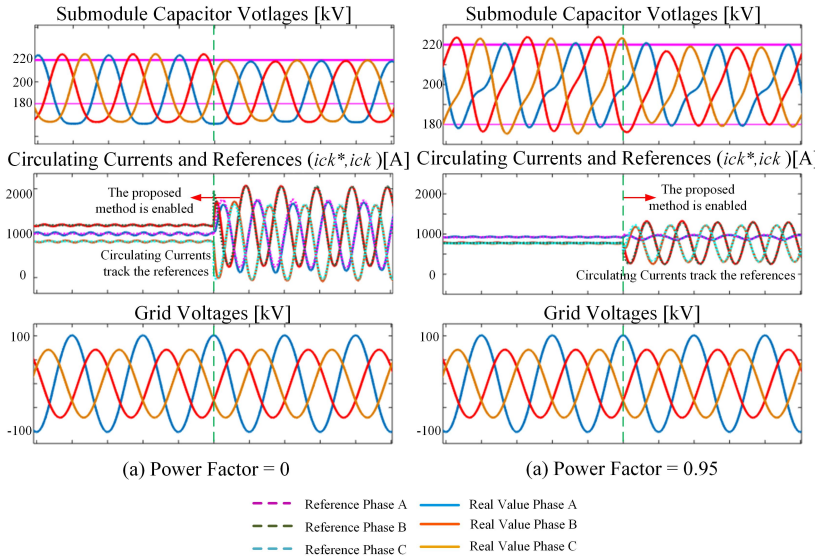

Fig. 19: Results when power factor=0 and 0.95

(3) The Results of Three Phase to Ground Fault

The simulation results of MMC under three phase to ground fault are shown in Fig. 18. In Fig. 18(b) and (c), the grid is under three phase to ground fault with a 0.7 grid dip severity factor. The grid voltages in the three phases are 70% of the rated grid voltage, 70 kV. Those fault voltages influence the charging of the capacitor voltages, then the capacitor voltage fluctuations are increased. The three-phase capacitor voltages are higher than the safe voltage limit (220 kV), which is shown in Fig. 18(b2). After enabling the proposed method, the capacitor voltages in three phases are reduced to the safe limit by injected the circulating currents, this can be seen from Fig. 18(c1) and (c2).

(4) The Results of Different Power Factors

The results of the proposed method under different power factor conditions are also shown in this report. The results show that the proposed method has a good ability to reduce the capacitor voltage fluctuation under different conditions. Fig. 19(a) presents that when the power factor equals to 0, the capacitor voltage fluctuation is still reduced

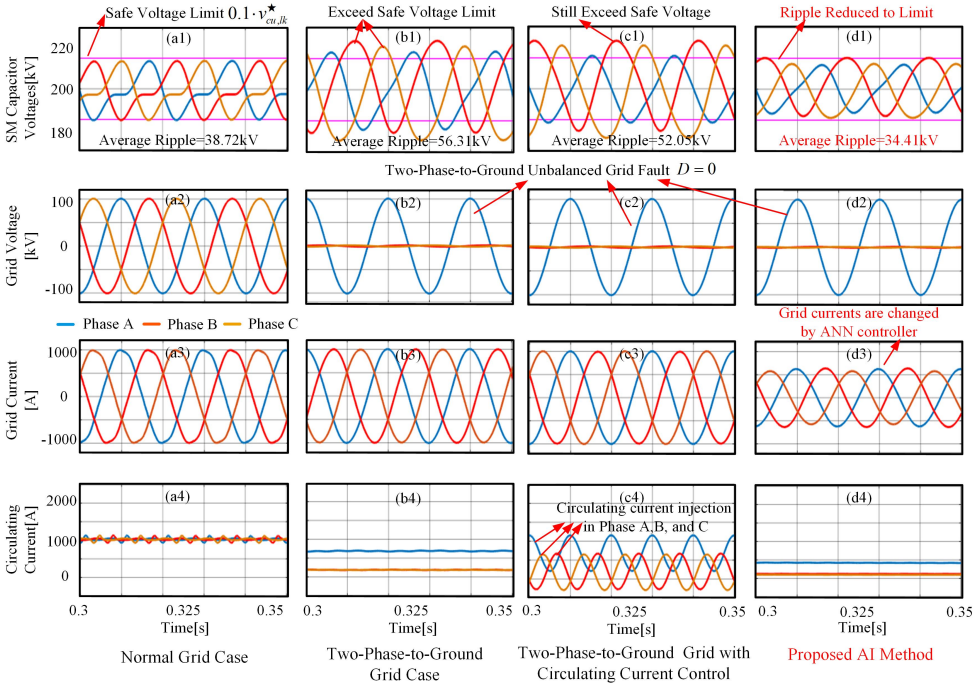

Fig. 20: Results with the proposed controller: (a) symmetrical grid; (b) double line to ground grid without proposed method; (c) double line to ground grid with circulating current injection; (d) proposed ML method.

by the proposed controller even though the shape of the capacitor voltage fluctuation is different. Fig. 19(b) also shows a good capacitor voltage reduction results when the power factor equals to 0.95.

3.6.1 The Results of High Grid Dip Severity Factor

The results under high grid dip severity factor are also shown. In Fig. 20(a), the capacitor voltages are balanced and not higher than the capacitor voltage limit. And the AC circulating current are suppressed by circulating current controller. The average capacitor voltage fluctuation is 38.72 kV.

Fig. 20(b) shows the results when two phases of grid are totally short circuit, i.e. D=0. The capacitor voltage fluctuation are high and asymmetrical. The average capacitor voltage fluctuation is 56.31 kV.

Fig. 20(c) shows the results under double line to ground fault when the AC circulating currents are injected. The average fluctuation is reduced to 52.05 kV, but the capacitor voltages still exceed the limit.

Fig. 20(d) shows the results of proposed ML method. From Fig. 20(d3), the output currents are reduced by the proposed ML based method. Then the capacitor voltages are reduced significantly. The average fluctuation here is reduced to 34.41 kV. All the capacitor voltages are below the safe voltage limit.

3.7 Conclusion

In this chapter, a comprehensive machine learning based capacitor voltage fluctuation reduction method is proposed to extend the operational region of MMCs under asymmetrical grid conditions. The machine learning model is trained by the acquired data to reduce and balance the submodule capacitor voltage fluctuation with asymmetrical grids. The MMC capacitor can always run in a safe voltage range under different asymmetrical grid faults. This machine learning approach to achieve complex control objectives in power electronics systems has the potential to be applied to many different power electronics applications.

4 Machine Learning Emulation of Model Predictive Controller for MMCs

4.1 Background

In this chapter, machine learning is applied to MMCs to achieve fast dynamic responses while reducing the computational burden on controllers. The traditional control structure of the MMCs is based on PI/PR based controller, these controller heavily rely on the accurate control bandwidth tunning based on the different operating conditions. What is more, there are several control loops and their bandwidth is overlapping, thus the stability issues will be rised. Model predictive control based controller can achieve a fast dynamic response while the parameter-free configuration. However, because of the nature of the MPC, the MPC will exhaustively search for a large number of possible switching signals to achieve its control goals, which will lead to a high computational burden on the controller.

In this chapter, machine learning technology is applied to emulate the MPC controller to achieve a fast dynamic response. What is more, the computation cost of the controller is significantly reduced because of the low computational burden characteristics of machine learning models.

The outline is as follows. In section 4.1, the concept of MPC is introduced first. The dynamic equations of the MPC are described and reproduced in this section. And then two machine learning networks are applied to emulate the MPC in section 4.2, the data collection procedures, and the training steps are also shown in 4.3. Finally, the simulation and experimental results are shown in 4.4 to verify the proposed methods.

4.2 Dynamic Equations of MPC MMC System

4.2.1 Model Predictive Control of MMC Scheme

The control scheme of MPC-MMC is introduced as follows [64], [65].
(1) The system variable values are measured by the measurement block. The system variables inlcude: upper/lower arm currents i_u, i_l; upper/lower capacitor voltages u_{cui}, u_{cli};
(2) Based on the dynamic equations (45) and (46) of MMC, all the possible output variables in next control period are predicted;
(3) The cost function is established based on (44) by considering the all the circulating current and output current values in the next control period;
(4) The best insert numbers of upper and lower arm are selected to achieve the lowest

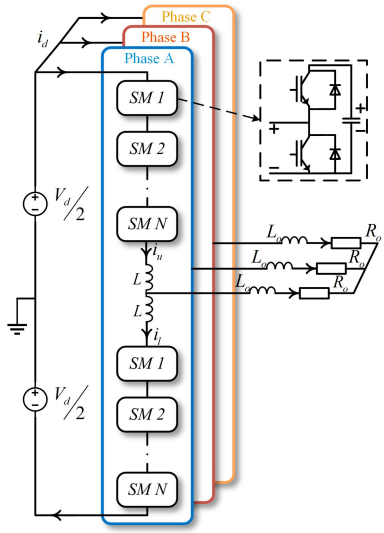

Fig. 21: MMC Topology Block Diagram

cost function;
(5) The best insert numbers of upper and lower arm are sent to control the MMC;
(6) Repeat step (1)-(5).

4.2.2 Dynamic Equations of MPC-MMC

In order to applying the MPC in MMCs, the dynamic equations of MMCs should be derived first. Fig. 21 shows the circuit diagram of the MMC system. From the circuit diagram, the Kirchhoff's voltage law can be used to derive the dynamic equations of the MMCs. The equations of the MMC circuit are derived [66], [67]:

$$\frac{V_d(t)}{2} - v_{cuk}(t) - L_{arm}\frac{di_{uk}(t)}{dt} = R_s i_{sk}(t) + L_s\frac{di_{sk}(t)}{dt} \tag{28}$$

$$\frac{V_d(t)}{2} - v_{clk}(t) - L_{arm}\frac{di_{lk}(t)}{dt} = -R_s i_{sk}(t) - L_s\frac{di_{sk}(t)}{dt} \tag{29}$$

Where $V_d(t)$ is the DC side voltage, $v_{cuk}(t)$ and $v_{clk}(t)$ are the arm voltages in phase A, B, and C, u and l represent upper arm and lower arm respectively, k represents the phase number (0 represents phase A, 1 represents B, and 2 represents C), R_s is load resistance and L_s is the load inductance, $i_{sk}(t)$ means the output current in phase k.

In this thesis, the definitions of the output current and circulating current in [68] and [69]:

$$i_{sk}(t) = i_{lk}(t) - i_{uk}(t) \tag{30}$$

$$i_{ck}(t) = \frac{1}{2}[i_{uk}(t) + i_{lk}(t)] - \frac{1}{3}i_d(t) \tag{31}$$

From (28) to (31), the output currents and circulating currents are:

$$\frac{di_{sk}(t)}{dt} = \frac{1}{L + 2L_0}[v_{clk}(t) - v_{cuk}(t) - 2R_0 i_{sk}(t)] \tag{32}$$

$$\frac{di_{ck}(t)}{dt} = \frac{1}{2L}[v_d(t) - v_{clk}(t) - v_{cuk}(t)] \tag{33}$$

The dynamic equations of capacitor voltage can be derived based on switching states, arm current, and submodule capacitance:

$$\frac{du_{cuki}(t)}{dt} = \frac{i_{uki}}{C_{SM}} \tag{34}$$

$$\frac{du_{clki}(t)}{dt} = \frac{i_{lki}}{C_{SM}} \tag{35}$$

Where u_{cukt} and u_{cukt} are the ith submodule capacitor voltages in upper and lower arm respectively (i=1...N), C_{SM} is the submodule capacitance.

The continuous dynamic equations (30) to (35) are needed to transfered the discrete model by applying the Euler forward equation as follows:

$$\frac{dx(t)}{dt} \approx \frac{x(k+1) - x(k)}{T_s} \tag{36}$$

Where x(k + 1) and $x(k)$ are the variable at k + 1 and k time period respectively.

Based on (36), the discrete dynamics of the output current, circulating current and the submodule capacitor voltages are derived based on (30)-(35):

$$i_j(k+1) = \frac{T_s}{L_{arm} + 2L_s}[u_{lj}(k+1) - u_{uj}(k+1)] + (1 - \frac{2T_s R_s}{L_0 + 2L_s})i_j(k) \tag{37}$$

$$i_c(k+1) = \frac{T_s}{2L_{arm}}[V_d - u_{uj}(k+1) - u_{lj}(k+1)] + i_c(k) \tag{38}$$

$$\begin{cases} u_{cui}(k+1) = \frac{T_s}{C_{SM}} i_r(k) + u_{cui}(k),\ S_{ri}(k) = 1 \\ u_{cui}(k+1) = u_{cui}(k),\ S_{ri}(k) = 0 \end{cases} \tag{39}$$

Where k+1 represents the k+1 time step, S_{ri} is the insert signal for the ith submodule capacitor, $S_{ri} = 1$ means insertion, $S_{ri} = 0$ means bypass.

In order to control the MMCs, three main control tasks should be achieved: (1). Controlling the output current to track the current reference; (2). Suppressing the circulating current to the pure DC component; (3). Balancing the capacitor voltages to a same capacitor voltage level. When the submodule number is high, the capacitor balancing block should be able to make the capacitor voltages to be the same, then the computational burden of the capacitor balancing block will be huge. To reduce the computational burden, the task of the capacitor voltage balancing can be done by independently block out of MPC. Then three tasks can be simplified to two task: Control the ac output current and suppress the circulating current.

Now, a relationship between output current, circulating current, and the switching states is needed to simplify the tasks. From (39) the sum of capacitor voltages can be derived.

$$\sum v_{cri}(k+1) = \frac{M_{ri} T_s}{C_{SM}} i_r(k) + \sum v_{cri}(k) \tag{40}$$

Where M_{ri} is the number of inserted submodules in upper or lower arm.

Assuming all the capacitor voltages are kept to the reference voltage, the arm voltage is:

$$v_r(k+1) = M_{ri} \frac{\sum v_{cri}(k+1)}{N} \tag{41}$$

Substituting (41) into (37), the relationship between output current and the switching state submodule is derived:

$$i_s(k+1) = \frac{2T_s}{L_{arm} + 2L_s} \left[\frac{M_l \sum v_{cli}(k+1) - M_u \sum v_{cui}(k+1)}{N} \right] + \left(1 - \frac{2T_s R_s}{L_{arm} + 2L_s} \right) i_s(k) \tag{42}$$

Also the substituting (41) to (38), the relationship between circulating current and the switching state submodule is derived:

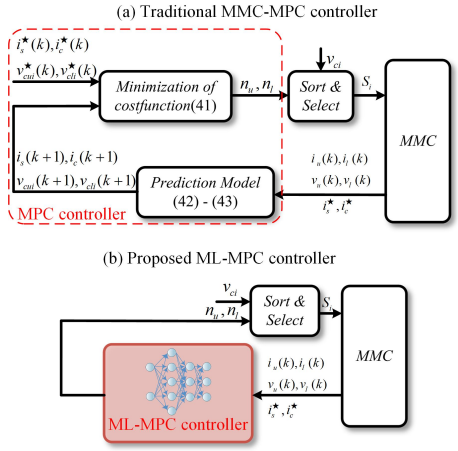

Fig. 22: MMC-MPC and AI-MPC Comparision

$$i_c(k+1) = \frac{T_s}{2L_{arm}}[V_d - \frac{M_l \sum v_{cli}(k+1) + M_u \sum v_{cui}(k+1)}{N}] + i_c(k) \tag{43}$$

Based on (42) and (43), the system variables (output and circulating current) can be controlled by selecting the inserted number of capacitor. And the capacitor voltages are balanced by external sort and select block. The cost function of the MPC MMC is:

$$g = \lambda_1 \left| i_s^*(k+1) - i_s(k+1) \right| + \lambda_2 \left| i_c(k+1) \right| \tag{44}$$

Where λ_1 and λ_2 are weighing factors of output circulating current respectively.

In the experimental hardware system, the digital controller always has the delay. That means, the control signals cannot be transmitted to the converter instantaneously due to hardware reason. Applying the method in [70] can compensate this delay. By predicting the variable values in k+2 time step, the time delay in k+1 time step is covered.

$$\begin{cases} i_s(k+2) = \boldsymbol{A}[(n_l(k+1) \cdot v_{cl}(k+2) - n_{cu}(k+1) v_{cu}(k+2))/N] + \boldsymbol{B} i_s(k+1) \\ \boldsymbol{A} = 2T_s/(L_{arm} + 2L_s) \\ \boldsymbol{B} = 1 - 2T_s R_s/(L_{arm} + 2L_s) \end{cases} \tag{45}$$

$$\begin{cases} i_c(k+2) = \boldsymbol{C}[v_d - (n_l(k+1) \cdot v_{cl}(k+2) + n_u(k+1) \cdot v_{cu}(k+2))/N] + i_c(k+1) \\ \boldsymbol{C} = T_s/(2L_s) \end{cases} \tag{46}$$

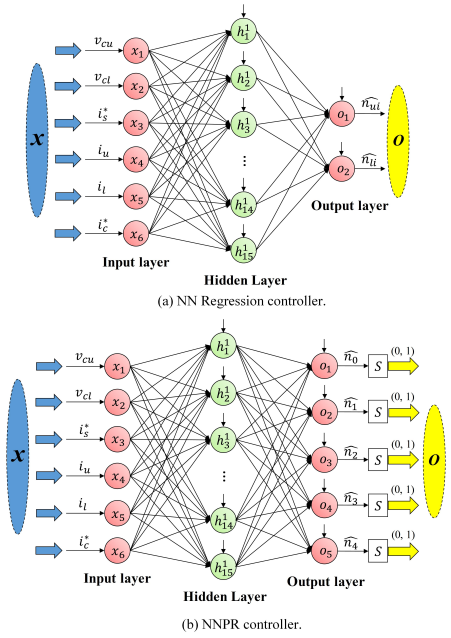

Fig. 23: Network Diagrams of two Machine Learning Networks

4.3 Emulation of MPC

During one control period, the MPC controller applies the same control pattern. So the input output relationship of MPC-MMC can be understood by analyzing only one control period. The key control principle of MPC-MMC is: all the possible circulating current values and output current values in next time period are predicted online, and the best inserted numbers are selected to minimize the cost function. This exhausted online searching pattern will occupy a lot of computing resources. What is more, this online searching pattern is a deterministic pattern. That means, when a fixed set of input parameters and a fixed cost function are chosen, the MPC algorithm always outputs a set of corresponding fixed output variables. In this chapter, the deterministic MPC input-output relationship is replaced by the machine learning networks. The exhausted online searching pattern is replaced by the computational efficient machine learning network. Then, we could achieve a lower computation burden controller.

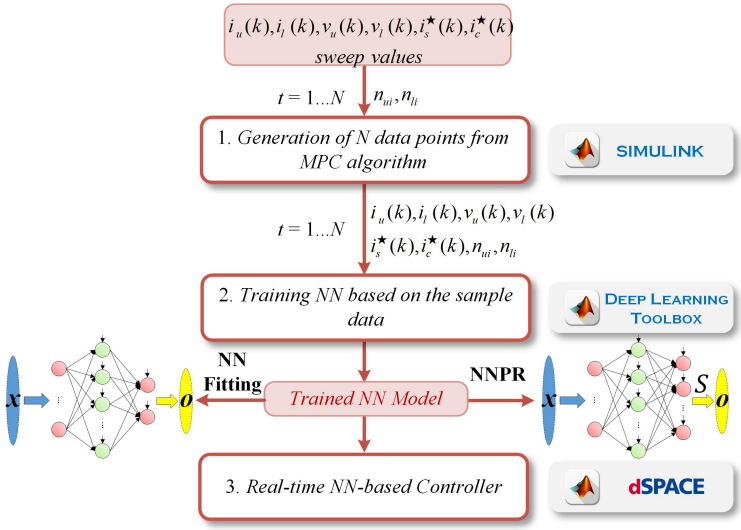

Fig. 24: Training Steps for the proposed ML MPC Controller

4.4 Data Collection and Network Training

Two ML based networks are proposed to emulate the behavior of the MPC-MMC controller: Neural Network (NN) regression and Neural Network pattern recognition (NNPR). The traditional MPC controller is replaced by the ML controller. The input variables are the same as the MPC controller: Upper/lower arm currents i_u, i_l, Upper/lower capacitor voltages u_{cui}, u_{cli}, and the reference of output current and circulating current i_s^*, i_c^*. The output variables of the ML controller are upper/lower arm input number n_u, n_l.

Those two networks need to be trained by the data which is collected from the traditional MPC controller. The training data for two networks are the same but the data processing method is different due to different NN output requirements. In NNPR, the output features must be 0 or 1 but the NN regression have no limit. So the structure of two networks are different. In this subsection, the two networks will be introduced in detail.

4.4.1 Introduction of Two Neural Networks

For the NN regression, as Fig. 23 (a) shows, a three layer structure is applied: one input layer, one hidden, and one output layer. The input-output relationship is represented

as follows:

$$(n_u,\ n_l) = F(v_{cu},\ v_{cl},\ i_s^*,\ i_c^*,\ i_u,\ i_l) \tag{47}$$

The output variables of the NN regression network are the inserted number of upper and lower arm MMC. In this study, the MMC has 4 submodules per arm. So the output have 5 integer values: 0, 1, 2, 3, 4, 5.

Regarding the NNPR network, the network structure is also a three layer structure. However, the output layer is different. In NNPR, the output unit can only output 0 or 1, only two output units to represent the insert number is not enough, so the NNPR will output the insert information for each specific submodule. In other words, the output unit number is 5. And also two NNPR network will be used to control the upper and lower arm MMC respectively. The input output relationship of NNPR is as follows:

$$(n_1,\ n_2,\ n_3,\ n_4,\ n_5\ ) = F(v_{cu},\ v_{cl},\ i_s^*,\ i_c^*,\ i_u,\ i_l) \tag{48}$$

Where n_z (z = 0, 1, 2, 3, 4) represents the output value of the NNPR for each specific submodule.

4.4.2 Data Collection and Network Training

Fig. 24 shows the data collection and network training steps of the proposed method. Each steps are introduced clearly as follows:

(1) Data Collection from MPC Block: The training data can be solely extracted from the MPC MMC controller by sweeping different input variables within the variable range. The sweeping data of the input variables v_{cu}, v_{cu} are [0:10:350]. 0 means the input variable starts at 0, 10 means the data resolution is 10, 350 means the input variable ends at 350, the data of input variables are like: 0V, 10V, 20V,...,350V. So there are 36 data points in total. The other sweeping variables are i_s^*, the range is [-6:1:6], there are 13 sampling points in output current. i_u, i_l: [-6:1:6], 13 sampling data in upper and lower current. i_c^* : [-2:0.2:2], 11 sampling points in circulating current. Therefore, the total data points of the training data can be calculated: 36*36*13*13*13*11=30.21 million data points. In this case, the data collection time is 76s.

(2) Network training: The collected data from MPC controller is randomly divided into three parts: the training data (70%), the validation data (15%), and the test data (15%). A work station PC is applied to train the NN regression network and NNPR networks. The training is done by the MATLAB Deep Learning Toolbox.

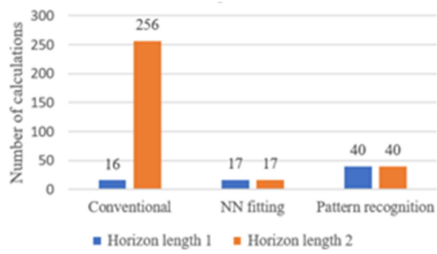

Fig. 25: Comparison of the number of calculations and the horizon length

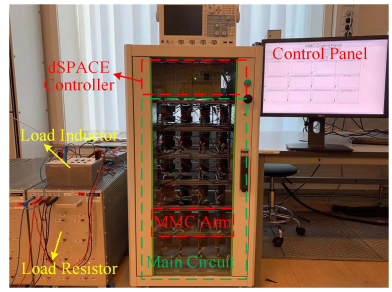

Fig. 26: The MMC Setup Diagram

4.4.3 Network Training Performance

After the network training, the training performance of NNPR is shown in Fig. 27. The output of NNPR has 5 features, each feature is a 0/1 classification problem. Each row of the confusion matrix from Fig. 27 represents an output unit for each submodule. And the each column of the confusion matrix represents the target data from the collected data. The green blocks of the confusion matrix give the information of the correctly classified data points and the red blocks give the information of the wrong prediction. From Fig. 27, 97.5% of the classification are correct. What is more, five grey cells in the 6th column and the other five grey cell in the 6th give the information of the classification for each feature. The accuracies of the 3rd and 4th features are only 1.1% and 0.4% respectively. So even though the overall training accuracy is high, the predicting accuracy of the 3rd and the 4the feature is low. The reason is, the data amount of the 3rd and 4th are only 0.56% and 0.62% of the total data. As a consequence of this, the control performance will be influenced.

Regarding the NN regression, the training performance is calculated. The predicted data is compared with the sample data to get the accuracy. In this case, the training accuracy of the NN regression is 93.2%, which is lower than the training ac-

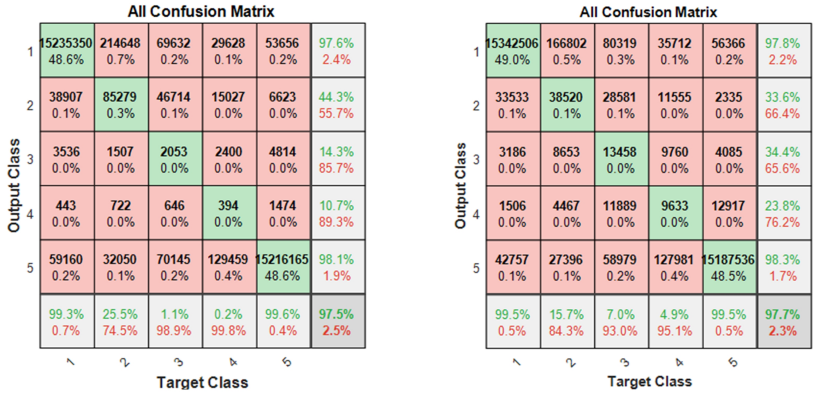

(a) NNPR training for upper arm

(b) NNPR training for lower arm

Fig. 27: Confusion matrix of NNPR training

curacy of the NNPR. However, the predicted accuracies of the 3rd and the 4th feature are 33.7% and 34.9% respectively, which are much higher than the accruacies in NNPR (1.1% and 0.4% respectively).

In Fig. 25, the calculation numbers of two networks based on the horizon length (HL) are presented. The calculation numbers of NN regression and NNPR are always 9 and 28 when the HL number is different. However, the calculation number of MPC will increase significantly when the HL is higher. The calculation number of MPC is 16 when the HL is one, and the calculation number of MPC increases to 256 when the HL is two. So, the calculation number of ML networks are lower than the MPC, which implys a lower computational burden.

4.5 Results

In this section, the simulation and experiment are achieved to verify the effeteness of the two proposed ML MPC controllers. The experimental MMC setup is a prototype with three phase half-bridge configuration. The DC voltage is 200V. The detailed parameter information is shown by Table. 5. The controller platform is based on DS1006 platform from dSPACE company. The measurement is achieved by DS4004 board. Each submodule is a half-bridge submodule with the hardware protection (Overcurrent and overvoltage protection). Fig. 26 shows the picture of the MMC setup.

Table 5: MMC Parameters

	Simulation	Experiment
Number of SMs per arm (N)	100	4
Rated DC voltage	200kV	200V
Rated active power	150MW	1kW
Nominal SM capacitance (C)	3.75mF	2000uF
Nominal SM capacitor voltage (Vc)	2kV	50V
Rated frequency	50Hz	50Hz
Arm inductance	50.9mH	10mH
Sample frequency	10kHz	10kHz
Grid voltage amplitude	100kV	83V

4.5.1 Steady State Results of NN Regression

The comparison of the MMC MPC controller and the proposed NN regression controller is presented in Fig. 28. First, as the Fig. 28 (a1) and (b1) show, the output currents of two controllers have almost the same performance. The load current total harmonic distortion (THD) of MPC controller is 0.021% and the load current THD is 0.023%. Second, the circulating currents are suppressed by two controllers. And also, the capacitor voltages are well balanced with the help of external sort and selecting block.

Fig. 29 shows the experimental results of different neuron numbers of the NN regression network. Theoretically, higher neuron number will have higher training performance. The standard to judge the training performance of different neuron numbers is mean squared error (MSE), lower MSE means better performance of the trained network. The MSE is 0.177 when the neuron number is 9, the MSE increases to 0.199 when the neuron number is 6, and the MSE further increases to 0.302 when the neuron number is 4. In Fig. 29 (a1), (b1), and (c1), the output currents are all well controlled by three different controllers.

Five different NN regression networks are trained by data sets with different data sizes. From fig. 30 (1)-(3), the output currents are not well controlled, and the training data sets have 4860, 22500, and 249018 points respectively. When the data points increase to 4889808, the output current currents in Fig. 30 (4) is acceptable. And then the output current is well controlled in Fig. 30 (5) when the data points is enough (31320432).

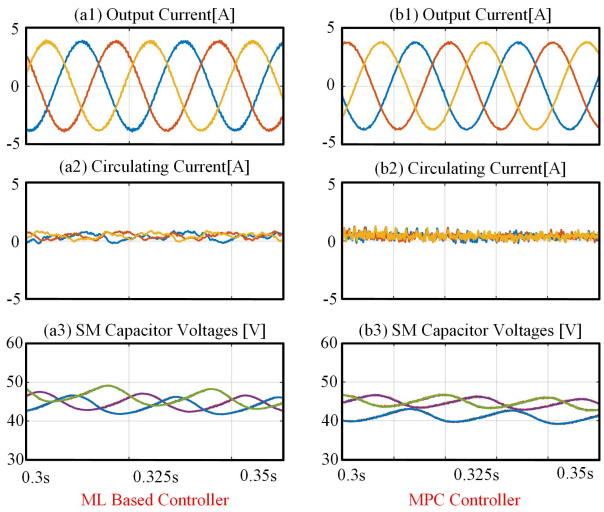

Fig. 28: Steady state experimental results of the traditonal MPC and the proposed NN regression

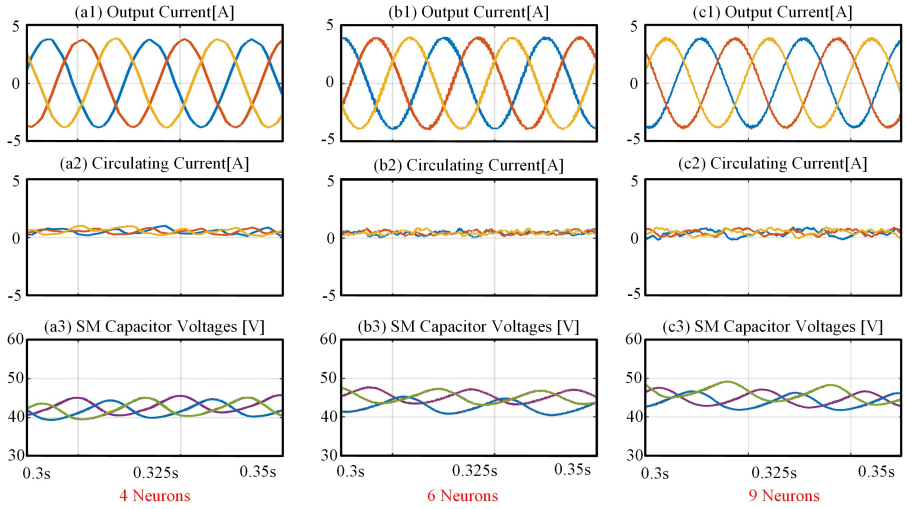

Fig. 29: Experimental results of ML controller with different neuron numbers

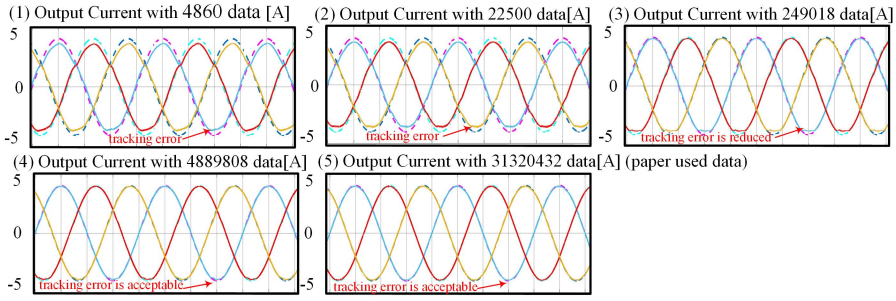

Fig. 30: Results of ML controller with different size of data

4.5.2 Dynamic Performance of NN Regression

The Fig. 31 shows the dynamic results of the NN regression method. The initial current reference amplitude is 4A, then suddenly it becomes 2A. And finally, it's back to 4A. The output current in Fig. 31 successfully allows instantaneous tracking of step reference values with a few microseconds.

The Fig. 32 shows the frequency dynamic of the NN regression method. The output current reference frequency is suddenly changed from 50Hz to 20Hz, and then 20Hz to 40Hz. Form the results, the proposed NN regression controller has a ability to track the suddenly changed reference frequencies with a few microseconds.

4.5.3 Computational Burden

The main merit of the proposed ML MPC controller is transferring MPC's exhausted online switching signal searching to offline network training. In this way, the online computation of the controller is reduced. In order to show this computational burden reduction of the proposed method. The experimental computation burden of different controllers are compared. Three control methods are compared, the first method is the MPC controller which is introduced in [71], the second method is the fast MPC model which is proposed in [31], and the third is the proposed ANN based controller. The computational burden is measured by the software dSPACE Profiler. Fig. 33 shows the computational burden comparison of those three methods. First of all, the mean turnaround time of the MPC method is the highest (9.790us) because the submodule capacitor voltage sorting and selecting is done by the controller. Second, the mean turnaround time of the fast MPC method is 1.615 us which is lower than the traditional MPC controller. Finally, the mean turnaround time of the propsoed ANN based controller is 1.112 us which is the lowest. Then the conclusion is that the proposed

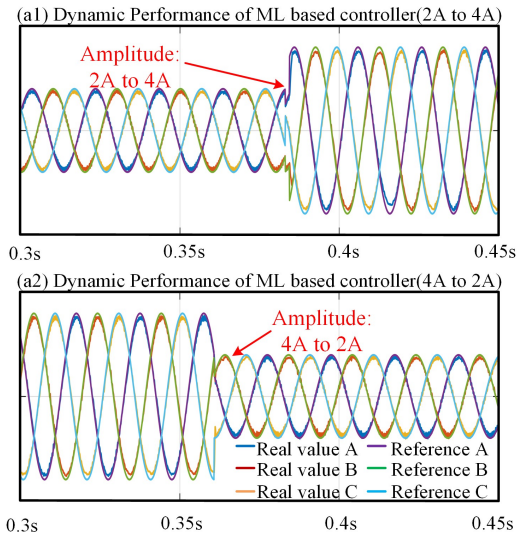

Fig. 31: Output current dynamic

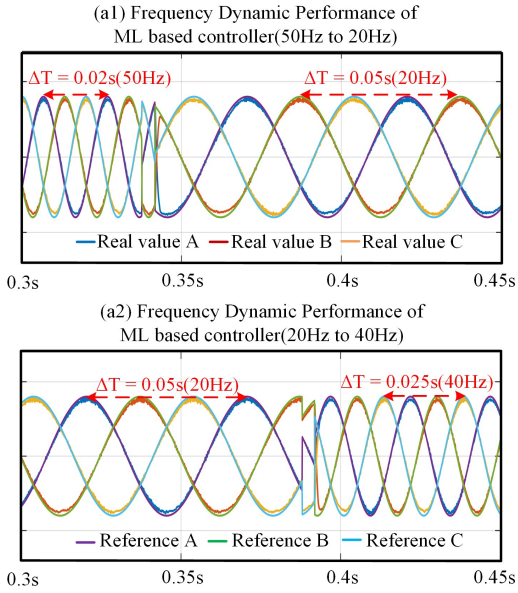

Fig. 32: Output current frequency dynamic

COMPUTATIONAL BURDEN

	ML	Fast MPC	MPC
Mean Turnaround Time (μs)	1.123	1.615	9.790
Max Turnaround Time (μs)	1.252	1.788	9.690
Min Turnaround Time (μs)	1.070	1.561	9.947

Fig. 33: The comparison of computational burden

controller is effective to reduce the computation burden.

4.5.4 The Results of the NNPR

The simulation and experimental results of two proposed controllers are compared in this section. First, the simulation steady state results of the two proposed controllers are shown in Fig. 34. Fig. 34 (a) presents the results of the MPC method, Fig. 34 (b) shows the results of the proposed NN regression method, and Fig. 34 (c) shows the results of the propsed NNPR method. From Fig. 34 (a1), (b1), and (c1), the output current are well controlled by those three controllers. From Fig. 34 (a2), (b2), and (c2), the AC circulating current are also suppressed by those controllers. However, the AC circulating current of NN regression has the highest RMS value (0.81 A) compared with MPC (0.71 A) and NNPR (0.73 A). In the end, the submodule capacitor voltages are equal by the control of those controllers.

The experimental steady state results of two proposed controllers are show in Fig. 35. The difference between simulation and experimental results is, the experimental output current of the NNPR has a high THD. This is because the poor training accuracy in some classes. The training accuracy of 2nd class, 3rd class, and 4th class are low to 15.7%, 1.1%, and 0.2% respectively. This poor training accuracy will not influence the performance of the simulation a lot because in simulated circuit the parameters are ideal. However, in experimental prototype, the noise and inaccurate circuit parameters will influence the performance.

The Fig. 36 (a) shows the dynamic results of the NN regression method. The initial current reference amplitude is 4 A, then suddenly it becomes 6 A. The output currents in Fig. 36 (a1) and (a2) show both proposed methods can successfully track the references within the sampling range and also with a fast response speed to the step reference and suddenly changed output current frequency.

In this chapter, the sampling range of output current is [-6 A, 6 A]. When the output current reference amplitude is higher than 6 A, the output data is out of training

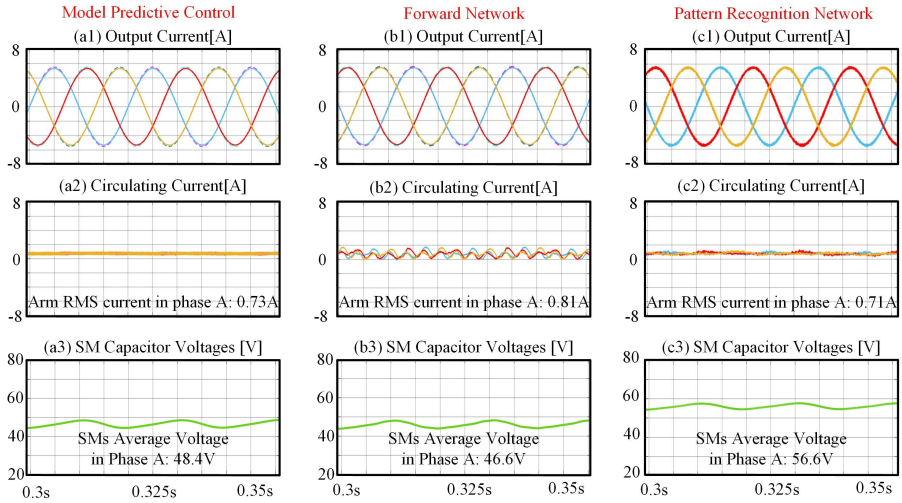

Fig. 34: Steady state performance of three controllers: (a) MPC controller, (b) NN regression controller, (c) NN pattern recognition controller.

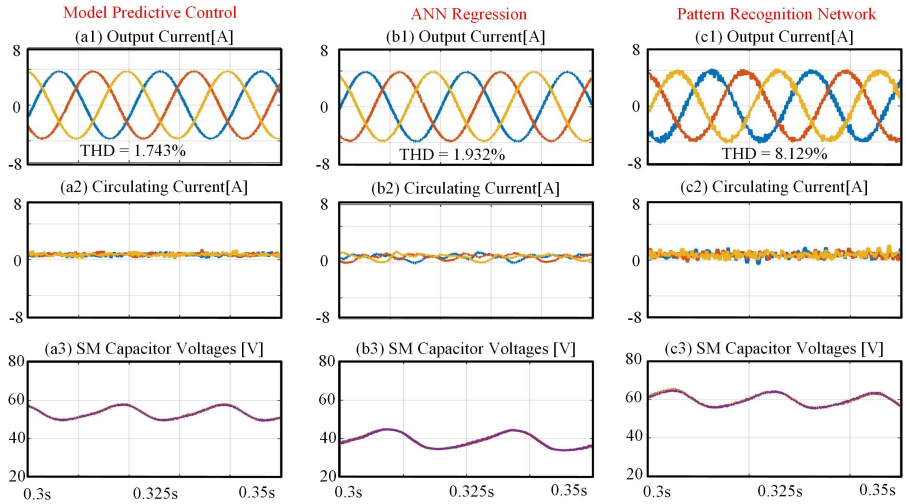

Fig. 35: Experimental results of the 1). MPC, 2). NN Regression Network Method, and 3). Pattern Recognition Network

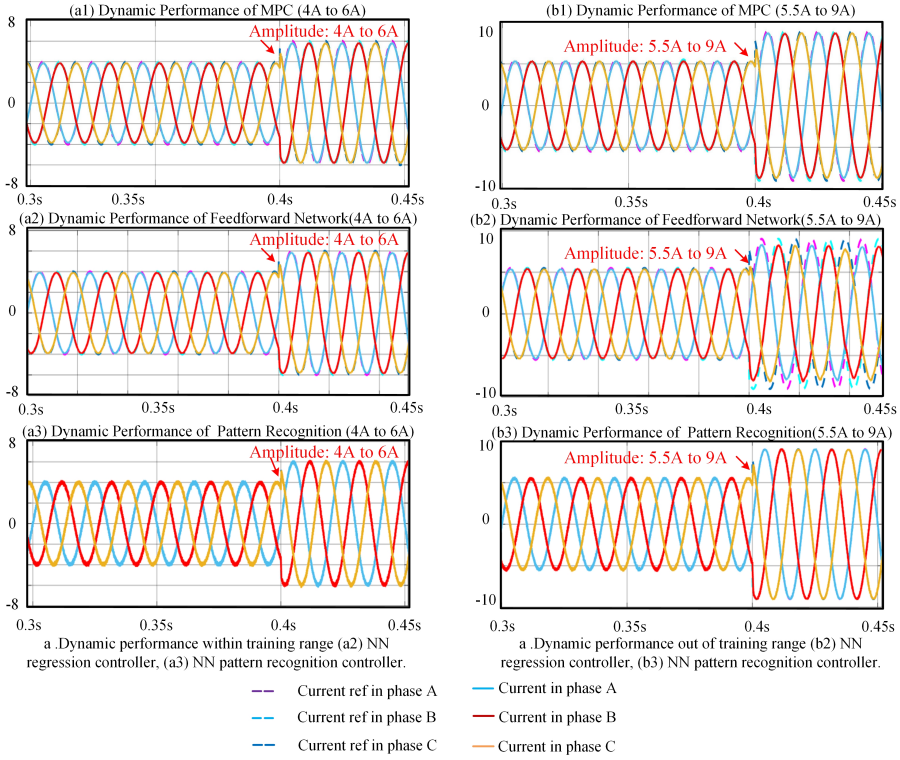

Fig. 36: The results of the proposed methods within or out of sampling range

range. The performance of the two proposed methods with out range data is shown in Fig. 36 (b). The amplitude of the output current reference is changed from 5.5 A to 9 A. The NNPR has a better ability to track the out range reference but NN regression cannot track the out range reference properly.

4.6 Conclusion

In this chapter, machine learning is applied to MMCs to maintain fast dynamic responses as MPC while reducing the computational burden on controllers. The machine learning network emulates the MPC controller with a low computational cost. This propsoed machine learning emulation could be a foundation of other computational efficient controller in future.

5 Conclusion

In this chapter, the main findings and the outcomes of the Ph.D. thesis Advanced Control Strategies of Modular Multilevel Converter are concluded. The conclusion section also summarizes how the Ph.D. thesis has addressed the project objectives The contributions of this thesis are introduced. And then the further research perspectives regarding the Ph.D. topic is discussed.

5.1 Summary

This project aims to improve the overall performance of MMCs in HVDC applications by proposing advanced control methods, enabling the MMCs have higher stability and better fault tolerance. First, some of the current problems of MMC are discussed and introduced, and then solutions to these problems are proposed. A brief description of each chapter is as follows.

In chapter 1, the background of the thesis is described in detailed: Renewable energy generation is a fast-growing industry, as countries around the world want to reduce carbon dioxide emissions by developing renewable energy sources, thereby mitigating climate change and building a better environment for future generations. MMC as a superior topology for building large scale HVDC systems. thus a flexible and efficient renewable energy transmission networks can be established. However, there are also some problems with using this topology, which are discussed in detail in this chapter. The first challenge is the high submodule capacitor voltages under asymmetric grid faults, which may cause several problems to the MMC such as submodule overvoltage trip, capacitance reduction, even the capacitor breakdown, etc. Another issue is when the MPC is applied in MMC to achieve a fast dynamic response, the computation burden of the controller will be high. A high computational burden can limit MPC MMC use in real-time controllers. Following to overcome those problems, new control strategies and methods are strongly demanded.

In Chapter 2, the first issue discussed in Chapter 1 will be resolved by controlling the internal characters of the MMC. By changing the circulating current reference value of the three-phase MMC, the charging mode of the bridge arm capacitor is changed, thus reducing the voltage ripple of the sub-module capacitor during grid imbalance. In this way, the submodule overvoltage trip, capacitance reduction can be prevented. This chapter derives the analytic formula for the submodule voltage, and by analyzing the individual components of the analytic formula, the causes of high submodule capacitor voltages at grid imbalances are first accurately understood. Then, by inserting the AC circulating current components, specific components of the submodule capacitor volt-

age are precisely eliminated, Thus reducing the ripple of the capacitor voltage under unbalanced grid conditions.

Although Chapter 2 presents a detailed analytical formula to analyze capacitor voltage in the presence of grid imbalances, this complex theoretical derivation can limit the wide application of this method. Chapter 3 introduces a more intuitive and simpler approach to reducing submodule capacitor voltage ripple than the one in Chapter 2. A machine learning model replaces the analytic formula in the previous chapter to generate a loop current reference to limit ripple. Both simulation and experimental results verify the effectiveness of the proposed method.

The second problem introduced in Chapter 1 is researched in Chapter 4. In Chapter 4, two different machine learning models are trained to simulate the control characteristics of a model-predictive controller, and resulting machine learning-based controller mimics the model predictive controller nearly perfectly in a computationally inexpensive way. Moreover, training data collection and neural network training are all presented in this chapter. Ultimately, the steady-state, dynamic performance of such machine learning based controllers is simulated and experimentally verified. Furthermore, the number of neurons, the size of the training data, and the computational burden of the controller are thoroughly compared and discussed.

5.2 Main Contributions of Thesis

(1) Providing an accurate symmetrical component method based capacitor voltage model under unbalanced grid faults for a three-phase modular multilevel converters

An in-depth and accurate submodule capacitor voltage ripple model is proposed, this model is the theoretical basis for understanding the phenomenon of submodule overvoltage under unbalanced grid faults. By decomposing the components in positive-sequence, negative-sequence, and zero-sequence, the submodule voltage ripple components affected by the unbalanced grid are decomposed one by one, and each ripple component that raises the voltage is clearly deduced. This model can give us a deep and clear representation of the capacitor voltage ripple in the submodule under unbalanced grid faults.

(2) Providing a convenient method of data acquisition for power electronic systems based on parallel simulation

An efficient and fast data acquisition method for power electronic systems is proposed in this paper, the method can scan all possible parameters of the power electronic system, and all possible parameters are input into the parallel simulation model by an automated code for rapid simulation, the result data and the corresponding scanned input parameters together constitute a database of the power electronic system. In this Ph.D. project, two set of data are collected:

- In Chapter 3, this data collection method is used to collect data on the capacitor voltage ripple of the submodule when the circulating amplitudes, unbalanced grid voltages, and output currents are changed. By this method, the original complex theoretical derivation formula is replaced by a comprehensive data set.
- In Chapter 4 of this paper, this data collection method collects input-output relationships specific to the MPC controller and, by scanning all possible variables, obtains a database of input-output relationships that are representation of the MPC control.

In addition, this method can be easily extended to other applications, such as parameter scanning of grid-connected converter controllers, to obtain stability data for the system which can help to design the controll parameters of the system.

(3) Development of machine learning-based methods to represent complex input-output relationships in MMC

A simple and intuitive machine learning method is proposed in this thesis to represent complex input-output relationships in a computationally efficient way. Machine learning models that represent the complex input-output relationships can be easily obtained by using the data obtained from the proposed data collection method. Three types of machine learning networks are trained in this paper:

- Use the data of the submodule capacitor voltage ripple to train a model to efficiently express the ripple amplitude of the submodule capacitor voltage under different unbalanced grid conditions.
- The deterministic input-output data from the MPC is used to train an ANN model that efficiently mimics the behavior of the MPC controller by way of a machine learning model, and achieve a higher training accruate at the same time.

5.2.1 Enhanced and revised control methods for MMC systems

4 control methods that improve MMC performance in different ways. These methods include:

- Two submodule capacitor voltage ripple balancing methods are proposed based on the propopsed analytical model of submodule.
- A fast and intuitive machine learning based method to balance and reduce the submodule capacitor voltage ripple under unbalanced grid conditions is proposed.
- A computation efficient ANN based MMC controller is proposed to control the MMC with a lower computational load.
- A NNPR based MMC controller is proposed to control the MMC with a ability to handle the data beyond the input range.

5.3 Research Perspectives

Although some models and control methods have been proposed in this PhD project, there are still some challenges that need to be overcome in the future.

- First, whether the method is based on machine learning or on theoretical derivation, it is assumed that the fault has been detected quickly and unmistakably by the fault detection module. However, this project does not include the fault detection algorithms. It could be beneficial to the integrate fault detection approach to the proposed methods to achieve a complete fault prevention strategy for MMC in case of grid imbalance.
- Although this Ph.D. project proposes a computationally less burden ML controller to control the MMC, there are still some open questions. First, when the MMC is caught in a fault, such as a grid failure or submodule failure, this project does not study the fault conditions control. Secondly, this Ph.D does not include all situations, and whether ML based controllers can effectively control all situations needs to be fully investigated. In the future, further research is needed on machine learning control in fault conditions and atypical situations.

References

[1] Terry P Hughes, Michele L Barnes, David R Bellwood, Joshua E Cinner, Graeme S Cumming, Jeremy BC Jackson, Joanie Kleypas, Ingrid A Van De Leemput, Janice M Lough, Tiffany H Morrison, et al. Coral reefs in the anthropocene. *Nature*, 546(7656):82–90, 2017.

[2] IEA. Global energy review 2020. http://www.iea.org/reports/global-energy-review-2020, 2020.

[3] IEA. World energy outlook 2019. https://www.iea.org/reports/world-energy-outlook-2019, 2019.

[4] Dragan Jovcic. *High voltage direct current transmission: converters, systems and DC grids*. John Wiley & Sons, 2019.

[5] Anton Lesnicar and Rainer Marquardt. An innovative modular multilevel converter topology suitable for a wide power range. In *2003 IEEE Bologna Power Tech Conference Proceedings,*, volume 3, pages 6–pp. IEEE, 2003.

[6] Zhujian Ou, Guangzhu Wang, and Lanhua Zhang. Modular multilevel converter control strategy based on arm current control under unbalanced grid condition. *IEEE Transactions on Power Electronics*, 33(5):3826–3836, 2017.

[7] Chunyi Guo, Jiayi Yang, and Chengyong Zhao. Investigation of small-signal dynamics of modular multilevel converter under unbalanced grid conditions. *IEEE Transactions on Industrial Electronics*, 66(3):2269–2279, 2018.

[8] Steffen Rohner, Steffen Bernet, Marc Hiller, and Rainer Sommer. Modulation, losses, and semiconductor requirements of modular multilevel converters. *IEEE transactions on Industrial Electronics*, 57(8):2633–2642, 2009.

[9] Kamran Sharifabadi, Lennart Harnefors, Hans-Peter Nee, Staffan Norrga, and Remus Teodorescu. *Design, control, and application of modular multilevel converters for HVDC transmission systems*. John Wiley & Sons, 2016.

[10] Qingrui Tu, Zheng Xu, Yong Chang, and Li Guan. Suppressing dc voltage ripples of mmc-hvdc under unbalanced grid conditions. *IEEE Transactions on Power Delivery*, 27(3):1332–1338, 2012.

[11] Deepak Ronanki and Sheldon S Williamson. Failure prediction of submodule capacitors in modular multilevel converter by monitoring the intrinsic capacitor voltage fluctuations. *IEEE Transactions on Industrial Electronics*, 67(4):2585–2594, 2019.

[12] Kalle Ilves, Antonios Antonopoulos, Lennart Harnefors, Staffan Norrga, Lennart Ängquist, and Hans-Peter Nee. Capacitor voltage ripple shaping in modular multilevel converters allowing for operating region extension. In *IECON 2011-37th Annual Conference of the IEEE Industrial Electronics Society*, pages 4403–4408. IEEE, 2011.

[13] Josep Pou, Salvador Ceballos, Georgios Konstantinou, Vassilios G Agelidis, Ricard Picas, and Jordi Zaragoza. Circulating current injection methods based on instantaneous information for the modular multilevel converter. *IEEE Transactions on Industrial Electronics*, 62(2):777–788, 2014.

[14] Rui Li, John E Fletcher, and Barry W Williams. Influence of third harmonic injection on modular multilevel converter-based high-voltage direct current transmission systems. *IET Generation, Transmission & Distribution*, 10(11):2764–2770, 2016.

[15] Georgios Konstantinou, Harith R Wickramasinghe, Salvador Ceballos, and Josep Pou. Offset pwm in modular multilevel converters for stored arm energy reduction. In *2016 IEEE 2nd Annual Southern Power Electronics Conference (SPEC)*, pages 1–6. IEEE, 2016.

[16] Mohamed S Diab, Ahmed M Massoud, Shehab Ahmed, and Barry W Williams. A dual modular multilevel converter with high-frequency magnetic links between submodules for mv open-end stator winding machine drives. *IEEE Transactions on Power Electronics*, 33(6):5142–5159, 2017.

[17] Xiaojie Shi, Zhiqiang Jack Wang, Bo Liu, Yalong Li, Leon M Tolbert, and Fred Wang. Steady-state modeling of modular multilevel converter under unbalanced grid conditions. *IEEE Transactions on Power Electronics*, 32(9):7306–7324, 2016.

[18] Ji-Woo Moon, Jung-Woo Park, Dae-Wook Kang, and Jang-Mok Kim. A control method of hvdc-modular multilevel converter based on arm current under the unbalanced voltage condition. *IEEE Transactions on Power Delivery*, 30(2):529–536, 2014.

[19] Michail Vasiladiotis, Nicolas Cherix, and Alfred Rufer. Impact of grid asymmetries on the operation and capacitive energy storage design of modular multilevel converters. *IEEE Transactions on Industrial Electronics*, 62(11):6697–6707, 2015.

[20] Jinke Li, Georgios Konstantinou, Harith R Wickramasinghe, Christopher David Townsend, and Josep Pou. Capacitor voltage reduction in modular multilevel converters under grid voltages unbalances. *IEEE Transactions on Power Delivery*, 2019.

[21] Shaohua Li, Xiuli Wang, Zhiqing Yao, Tai Li, and Zhong Peng. Circulating current suppressing strategy for mmc-hvdc based on nonideal proportional resonant controllers under unbalanced grid conditions. *IEEE Transactions on Power Electronics*, 30(1):387–397, 2014.

[22] Qichen Yang, Maryam Saeedifard, and Marcelo A Perez. Sliding mode control of the modular multilevel converter. *IEEE Transactions on Industrial Electronics*, 66(2):887–897, 2018.

[23] Apparao Dekka, Bin Wu, Venkata Yaramasu, Ricardo Lizana Fuentes, and Navid R Zargari. Model predictive control of high-power modular multilevel converters—an overview. *IEEE Journal of Emerging and Selected Topics in Power Electronics*, 7(1):168–183, 2018.

[24] Zheng Gong, Xiaojie Wu, Peng Dai, and Rongwu Zhu. Modulated model predictive control for mmc-based active front-end rectifiers under unbalanced grid conditions. *IEEE Transactions on Industrial Electronics*, 66(3):2398–2409, 2018.

[25] Mohsen Vatani, Behrooz Bahrani, Maryam Saeedifard, and Morten Hovd. Indirect finite control set model predictive control of modular multilevel converters. *IEEE Transactions on Smart Grid*, 6(3):1520–1529, 2014.

[26] Yue Wang, Wulong Cong, Ming Li, Ning Li, Mu Cao, and Wanjun Lei. Model predictive control of modular multilevel converter with reduced computational load. In *2014*

IEEE Applied Power Electronics Conference and Exposition-APEC 2014, pages 1776–1779. IEEE, 2014.

[27] Hamid Mahmoudi, Mohsen Aleenejad, and Reza Ahmadi. Modulated model predictive control of modular multilevel converters in vsc-hvdc systems. *IEEE Transactions on Power Delivery*, 33(5):2115–2124, 2017.

[28] Venkata Yaramasu and Bin Wu. Predictive control of a three-level boost converter and an npc inverter for high-power pmsg-based medium voltage wind energy conversion systems. *IEEE Transactions on Power Electronics*, 29(10):5308–5322, 2013.

[29] Apparao Dekka, Bin Wu, and Navid R Zargari. Minimization of dc-bus current ripple in modular multilevel converter under unbalanced conditions. *IEEE Transactions on Power Electronics*, 32(6):4125–4131, 2016.

[30] Jingjing Huang, Bo Yang, Fanghong Guo, Zaifu Wang, Xiangqian Tong, Aimin Zhang, and Jianfang Xiao. Priority sorting approach for modular multilevel converter based on simplified model predictive control. *IEEE Transactions on Industrial Electronics*, 65(6):4819–4830, 2017.

[31] Zheng Gong, Peng Dai, Xibo Yuan, Xiaojie Wu, and Guosheng Guo. Design and experimental evaluation of fast model predictive control for modular multilevel converters. *IEEE Transactions on Industrial Electronics*, 63(6):3845–3856, 2015.

[32] Tom M Mitchell et al. Machine learning. 1997. *Burr Ridge, IL: McGraw Hill*, 45(37):870–877, 1997.

[33] Shuai Zhao, Frede Blaabjerg, and Huai Wang. An overview of artificial intelligence applications for power electronics. 2020.

[34] Tomislav Dragičević, Patrick Wheeler, and Frede Blaabjerg. Artificial intelligence aided automated design for reliability of power electronic systems. *IEEE Transactions on Power Electronics*, 34(8):7161–7171, 2018.

[35] Tomislav Dragičević and Mateja Novak. Weighting factor design in model predictive control of power electronic converters: An artificial neural network approach. *IEEE Transactions on Industrial Electronics*, 66(11):8870–8880, 2018.

[36] Peng Xiao, Ganesh Kumar Venayagamoorthy, Keith A Corzine, and Jing Huang. Recurrent neural networks based impedance measurement technique for power electronic systems. *IEEE transactions on power electronics*, 25(2):382–390, 2009.

[37] Fujin Deng and Zhe Chen. Voltage-balancing method for modular multilevel converters under phase-shifted carrier-based pulsewidth modulation. *IEEE Transactions on Industrial Electronics*, 62(7):4158–4169, 2015.

[38] Kurt Friedrich. Modern hvdc plus application of vsc in modular multilevel converter topology. In *2010 IEEE International Symposium on Industrial Electronics*, pages 3807–3810. IEEE, 2010.

[39] Rainer Marquardt. Modular multilevel converter: An universal concept for hvdc-networks and extended dc-bus-applications. In *The 2010 International Power Electronics Conference-ECCE ASIA-*, pages 502–507. IEEE, 2010.

[40] Eduardo Prieto-Araujo, Adria Junyent-Ferre, Gerard Clariana-Colet, and Oriol Gomis-Bellmunt. Control of modular multilevel converters under singular unbalanced voltage conditions with equal positive and negative sequence components. *IEEE Transactions on Power Systems*, 32(3):2131–2141, 2016.

[41] Qingrui Tu, Zheng Xu, and Lie Xu. Reduced switching-frequency modulation and circulating current suppression for modular multilevel converters. *IEEE transactions on power delivery*, 26(3):2009–2017, 2011.

[42] OA Giddani, Grain Philip Adam, Olimpo Anaya-Lara, Graeme Burt, and KL Lo. Control strategies of vsc-hvdc transmission system for wind power integration to meet gb grid code requirements. In *SPEEDAM 2010*, pages 385–390. IEEE, 2010.

[43] Remus Teodorescu, Marco Liserre, and Pedro Rodriguez. *Grid converters for photovoltaic and wind power systems*, volume 29. John Wiley & Sons, 2011.

[44] Jun Wang, Xu Han, Hao Ma, and Zhihong Bai. Analysis and injection control of circulating current for modular multilevel converters. *IEEE Transactions on Industrial Electronics*, 66(3):2280–2290, 2018.

[45] Remus Teodorescu, Frede Blaabjerg, Marco Liserre, and P Chiang Loh. Proportional-resonant controllers and filters for grid-connected voltage-source converters. *IEE Proceedings-Electric Power Applications*, 153(5):750–762, 2006.

[46] Yufei Yue, Fujun Ma, An Luo, Qianming Xu, and Longyu Xie. A circulating current suppressing method of mmc based statcom for negative-sequence compensation. In *2016 IEEE 8th International Power Electronics and Motion Control Conference (IPEMC-ECCE Asia)*, pages 3566–3572. IEEE, 2016.

[47] Aaron S Jackson, Adrian Bulat, Vasileios Argyriou, and Georgios Tzimiropoulos. Large pose 3d face reconstruction from a single image via direct volumetric cnn regression. In *Proceedings of the IEEE International Conference on Computer Vision*, pages 1031–1039, 2017.

[48] Adrian Rosebrock. Eye blink detection with opencv, python, and dlib, 2017.

[49] Shai Shalev-Shwartz, Shaked Shammah, and Amnon Shashua. Safe, multi-agent, reinforcement learning for autonomous driving. *arXiv preprint arXiv:1610.03295*, 2016.

[50] Ürün Dogan, Johann Edelbrunner, and Ioannis Iossifidis. Autonomous driving: A comparison of machine learning techniques by means of the prediction of lane change behavior. In *2011 IEEE International Conference on Robotics and Biomimetics*, pages 1837–1843. IEEE, 2011.

[51] Igor Mordatch and Pieter Abbeel. Emergence of grounded compositional language in multi-agent populations. *arXiv preprint arXiv:1703.04908*, 2017.

[52] Christopher D Manning, Mihai Surdeanu, John Bauer, Jenny Rose Finkel, Steven Bethard, and David McClosky. The stanford corenlp natural language processing toolkit. In *Proceedings of 52nd annual meeting of the association for computational linguistics: system demonstrations*, pages 55–60, 2014.

[53] Rich Caruana and Alexandru Niculescu-Mizil. An empirical comparison of supervised learning algorithms. In *Proceedings of the 23rd international conference on Machine learning*, pages 161–168, 2006.

[54] Horace B Barlow. Unsupervised learning. *Neural computation*, 1(3):295–311, 1989.

[55] Richard S Sutton, Andrew G Barto, et al. *Introduction to reinforcement learning*, volume 135. MIT press Cambridge, 1998.

[56] T. Tanaka, K. Ma, H. Wang, and F. Blaabjerg. Asymmetrical reactive power capability of modular multilevel cascade converter based statcoms for offshore wind farm. *IEEE Transactions on Power Electronics*, 34(6):5147–5164, 2019.

[57] Takaaki Tanaka. *Control and Optimization of Modular Multilevel Cascaded Statcom Converters for Offshore Wind Application*. PhD thesis, Aalborg Universitetsforlag, 2018.

[58] Math HJ Bollen. Understanding power quality problems. In *Voltage sags and Interruptions*. IEEE press, 2000.

[59] Suman Debnath, Jiangchao Qin, Behrooz Bahrani, Maryam Saeedifard, and Peter Barbosa. Operation, control, and applications of the modular multilevel converter: A review. *IEEE transactions on power electronics*, 30(1):37–53, 2014.

[60] Heejin Kim, Sangmin Kim, Yong-Ho Chung, Dong-Wook Yoo, Chan-Ki Kim, and Kyeon Hur. Operating region of modular multilevel converter for hvdc with controlled second-order harmonic circulating current: Elaborating pq capability. *IEEE Transactions on Power Delivery*, 31(2):493–502, 2015.

[61] Gilbert Bergna, Erik Berne, Philippe Egrot, Pierre Lefranc, Amir Arzande, Jean-Claude Vannier, and Marta Molinas. An energy-based controller for hvdc modular multilevel converter in decoupled double synchronous reference frame for voltage oscillation reduction. *IEEE Transactions on Industrial Electronics*, 60(6):2360–2371, 2012.

[62] Michaël MC Merlin and Tim C Green. Cell capacitor sizing in multilevel converters: cases of the modular multilevel converter and alternate arm converter. *IET Power Electronics*, 8(3):350–360, 2014.

[63] Sixing Du, Apparao Dekka, Bin Wu, and Navid Zargari. *Modular multilevel converters: analysis, control, and applications*. John Wiley & Sons, 2017.

[64] P. Guo, Z. He, Y. Yue, Q. Xu, X. Huang, Y. Chen, and A. Luo. A novel two-stage model predictive control for modular multilevel converter with reduced computation. *IEEE Transactions on Industrial Electronics*, 66(3):2410–2422, 2019.

[65] D. Zhou, P. Tu, H. Qiu, and Y. Tang. Finite-control-set model predictive control of modular multilevel converters with cascaded open-circuit fault ride-through. *IEEE Journal of Emerging and Selected Topics in Power Electronics*, 8(3):2943–2953, 2020.

[66] L. Harnefors, A. Antonopoulos, K. Ilves, and H. Nee. Global asymptotic stability of current-controlled modular multilevel converters. *IEEE Transactions on Power Electronics*, 30(1):249–258, 2015.

[67] K. Ilves, L. Harnefors, S. Norrga, and H. Nee. Predictive sorting algorithm for modular multilevel converters minimizing the spread in the submodule capacitor voltages. *IEEE Transactions on Power Electronics*, 30(1):440–449, 2015.

[68] N. Ahmed, L. Ängquist, S. Norrga, A. Antonopoulos, L. Harnefors, and H. Nee. A computationally efficient continuous model for the modular multilevel converter. *IEEE Journal of Emerging and Selected Topics in Power Electronics*, 2(4):1139–1148, 2014.

[69] K. Jacobs, D. Johannesson, S. Norrga, and H. Nee. Mmc converter cells employing ultrahigh-voltage sic bipolar power semiconductors. In *2017 19th European Conference on Power Electronics and Applications (EPE'17 ECCE Europe)*, pages P.1–P.10, 2017.

[70] P. Cortes, J. Rodriguez, C. Silva, and A. Flores. Delay compensation in model predictive current control of a three-phase inverter. *IEEE Transactions on Industrial Electronics*, 59(2):1323–1325, 2012.

[71] Jiangchao Qin and Maryam Saeedifard. Predictive control of a three-phase dc-ac modular multilevel converter. In *2012 IEEE Energy Conversion Congress and Exposition (ECCE)*, pages 3500–3505. IEEE, 2012.

Part II

Papers

MDPI

Article

New Modeling and Mitigation Control of Submodule-Capacitor Voltage Ripple of Modular Multilevel Converter Under Unbalanced Grid Conditions

Songda Wang, Danyang Bao *, Gustavo Gontijo, Sanjay K Chaudhary and Remus Teodorescu

Department of Energy Technology, Aalborg University, 9220 Aalborg East, Denmark; skc@et.aau.dk (S.C.); ret@et.aau.dk (R.T.)

* Correspondence: baodanyang@szpt.edu.cn (D. B)

Version October 17, 2020 submitted to Journal Not Specified

Abstract: The modular multilevel converter needs to deal with a voltage ripple in its submodule capacitors under normal grid conditions. In order for the converter to operate in a safe and reliable fashion, the submodule-capacitor capacitance must be designed in such a way as to maintain the voltage ripple within a pre-defined range (usually $\pm 10\%$ of the nominal capacitor voltage). However, under unbalanced grid conditions, the submodule-capacitor voltage ripple increases. Depending on the imbalance level, the voltage ripple can be considerably high and it can exceed the pre-defined safe limits. If this occurs, the converter will trip, in order to protect its semiconductor devices, which can lead to serious stability problems for the electrical grid. Circulating currents correspond to a degree of freedom of the modular multilevel converter as they can be used to compensate for the submodule-capacitor ripple without affecting the output-current control. However, in order to properly compensate the voltage ripple under unbalanced grid conditions, an specific circulating-current profile needs to be injected. The definition of such profile might not be an easy task. In this paper, a new modeling of the modular multilevel converter submodule-capacitor voltage ripple under unbalanced grid conditions is proposed. This modeling is based on the symmetrical components and it allows for a very clear understanding of the submodule-capacitor-voltage-ripple behavior under unbalanced grid conditions. This way, the proper circulating-current profile to be injected can be obtained, allowing for the right compensation of the voltage ripple. Based on this approach, two new voltage-ripple compensation methods are proposed in this paper. Simulations are carried out to validate the analytical description of the submodule-capacitor voltage ripple proposed in this paper. Moreover, simulation and experimental results are provided to validate the new compensation techniques introduced in this paper.

Keywords: Modular multilevel converter, submodule-capacitor voltage ripple, unbalanced grid conditions.

1. Introduction

The modular multilevel converter (MMC), illustrated in Figure 1, is the standard power-electronic solution for high-power applications such as the high-voltage direct-current (HVDC) transmission systems that operate as voltage sources [1], [2]. This is because the MMC can reach high voltage levels, due to its modularity and scalability [3], [4], with high flexibility, efficiency, reliability and power quality [5], [6]. Nonetheless, the MMC presents a high number of components including semiconductor devices and submodule capacitors. These submodule capacitors are quite bulky and heavy since

they need to be designed with a considerably high capacitance, in such a way as to maintain the submodule-capacitor voltage ripple within safe limits. In other words, as a natural consequence of the MMC topology and operation, a voltage ripple exists in the submodule capacitor under normal operation conditions [7]. Different grid phenomenon such as faults and imbalance will affect the profile and the amplitude of the submodule-capacitor voltage ripple and some dangerous situations can eventually occur. This way, it is important to analyze the MMC submodule-capacitor voltage ripple under different grid conditions.

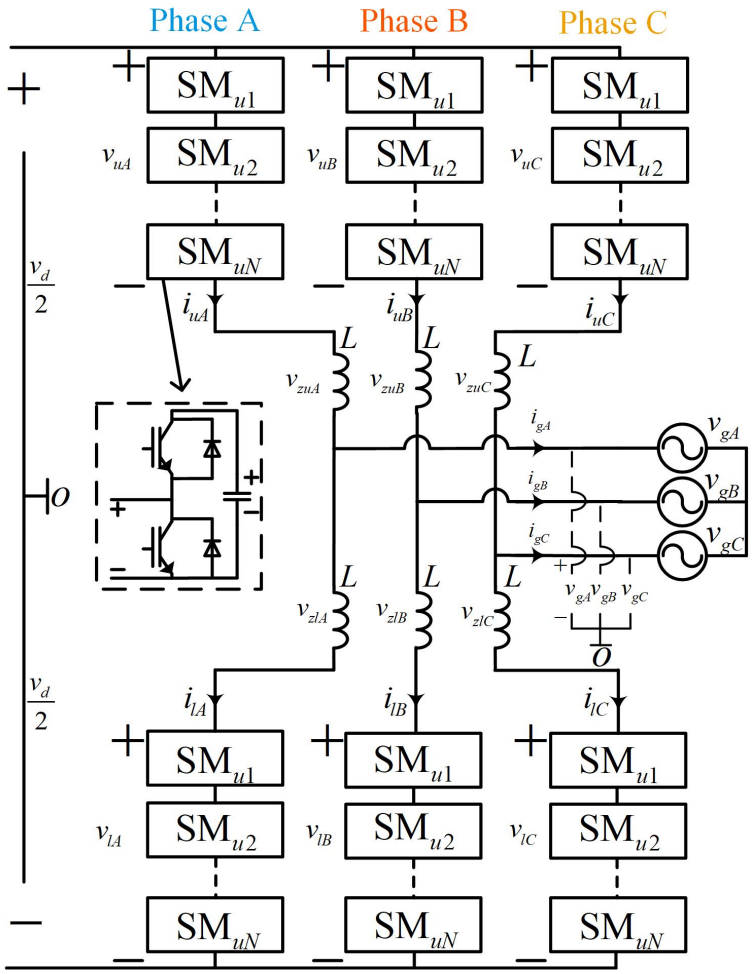

Figure 1. MMC topology diagram

Under balanced grid conditions, the current that flows through the MMC arms is composed of an AC term with the positive-sequence component of the grid fundamental frequency and of a DC term related to the MMC DC-link current [8]. The interaction of the mentioned arm current and the MMC arm insertion index results in a submodule-capacitor voltage ripple composed of the positive-sequence component of the grid fundamental frequency as well as of the the negative-sequence component of double fundamental frequency [9]. Under unbalanced grid conditions, however, the AC currents flowing through the MMC arms will be different. As illustrated in Figure 1, the MMC positive and negative DC terminals form neutral points for the converter phases, which are represented by the converter arms. Thus, under unbalanced grid conditions, AC currents with the negative-sequence component of the grid fundamental frequency will flow through the MMC arms. Depending on the converter transformer connection, or if it is a transformer-less connection, AC currents with the zero-sequence component of the grid fundamental frequency will also flow through the MMC arms [10], [11]. The zero-sequence currents flowing through each phase of the MMC (each arm) do not

sum to zero in the neutral points corresponding to the positive and negative DC terminals of the converter. Thus, the zero-sequence currents will flow towards the MMC DC link producing a DC-side voltage ripple that could be harmful for the converter. In [10] and [11], control methods are proposed to compensate for the MMC DC-link ripple under unbalanced grid conditions. Another consequence of the MMC operation under unbalanced grid conditions is the appearance of extra circulating-current components that will increase the converter conduction losses if they are not properly suppressed. In [12], [13] and [14], detailed analytical models are proposed to describe the MMC circulating currents under unbalanced grid conditions. Moreover, control techniques are proposed to mitigate these extra undesired circulating-current components. Finally, another consequence of the MMC operation under unbalanced grid conditions is the increase of the submodule-capacitor voltage ripple. In other words, even if all the undesired circulating currents are properly compensated and if there are no paths for zero-sequence components to flow through, under unbalanced grid conditions, a negative-sequence current component with the fundamental frequency will flow through the MMC arms, in addition to the positive-sequence component with the fundamental frequency and the DC component. This extra component will increase the submodule-capacitor charging current, increasing the voltage ripple as well, and eventually leading to dangerous situations for the converter. Many different problems can occur due to the increased submodule-capacitor voltage ripple under unbalanced grid conditions. If the imbalance level of the grid voltage is high, a considerably high submodule-capacitor voltage ripple can occur, which could exceed the safe voltage limits of the submodule semiconductor devices [15]. In a MMC-based HVDC transmission system, when a submodule overvoltage occurs, the converter station will shut down in order to avoid the destruction of its semiconductor devices. The tripping of a HVDC transmission system can result in many serious stability issues in the power system and, thus, this situation should be avoided. Even if the increased voltage ripple does not exceed the converter tripping limits, it will slowly deteriorate the submodule capacitors due to the overvoltage vaporization phenomenon [16], affecting their life spam. Moreover, the deterioration of the submodule capacitors will lead to the reduction of their original capacitance (which was designed to maintain the voltage ripple within a pre-defined range). The reduction of the submodule-capacitor capacitance will lead to an increased voltage ripple that might exceed the breakdown voltage of such capacitors resulting in an internal short circuit. Since the MMC submodule is built with a set of many series-connected capacitors, if one of these capacitors is damaged, the remaining capacitors in the string will have to withstand a higher voltage and, thus, a cascade failure might occur with them if their breakdown voltages are exceeded. The MMC submodule-capacitor voltage ripple must be properly compensated in order to avoid the mentioned problems under unbalanced grid conditions.

Many papers in the literature propose analytical descriptions and compensation methods for the MMC submodule-capacitor voltage ripple under balanced grid conditions. In [17], a mathematical description of the MMC arm power is introduced. Based on this arm-power model, the submodule-capacitor voltage ripple is described in [18]. One strategy to reduce the submodule-capacitor ripple is by injecting specific AC circulating-current components as proposed in [19] and [20]. The circulating current is an internal variable of the converter that can be used to suppress the submodule-capacitor voltage ripple without affecting the MMC external variables such as the output current. Of course, it is a tradeoff between limiting the circulating currents, to reduce conduction losses, and limiting the submodule-capacitor voltage ripple by injecting circulating currents. However, a clear and accurate description of the MMC submodule-capacitor voltage ripple allows for the analytical derivation of specific circulating-current terms to be injected in order to mitigate the voltage ripple. The other undesired circulating-current components can still be suppressed. Thus, the first contribution of this paper is the introduction of a new analytical description of the MMC submodule-capacitor voltage ripple under unbalanced grid conditions. This new approach is based on the symmetrical components and it allows for a clear comprehension of the MMC submodule-capacitor voltage behavior under unbalanced grid conditions. Through the proposed equations, it becomes clear that, under unbalanced grid conditions, some extra terms appear in the submodule-capacitor voltage

ripple such as the positive-sequence and zero-sequence components with double the fundamental frequency and the negative-sequence component with the fundamental frequency. Based on this accurate description of the submodule-capacitor voltage ripple, two compensation techniques based on the circulating-current injection are proposed in this paper as new contributions.

Some papers in the literature present different approaches to compensate for the MMC submodule-capacitor voltage ripple under unbalanced grid conditions. In [21], a compensation technique is proposed, which is based on the offset pulsewidth modulation (OPWM) and in the zero-sequence voltage injection. In [22], a compensation strategy is proposed, which is similar to the approach used in the present paper (based on circulating-current injection). However, in [22], the authors define the circulating-current term to be injected based on the the MMC-arm power. In this approach, the zero-sequence component with double the fundamental frequency that appears in the submodule-capacitor ripple is not evident and, thus, it is not compensated. In other words, the detailed and accurate analytical description of the submodule-capacitor voltage ripple, proposed in the present paper, allows for a more clear comprehension of such ripple, which results in an enhanced and more accurate compensation of it, through the circulating-current injection method. In this paper, a comprehensive analytical model of capacitor-voltage ripple is proposed. This model describes the relationship between the unbalanced grid voltages/currents and the MMC circulating currents. According to the proposed model, under unbalanced grid conditions, an extra zero-sequence component appears in the submodule-capacitor voltage ripple and the positive-sequence and negative-sequence components of the ripple are unbalanced among the three phase of the MMC. The submodule-capacitor voltage ripple can be predicted precisely through the proposed model and, thus, based on this model, two voltage-balancing methods are proposed to reduce and balance the submodule-capacitor voltage ripple under unbalanced grid conditions. Simulation and experimental results are presented to verify the effectiveness of the proposed methods.

2. Analytical description of submodule-capacitor voltage under unbalanced grid conditions

In this section, an new analytical description of the MMC submodule-capacitor voltage under unbalanced grid conditions is proposed. The proposed equations are an extension of the analytical method presented in [18]. In Figure 1, the basic topology of the three-phase MMC analyzed in this paper is illustrated. This converter is composed of three legs, in which each of these legs are composed of one upper arm and one lower arm. Each arm is composed of one string of N half-bridge (HB) submodules connected in series and one arm inductor. The arm inductor is modeled by an inductance (L) in combination with a resistance (R). Through the symmetrical components theory, an unbalanced voltage can be represented by the combination of a positive-sequence component, a negative-sequence component and a zero-sequence component. The zero-sequence component can be neglected in a three-phase system with its neutral point not grounded [23], which is the assumption made in this paper. Thus, the grid voltage (v_{gk}) can be described as follows:

$$v_{gk} = \widehat{V}_{+1}\cos(\omega t - \frac{2}{3}k\pi) + \widehat{V}_{-1}\cos(\omega t - \frac{4}{3}k\pi) \tag{1}$$

In which ω is the grid fundamental frequency, $\widehat{V}_{+1}$ and $\widehat{V}_{-1}$ are the amplitudes of the positive-sequence and negative-sequence components of the grid voltage, respectively, k means phase number (0 for A, 1 for B, 2 for C). Similarly, the grid current can be described as follows:

$$i_{gk} = \widehat{I}_{+1}\cos(\omega t - \frac{2}{3}k\pi + \varphi) + \widehat{I}_{-1}\cos(\omega t - \frac{4}{3}k\pi + \varphi) \tag{2}$$

The MMC upper and lower arm voltages (v_{uk} and v_{lk}, respectively) can be defined as follows by applying Kirchhoff's law to the circuit shown in Fig.1:

$$\begin{bmatrix} v_{uk} \\ v_{lk} \end{bmatrix} = \begin{bmatrix} \frac{1}{2}v_d - v_{gk} - v_{zuk} \\ \frac{1}{2}v_d + v_{gk} - v_{zlk} \end{bmatrix} \tag{3}$$

In which v_d is the MMC DC-link voltage, and v_{zuk} and v_{zlk} are the voltage drops across the upper-arm and lower-arm impedances, respectively. The upper-arm and lower-arm currents (i_{uk} and i_{lk}, respectively) are defined as follows:

$$\begin{bmatrix} i_{uk} \\ i_{lk} \end{bmatrix} = \begin{bmatrix} i_{ck} + \frac{1}{2} i_{gk} \\ i_{ck} - \frac{1}{2} i_{gk} \end{bmatrix} \tag{4}$$

In which i_{ck} is the MMC internal circulating current. In this paper, the undesired AC components of the circulating current are considered to be completely suppressed through a proper control technique and, thus, the circulating current is assumed to be a purely DC signal ($i_{ck} = I_{cDCk}$). The MMC upper-arm and lower-arm power (p_{uk} and p_{lk}, respectively) can be calculated as follows:

$$\begin{bmatrix} p_{uk} \\ p_{lk} \end{bmatrix} = \begin{bmatrix} v_{uk} \cdot i_{uk} \\ v_{lk} \cdot i_{lk} \end{bmatrix} \tag{5}$$

In order to facilitate the analytical equations derivation, the sum and delta power terms ($P_{\Sigma k}$ and $P_{\Delta k}$, respectively) are defined as follows:

$$\begin{bmatrix} P_{\Sigma k} \\ P_{\Delta k} \end{bmatrix} = \begin{bmatrix} p_{uk} + p_{lk} \\ p_{uk} - p_{lk} \end{bmatrix} \tag{6}$$

By substituting (1), (2), (3), (4) and (5) into (6), the following two equations are obtained:

$$\begin{aligned} P_{\Sigma k} = i_{ck} v_d - \frac{1}{2}\widehat{V}_{+1}\widehat{I}_{+1}\cos\varphi - \frac{1}{2}\widehat{V}_{+1}\widehat{I}_{-1}\cos\varphi - \frac{1}{2}\widehat{V}_{-1}\widehat{I}_{+1}\cos\varphi - \frac{1}{2}\widehat{V}_{-1}\widehat{I}_{-1}\cos\varphi - \\ \frac{1}{2}\widehat{V}_{+1}\widehat{I}_{+1}\cos(2\omega t + \theta_{vk-} + \varphi) - \frac{1}{2}\cos\widehat{V}_{-1}\widehat{I}_{-1}(2\omega t + \theta_{vk+} - \varphi) - \\ \frac{1}{2}\widehat{V}_{+1}\widehat{I}_{-1}\cos(2\omega t - \varphi) - \frac{1}{2}\widehat{V}_{-1}\widehat{I}_{+1}\cos(2\omega t + \varphi) \end{aligned} \tag{7}$$

And

$$\begin{aligned} P_{\Delta k} = \frac{1}{2} v_d \widehat{I}_{+1}\cos(\omega t + \theta_{vk+} + \varphi) + \frac{1}{2} v_d \widehat{I}_{-1}\cos(\omega t + \theta_{vk-} - \varphi) - \\ 2\widehat{V}_{+1} I_{cDCk}\cos(\omega t + \theta_{vk+}) - 2\widehat{V}_{-1} I_{cDCk}\cos(\omega t + \theta_{vk-}) \end{aligned} \tag{8}$$

It is important to notice that since the grid voltage is unbalanced and the MMC DC-link voltage is constant, then the DC component of the circulating current is different for each phase (each arm). In other words, the DC component of the circulating current of each phase should be calculated as follows:

$$I_{cDCk} = \frac{P_{gk}}{v_d} \tag{9}$$

In which P_{gk} is the average value of the instantaneous grid power (p_{gk}) for three phases. By integrating the sum and delta power (described in (7) and (8), respectively), the sum and delta energy ($W_{\Sigma k}$ and $W_{\Delta k}$, respectively) are obtained as follows:

$$W_{\Sigma k} = W_{\Sigma kDC} - \underbrace{\frac{\widehat{V}_{+1}\widehat{I}_{+1}\sin(2\omega t + \theta_{vk-} + \varphi)}{4\omega} - \frac{\widehat{V}_{-1}\widehat{I}_{+1}\sin(2\omega t + \varphi)}{4\omega}}_{\Delta W_{\Sigma k}(1)} - \underbrace{\frac{\widehat{V}_{+1}\widehat{I}_{-1}\sin(2\omega t - \varphi)}{4\omega} - \frac{\widehat{V}_{-1}\widehat{I}_{-1}\sin(2\omega t + \theta_{vk+} - \varphi)}{4\omega}}_{\Delta W_{\Sigma k}(2)} \tag{10}$$

And

$$W_{\Delta k} = W_{\Delta kDC} + \underbrace{\frac{v_d\widehat{I}_{+1}\sin(\omega t + \theta_{vk+} - \varphi)}{2\omega} + \frac{v_d\widehat{I}_{-1}\sin(\omega t + \theta_{vk-} - \varphi)}{2\omega}]}_{\Delta W_{\Delta k}(1)} - \underbrace{\frac{2V_{+1}I_{cDCk}\sin(\omega t + \theta_{vk+})}{\omega} - \frac{2\widehat{V}_{-1}I_{cDCk}\sin(\omega t + \theta_{vk-})}{\omega}}_{\Delta W_{\Delta k}(2)} \tag{11}$$

The sum energy consists in two terms: the sum DC energy ($W_{\Sigma kDC}$) and the sum AC energy. The sum AC energy is also composed of two terms: ($\Delta W_{\Sigma k} = \Delta W_{\Sigma k}(1) + \Delta W_{\Sigma k}(2)$). Similarly, the delta energy is composed of two terms: delta DC energy ($W_{\Delta k}$) and delta AC energy ($\Delta W_{\Delta k} = \Delta W_{\Delta k}(1) + \Delta W_{\Delta k}(2)$). Similarly to (6), the sum energy and delta energy (W_{uk} and W_{lk}, respectively) can be defined as follows as functions of the upper-arm energy and lower-arm energy:

$$\begin{bmatrix} W_{\Sigma k} \\ W_{\Delta k} \end{bmatrix} = \begin{bmatrix} W_{uk} + W_{lk} \\ W_{uk} - W_{lk} \end{bmatrix} \tag{12}$$

The energy stored in the MMC capacitors can be calculated as follows:

$$W^i_{cu,lk} = \frac{C}{2}(v^i_{cu,lk})^2 \tag{13}$$

In which C is the submodule-capacitor capacitance, $v_{cu,lk}$ is the capacitor voltage and $i = 1, 2, ..., N$ represents the submodule number in the MMC arm. In this paper, an average model is considered [18] in which all the capacitors in each MMC arm are represented by an equivalent capacitor with capacitance equal to $\frac{C}{N}$ and with voltage equal to the sum of each voltage in each submodule capacitor ($v^{\Sigma}_{cu,lk}$). It means that the upper-arm and lower-arm energies are equal to the energy in this equivalent capacitor. In other words:

$$W_{u,lk} = \frac{C}{2N}(v^{\Sigma}_{cu,lk})^2 \tag{14}$$

According to (14), the voltage in the equivalent capacitor can be calculated as follows:

$$v^{\Sigma}_{cu,lk} = \sqrt{\frac{2N}{C}W_{u,lk}} \tag{15}$$

As explained in [18], by calculating the upper-arm energy (W_{uk}) and lower-arm energy (W_{lk}), through (10), (11) and (12), and by substituting these terms into (15), the following equations are obtained after some approximations:

$$v^{\Sigma}_{cuk} \approx v_d + \frac{N}{2CV_d}(\Delta W_{\Sigma k} + \Delta W_{\Delta k}) \tag{16}$$

And

$$v_{clk}^{\Sigma} \approx v_d + \frac{N}{2CV_d}(\Delta W_{\Sigma k} - \Delta W_{\Delta k}) \tag{17}$$

Equations (16) and (17) are composed of a DC term and of an AC term. The DC term corresponds to the average voltage value in the equivalent capacitor, whereas the AC term corresponds to the ripple in the equivalent capacitor. The two AC terms in (16) and (17) are defined as follows:

$$v_{ck(\Delta W_{\Sigma})}^{\Sigma} = \frac{N}{2CV_d}\Delta W_{\Sigma k} \tag{18}$$

And

$$v_{ck(\Delta W_{\Delta})}^{\Sigma} = \frac{N}{2CV_d}\Delta W_{\Delta k} \tag{19}$$

By substituting the terms of (10) and (11) into (18) and (19) the following is obtained:

$$\begin{aligned} v_{ck(\Delta W_{\Sigma})}^{\Sigma} = \frac{N}{2CV_d}\Bigg[& \underbrace{-\frac{\widehat{V}_{+1}\widehat{I}_{+1}\sin(2\omega t + \theta_{vk-} + \varphi)}{4\omega}}_{Negative-sequence\ component} \underbrace{-\frac{\widehat{V}_{-1}\widehat{I}_{-1}\sin(2\omega t + \theta_{vk+} - \varphi)}{4\omega}}_{Positive-sequence\ component}\Bigg] \\ + \frac{N}{2CV_d}\Bigg[& \underbrace{-\frac{\widehat{V}_{+1}\widehat{I}_{-1}\sin(2\omega t - \varphi)}{4\omega} - \frac{\widehat{V}_{-1}\widehat{I}_{+1}\sin(2\omega t + \varphi)}{4\omega}}_{Zero-sequence\ component}\Bigg] \end{aligned} \tag{20}$$

And

$$\begin{aligned} v_{ck(\Delta W_{\Delta})}^{\Sigma} = \frac{N}{2CV_d}\Bigg[& \underbrace{\frac{1}{2\omega}V_d\widehat{I}_{+1}\sin(\omega t + \theta_{vk+} - \varphi)}_{Positive-sequence\ component} + \underbrace{\frac{1}{2\omega}V_d\widehat{I}_{-1}\sin(\omega t + \theta_{vk-} - \varphi)}_{Negative-sequence\ component}\Bigg] \\ + \frac{N}{2CV_d}\Bigg[& \underbrace{-\frac{2}{\omega}\widehat{V}_{+1}i_{cDCk}\sin(\omega t + \theta_{vk+})}_{Delta\ ripple\ part\ 1} \underbrace{-\frac{2}{\omega}\widehat{V}_{-1}i_{cDCk}\sin(\omega t + \theta_{vk-})}_{Delta\ ripple\ part\ 2}\Bigg] \end{aligned} \tag{21}$$

In this paper, it is considered that the MMC output current is controlled in such a way as to be composed of only positive-sequence component even during the unbalanced grid conditions. In other words, the negative-sequence component is compensated ($\widehat{I}_{-1} = 0$) through a control action. Thus, some terms of (20) and (21) are eliminated resulting in the following two equations:

$$v_{ck(\Delta W_{\Sigma})}^{\Sigma} = \frac{N}{2CV_d}\Bigg[\underbrace{-\frac{\widehat{V}_{+1}\widehat{I}_{+1}\sin(2\omega t + \theta_{vk-} + \varphi)}{4\omega}}_{Negative-sequence\ component} \underbrace{-\frac{\widehat{V}_{-1}\widehat{I}_{+1}\sin(2\omega t + \varphi)}{4\omega}}_{Zero-sequence\ component}\Bigg] \tag{22}$$

And

$$v^{\Sigma}_{ck(\Delta W_{\Delta})} = \frac{N}{2CV_d}\left[\underbrace{\frac{1}{2\omega}V_d\widehat{I}_{+1}\sin(\omega t+\theta_{vk+}-\varphi)}_{Positive-sequence\ component}\right] + \frac{N}{2CV_d}\left[\underbrace{-\frac{2}{\omega}\widehat{V}_{+1}I_{cDCk}\sin(\omega t+\theta_{vk+})}_{Delta\ ripple\ 1}\underbrace{-\frac{2}{\omega}\widehat{V}_{-1}I_{cDCk}\sin(\omega t+\theta_{vk-})}_{Delta\ ripple\ 2}\right] \quad (23)$$

In other words, even if all the control actions are taken to compensate for the negative-sequence grid voltage and to suppress all the undesired AC components of the converter circulating current, still the submodule-capacitor ripple will be composed of the terms described in (22) and (23). There are two additional ripple terms, in comparison to the balanced grid case, which are caused by the negative-sequence grid voltage ($\widehat{V}_{-1}$). In other words, under balanced grid conditions, the MMC submodule-capacitor voltage ripple would be identical to the one described by (22) and (23) if the two terms containing $\widehat{V}_{-1}$ were removed. The ripple behavior under balanced grid conditions is demonstrated in [18]. The MMC submodule-capacitor voltage ripple under unbalanced grid conditions (described through equations (22) and (23)) is illustrated in Figure 2.

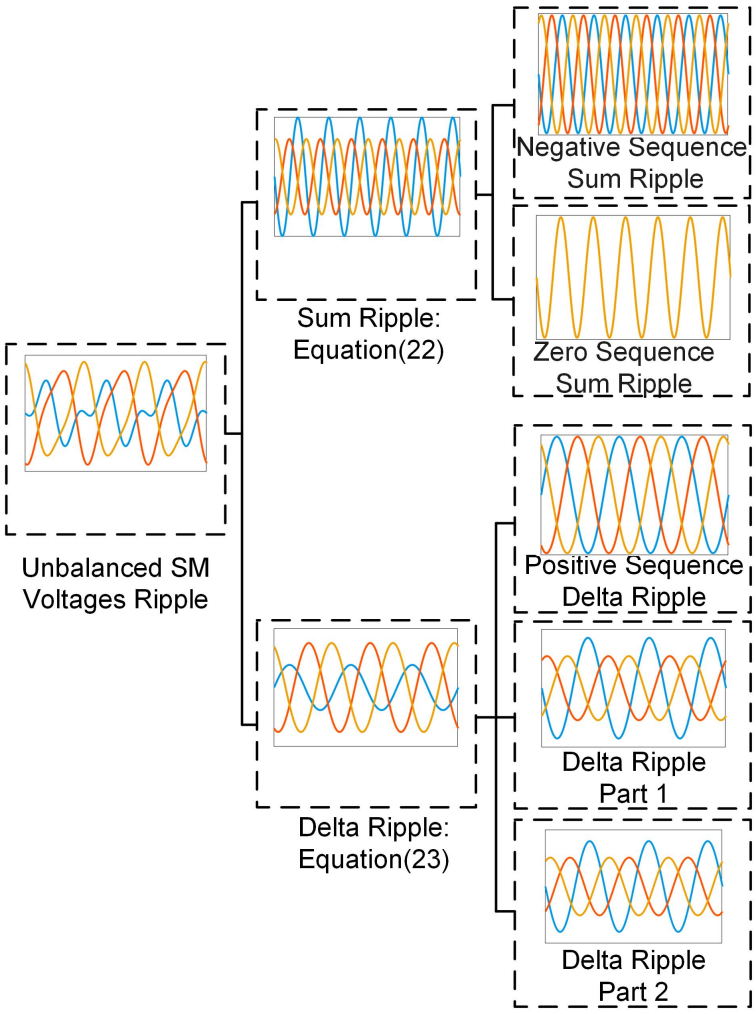

Figure 2. Illustration of MMC submodule-capacitor voltage-ripple components under unbalanced grid conditions.

Table 1. MMC Parameters

	Simulation	Experiment
Submodule number in one arm(N)	100	4
DC line voltage	200 kV	200 V
Active power	150 MW	1 kW
Submodule capacitance (C)	3.75 mF	2000 uF
Submodule capacitor voltage (Vc)	2 kV	50 V
AC system frequency	50 Hz	50 Hz
Inductance in the arm	50.9 mH	10 mH
Sampling frequency	10k Hz	10k Hz
Amplitude of the grid	100 kV	83 V

In order to validate the analytical equations proposed in this paper, a simulation is carried out through the software Simulink/Matlab. In this simulation, the MMC is modeled according to Figure 1. In order to calculate the equations obtained in this paper, the block diagram illustrated in Figure 3 was also implemented in Simulink/Matlab. The MMC parameters used in both simulations are the ones described in Table 1.

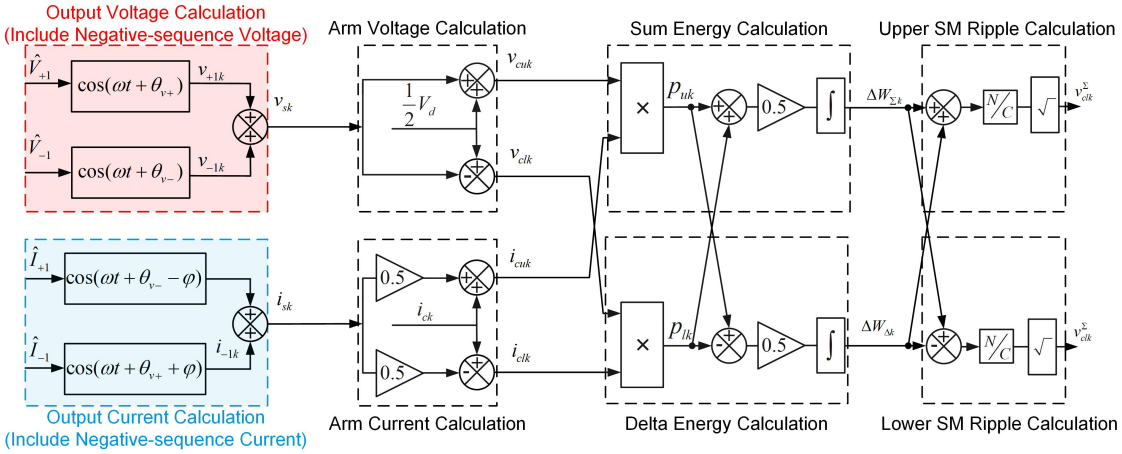

Figure 3. Block diagram of submodule-capacitor voltage analytical derivation.

The results obtained in the simulations with the real system (illustrated in Figure 1) and with the proposed analytical method (represented by the block diagram shown in Figure 3) are depicted in Figure 4. By analyzing this figure, it becomes clear that the analytical description of the MMC submodule-capacitor voltage under unbalanced grid conditions is very precise, as the simulation results match with high accuracy.

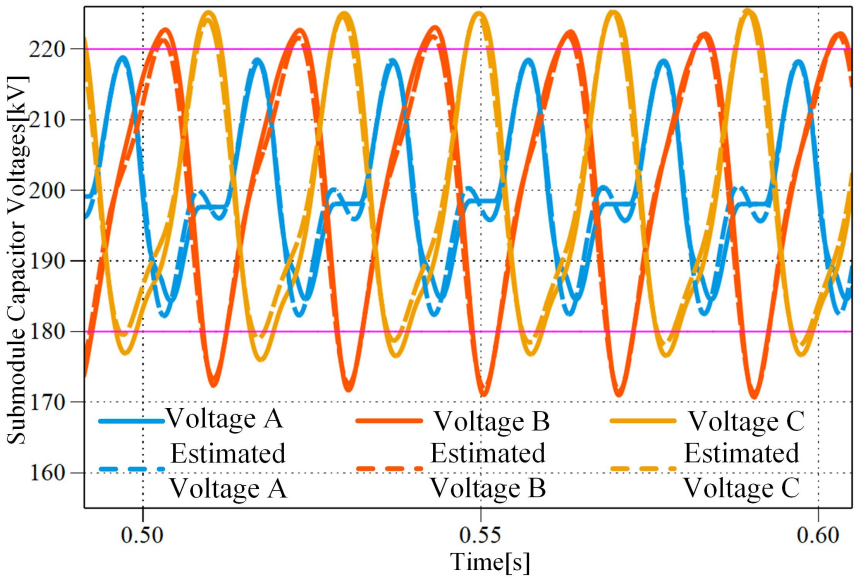

Figure 4. Estimated submodule capacitor voltages and the simulated submodule capacitor voltages

3. Submodule capacitor voltage ripple reduction methods

After the derivation of submodule-capacitor voltage equations in Section 2, in this section, the submodule-capacitor voltage-ripple-reduction methods based on the derived equations will be proposed. From equation (22) and (23), we can conclude that the following variables affect the submodule-capacitor voltage: positive-sequence grid voltage ($\widehat{V}_{+1}$), negative-sequence grid voltage ($\widehat{V}_{-1}$), positive-sequence output current ($\widehat{I}_{+1}$), DC voltage (V_d), and DC component of circulating current (I_{cDCk}). All these variables are imposed by grid codes or cannot be changed. In order to optimize the submodule-capacitor voltage in (22) and (23), a new variable should be selected. Injecting AC circulating current is a suitable choice to reduce the submodule-capacitor voltage. Circulating current is a current that flows internally in the converter as it oly affects the internal behavior of the MMC. Now, the circulating current is defined as containing both DC and AC components as follows:

$$i_{ck} = \frac{i_{uk} + i_{lk}}{2} = i_{cDCk} + i_{cACk} \tag{24}$$

Based on [19], the submodule-capacitor voltage ripple can be reduced by injecting AC circulating currents under balanced grid conditions. However, these methods are only designed for the balanced case, as they disregard the unbalanced grid conditions. In the following subsection, the AC component of the MMC circulating current is also considered to derive the equations of the submodule-capacitor voltages since, in Section 2, the AC component was disregarded as the circulating current was considered to be only composed of the DC component. This way, the proper amplitude of the AC component of the circulating current can be calculated, which is the optimum one required to reduce the submodule-capacitor voltage ripple.

3.1. Submodule Capacitor Voltage Balancing Method A

The definition of circulating current is that it is a current that flows in the same direction through both the MMC upper and lower arms. Thus, the circulating current charges equally the submodule capacitors of the upper and of the lower arm. So, the circulating current only affects the sum capacitor voltage ripple as described in (22). In this paper, the AC circulating current injected for the voltage-ripple compensation is composed of a negative–sequence double-frequency component ($\widehat{I}_{cAC2}$) and of a zero-sequence double-frequency component ($\widehat{I}_{cAC0}$). These circulating-current components

can eliminate the sum capacitor voltage ripple as described below. The first compensation technique proposed in this paper consists in considering the MMC circulating current to be equal to:

$$i_{ck} = I_{cDCk} + \widehat{I}_{cAC2}\cos(2\omega t + \theta_{vk-}) + \widehat{I}_{cAC0}\cos(2\omega t) \tag{25}$$

By substituting (25) into (4) and by repeating the derivation steps of Section 2 the new equation that describes the sum-capacitor term is the following:

$$v^{\Sigma}_{ck(\Delta W_{\Sigma})} = \frac{N}{2CV_d}\left[\underbrace{\frac{V_d\widehat{I}_{cAC2k}\sin(2\omega t + \theta_{vk-})}{2\omega} - \frac{\widehat{V}_{+1}\widehat{I}_{+1}\sin(2\omega t + \theta_{vk-} + \varphi)}{4\omega}}_{Negative-sequence\ sum\ ripple}\right]$$
$$+ \frac{N}{2CV_d}\left[\underbrace{\frac{V_d\widehat{I}_{cAC0k}\sin(2\omega t)}{2\omega} - \frac{\widehat{V}_{-1}\widehat{I}_{+1}\sin(2\omega t + \varphi)}{4\omega}}_{Zero-sequence\ sum\ ripple}\right] \tag{26}$$

The new equation that describes the MMC sum-capacitor voltage is composed of terms that have the same frequency and phase angle and, thus, these terms can cancel each other out if the proper amplitude of the circulating-current components are set. The proper amplitude of the circulating components are the following:

$$\widehat{I}_{cAC2k} = \frac{\widehat{V}_{+1}\widehat{I}_{+1}}{2V_d}, \quad \widehat{I}_{cAC0k} = \frac{\widehat{V}_{-1}\widehat{I}_{+1}}{2V_d} \tag{27}$$

Thus, the reference signal of the AC circulating current to be injected for the submodule-capacitor voltage-ripple compensation is the following:

$$I^{*}_{cACk} = \widehat{I}_{cAC2k}\cos(2\omega t + \theta_{vk-}) + \widehat{I}_{cAC0k}\cos(2\omega t) \tag{28}$$

If the current represented in (28) is injected, then the sum submodule-capacitor voltage ripple ($v^{\Sigma}_{ck(\Delta W_{\Sigma})}$) will be null. This fact can be confirmed by substituting (27) into (26). Since an arbitrary unbalanced grid can be represented by the combination of positive- and negative-sequence components, then this method is an universal approach to reduce capacitor voltage ripple under unbalanced grid conditions. The advantage of this method in relation to the one proposed in [22] is that, in [22], only the negative-sequence double-fundamental component is injected whereas, in this paper, also the zero-sequence component is considered in the injected circulating current. Thus, an improved compensation is obtained. The method proposed in this subsection is illustrated in Figure 5.

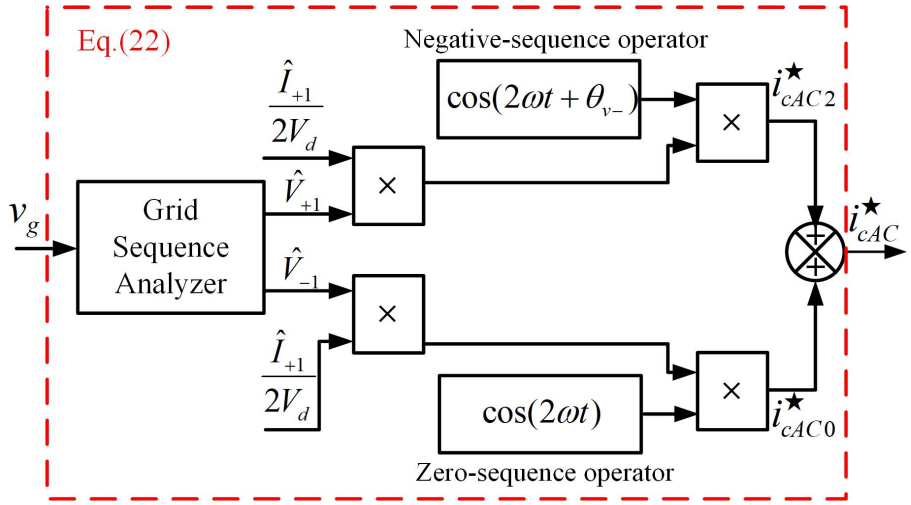

Figure 5. Block diagram of Method A

3.2. Submodule Capacitor Voltage Balancing Method B

As shown in Figure 4, the amplitude of the submodule-capacitor voltage ripple in phases B and C exceed its limit, which is equal to 10% of the submodule-capacitor rated voltage. The submodule-capacitor voltage ripple in phase A is still within the allowed range. That is to say, the submodule capacitors in phase A can still work in a safe fashion without any circulating current injection. In other words, intuitively, there is no need to inject circulating current in phase A to reduce the ripple. Only injecting circulating current in phase B and C is enough to limit the submodule-capacitor voltage ripple within the safe limits. The block diagram of Method B is shown in Figure 6. When the submodule-capacitor voltage ripple of one phase exceeds its limit, then circulating current is injected, only in this phase, in order to limit the voltage ripple. The circulating current to be injected in the one described in (28), which is same as in Method A. If the submodule-capacitor voltage ripple of a given phase does not exceed its limit, no circulating current is injected in this phase.

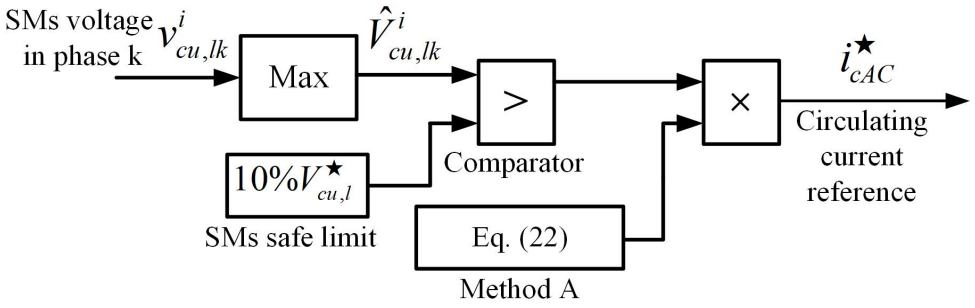

Figure 6. Block diagram of Method B

4. Results

The controller structure of the MMC controller is presented in Figure 7. Two variables of MMC need to be controlled by corresponding controllers: circulating currents need to be suppressed to pure DC and output currents need to be controlled to track the output current reference. Therefore, two independent controllers are needed: the controller of the circulating currents and the controller of output currents. In this paper, the AC circulating currents are injected by method A and method B. So the circulating current controller is also able to track the AC circulating current by the PR controller. What is more, in order to stabilize the energy of the MMC system, energy control will be embedded in the circulating current controller.

Table 2. Submodule Capacitor Voltage Ripple Values of Proposed Methods

	Normal Grid	No Injection	Method A	Method B
Average Ripple	38.37kV	44.96kV	31.65kV	38.09kV
Amplitude A	218.3kV	218.41kV	207.9kV	218.6kV
Amplitude B	218.2kV	222.4kV	219.8kV	219.9kV
Amplitude C	218.3kV	225.3kV	218.9kV	218.5kV
Unbalanced Degree	0.05%	3.08%	5.41%	0.70%

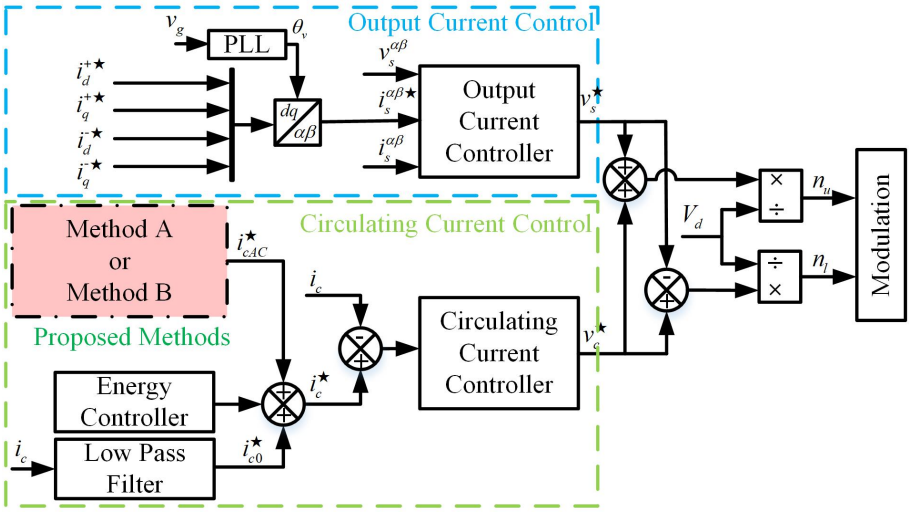

Figure 7. The structure of the proposed MMC controller

4.1. Simulation Results

he simulation of grid-connected MMC system in this paper is carried out to validate the proposed algorithms. The parameters of the simulation model are shown in Table 2. To simplify the simulation model, the average arm model is applied [18]. Fig. 8(a1-a3) present the grid voltages, capacitor voltages, and circulating currents under a balanced grid. A 100kV amplitude three-phase symmetrical voltage is shown in Fig. 8(a1). Fig. 8(a2) presents that the submodule capacitor voltages are also three phase symmetrical and all the capacitor voltages are below the safe limit (10% of the rated submodule capacitor voltage, 220kV). The three-phase circulating currents are suppressed to the pure DC components by circulating currents. Detailed numbers are shown in Table 3.

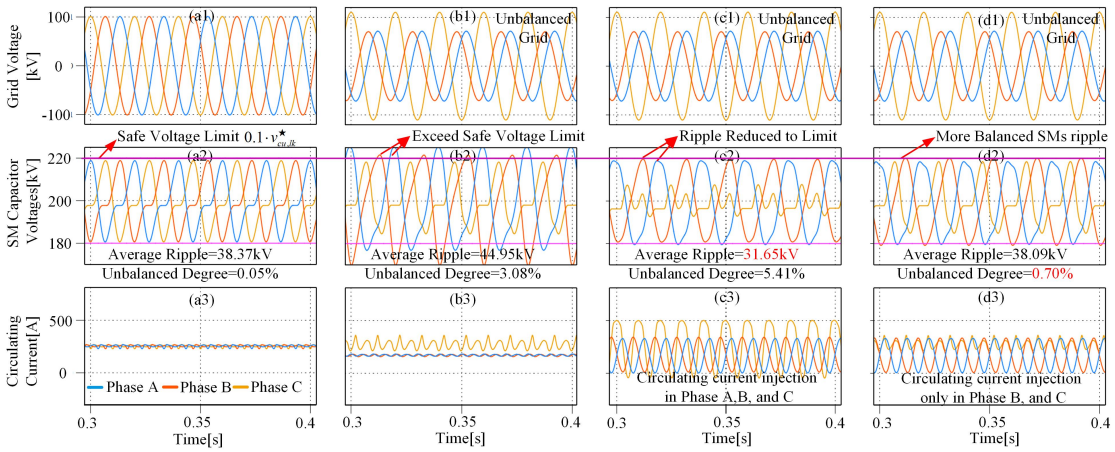

Figure 8. Simulation results, (a) Balanced Grid, (b) Unbalanced grid without circulating current injection, (c) Results of Method A, (d) Results of method B.

Fig. 8(b1-b3) present the simulation results of the grid connected MMC system under an unbalanced grid. The amplitudes of positive-sequence and negative-sequence components are 0.8 $\widehat{V}_s$ and 0.4 $\widehat{V}_s$ respectively. From Fig. 8(b2), capacitor voltages in phase B (222.45kV) and C (225.32kV) are higher than the safe voltage limit (220kV). In this case, those high capacitor voltages will trip the MMC system. A unbalanced degree (UD) of submodule capacitor voltage ripple is defined in (22), the unbalanced degree in this case is 3.08% and the average capacitor voltage ripple is 44.96kV. Also the DC circulating currents are changed by the unbalanced grid as Fig. 8(b3) shows.

$$UD = \frac{max(V_a, V_b, V_c) - min(V_a, V_b, V_c)}{V_{avg}}, \quad V_{avg} = \frac{V_a + V_b + V_c}{3} \tag{29}$$

Fig. 8(c1-c3) shows the simulation results of MMC system under an unbalanced grid when the proposed method A is enabled. The calculated injected circulating currents components are injected to the MMC converter (Fig.8(c3)). Then the capacitor voltages ripple are reduced significantly, especially in phase A as Fig.8(c2) shows. The average submodule capacitor voltage is reduced to 31.65kV which is reduced by 29.6% compared to the case without circulating current injection. The UD here is 5.41%.

Fig. 8(d1-d3) shows the simulation results of MMC system under an unbalanced grid when the proposed method B is enabled. Since capacitor voltage ripple in phase A does not exceed the safe limit, the circulating current in phase A does not need to be injected to reduce the capacitor ripple. Therefore only phase B and C are injected the circulating currents as Fig.8(d3) shows. Then the average capacitor voltage in this case is reduced to 38.09kV and the UD is only 0.7%.

The average submodule capacitor voltages in method A and method B are both reduced compared to the no injection condition. This low average ripple is mainly due to the fact that the ripple of phase A is much reduced. However, the ripple reduction in phase A is meaningless because ripple in phase A never exceeds the safety voltage in the no injection condition. Circulating current in phase will only increase the losses of the MMC system. In this paper, we recommend method B to achieve a more balanced submodule capacitor voltage and lower losses.

4.2. Experimental Results

To evaluate the performance of the proposed ripple reduction methods, the experiment is implemented. The experiment is carried out in a scale-down three-phase grid-connected MMC setup with 4 half-bridge SMs per arm. Table 2 shows the parameters of the experiment setup. The control system is implemented using DS1006 board. The experimental setup works as a three-phase MMC inverter. The level shift carrier modulation method is applied with the sort and select algorithm. In experiment, the switching frequency is 2kHz.

Like the simulation results, the SM capacitor voltage ripple becomes unbalanced which is shown in Fig. 10(b2), the amplitude of SMs voltage ripple in phase B and C is 30.3V. The average ripple is 2.07V. The unbalanced degree here is 1.28%. In Fig. 10(b2), the three phase capacitor voltages have an unstable non-periodic waveform, this is because the energy of three phase under unbalanced grid conditions are not stable during no circulating current injection.

Fig. 10(c2) presents the average SM capacitor ripple is reduced from 2.07V to 1.19V. The amplitude in phase B and C also reduced to a safe level. The unbalanced degree here is 1.11%. The unbalanced SM capacitor voltage ripple is further balanced by Method B. The unbalanced degree decreased to 0.42%.

Since this setup is only for laboratory verification, there are some limits on the experiment results part. First, the experiment SM capacitor voltage ripple is relatively low due to the setup capacitance is high to guarantee the stability of the experimental platform. Second, the DC voltage in the setup is the only 120V, so the DC circulating current is not high enough to see the difference during an unbalanced grid condition.

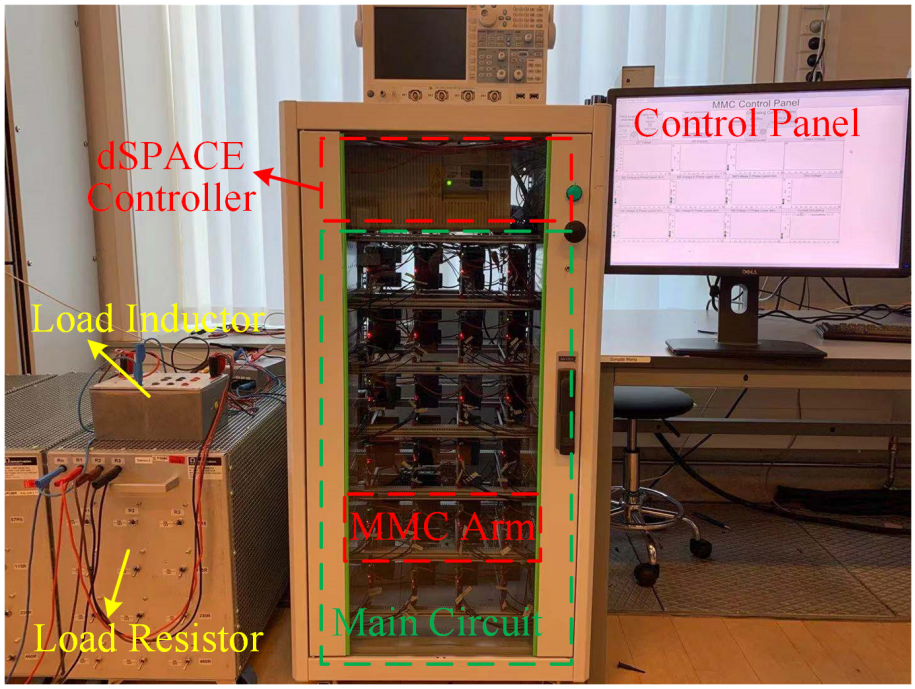

Figure 9. MMC Experimental Setup

Table 3. Submodule Capacitor Voltage Ripple Values of Proposed Methods: Experiment

	Normal Grid	No Injection	Method A	Method B
Average Ripple	1.58V	2.07V	1.19V	1.48V
Amplitude A	30.92V	30.90V	30.55V	30.95V
Amplitude B	30.85V	31.30V	30.83V	30.82V
Amplitude C	30.90V	31.30V	30.89V	30.90V
Unbalanced Degree	0.23%	1.28%	1.11%	0.42%

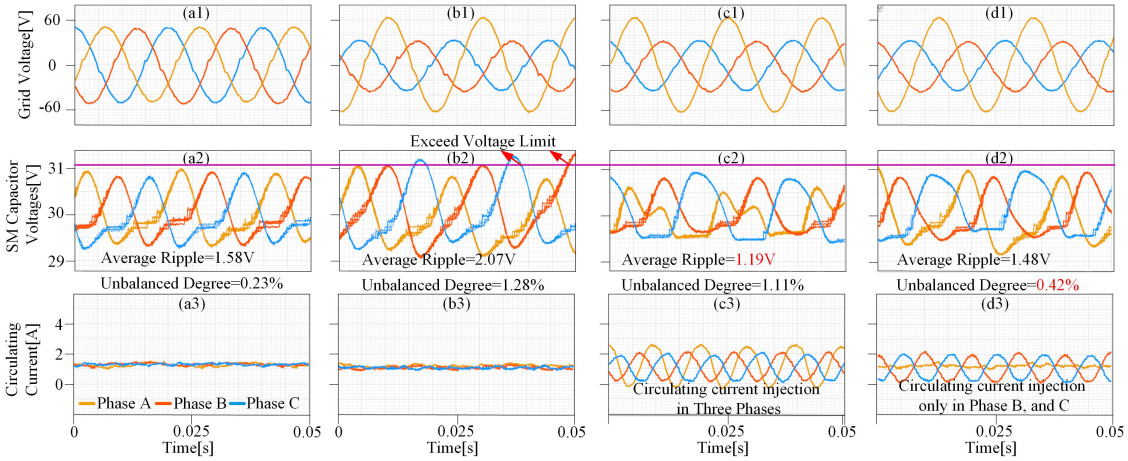

Figure 10. Experimental results, (a) Balanced Grid, (b) Unbalanced grid without circulating current injection, (c) Results of Method A, (d) Results of method B.

5. Conclusion

In this paper, a comprehensive solution to solve the high submodule capacitor voltage problem under unbalanced grid conditions is proposed. First, the analytical tool to indicate the different components of the capacitor voltage under unbalanced grid conditions is proposed. The formation

mechanism of the high capacitor voltage ripple can be understood in an Intuitive and accurate way. What is more, based on the analytical model of the capacitor voltage, two submodule capacitor voltage reduction methods are proposed. The injected circulating current is calculated based on the analytical model in an easy way. Then, both the simulation and experiment are carried out to verify the effectiveness of the two capacitor voltage reduction methods. This proposed solution has the potential to be a competitive solution to the high submodule capacitor voltage problem under unbalanced grid conditions.

References

1. Ahmadijokani, M.; Mehrasa, M.; Sleiman, M.; Sharifzadeh, M.; Sheikholeslami, A.; Al-Haddad, K. A Back-Stepping Control Method for Modular Multilevel Converters. *IEEE Transactions on Industrial Electronics* **2020**.
2. Mehrasa, M.; Pouresmaeil, E.; Zabihi, S.; Catalão, J.P. Dynamic model, control and stability analysis of MMC in HVDC transmission systems. *IEEE Transactions on Power Delivery* **2016**, *32*, 1471–1482.
3. Ou, Z.; Wang, G.; Zhang, L. Modular multilevel converter control strategy based on arm current control under unbalanced grid condition. *IEEE Transactions on Power Electronics* **2017**, *33*, 3826–3836.
4. Guo, C.; Yang, J.; Zhao, C. Investigation of small-signal dynamics of modular multilevel converter under unbalanced grid conditions. *IEEE Transactions on Industrial Electronics* **2018**, *66*, 2269–2279.
5. Lesnicar, A.; Marquardt, R. An innovative modular multilevel converter topology suitable for a wide power range. 2003 IEEE Bologna Power Tech Conference Proceedings,. IEEE, 2003, Vol. 3, pp. 6–pp.
6. Rohner, S.; Bernet, S.; Hiller, M.; Sommer, R. Modulation, losses, and semiconductor requirements of modular multilevel converters. *IEEE transactions on Industrial Electronics* **2009**, *57*, 2633–2642.
7. Wang, K.; Li, Y.; Zheng, Z.; Xu, L. Voltage balancing and fluctuation-suppression methods of floating capacitors in a new modular multilevel converter. *IEEE Transactions on Industrial Electronics* **2012**, *60*, 1943–1954.
8. Antonopoulos, A.; Angquist, L.; Nee, H.P. On dynamics and voltage control of the modular multilevel converter. 2009 13th European Conference on Power Electronics and Applications. IEEE, 2009, pp. 1–10.
9. Nami, A.; Liang, J.; Dijkhuizen, F.; Demetriades, G.D. Modular multilevel converters for HVDC applications: Review on converter cells and functionalities. *IEEE Transactions on Power Electronics* **2014**, *30*, 18–36.
10. Guan, M.; Xu, Z. Modeling and control of a modular multilevel converter-based HVDC system under unbalanced grid conditions. *IEEE transactions on power electronics* **2012**, *27*, 4858–4867.
11. Tu, Q.; Xu, Z.; Chang, Y.; Guan, L. Suppressing DC voltage ripples of MMC-HVDC under unbalanced grid conditions. *IEEE Transactions on Power Delivery* **2012**, *27*, 1332–1338.
12. Moon, J.W.; Kim, C.S.; Park, J.W.; Kang, D.W.; Kim, J.M. Circulating current control in MMC under the unbalanced voltage. *IEEE Transactions on Power delivery* **2013**, *28*, 1952–1959.
13. Moon, J.W.; Park, J.W.; Kang, D.W.; Kim, J.M. A control method of HVDC-modular multilevel converter based on arm current under the unbalanced voltage condition. *IEEE Transactions on Power Delivery* **2014**, *30*, 529–536.
14. Shi, X.; Li, Y.; Wang, Z.; Liu, B.; Tolbert, L.M.; Wang, F. Steady-state analysis of modular multilevel converter (MMC) under unbalanced grid conditions. 2016 IEEE Applied Power Electronics Conference and Exposition (APEC). IEEE, 2016, pp. 2637–2644.
15. Ilves, K.; Norrga, S.; Harnefors, L.; Nee, H.P. On energy storage requirements in modular multilevel converters. *IEEE transactions on power electronics* **2013**, *29*, 77–88.
16. Ronanki, D.; Williamson, S.S. Failure prediction of submodule capacitors in modular multilevel converter by monitoring the intrinsic capacitor voltage fluctuations. *IEEE Transactions on Industrial Electronics* **2019**, *67*, 2585–2594.
17. Harnefors, L.; Antonopoulos, A.; Norrga, S.; Angquist, L.; Nee, H.P. Dynamic analysis of modular multilevel converters. *IEEE Transactions on Industrial Electronics* **2012**, *60*, 2526–2537.
18. Sharifabadi, K.; Harnefors, L.; Nee, H.P.; Norrga, S.; Teodorescu, R. *Design, control, and application of modular multilevel converters for HVDC transmission systems*; John Wiley & Sons, 2016.

19. Ilves, K.; Antonopoulos, A.; Harnefors, L.; Norrga, S.; Ängquist, L.; Nee, H.P. Capacitor voltage ripple shaping in modular multilevel converters allowing for operating region extension. IECON 2011-37th Annual Conference of the IEEE Industrial Electronics Society. IEEE, 2011, pp. 4403–4408.
20. Pou, J.; Ceballos, S.; Konstantinou, G.; Agelidis, V.G.; Picas, R.; Zaragoza, J. Circulating current injection methods based on instantaneous information for the modular multilevel converter. *IEEE Transactions on Industrial Electronics* **2014**, *62*, 777–788.
21. Li, J.; Konstantinou, G.; Wickramasinghe, H.R.; Townsend, C.D.; Pou, J. Capacitor Voltage Reduction in Modular Multilevel Converters under Grid Voltages Unbalances. *IEEE Transactions on Power Delivery* **2019**, *35*, 160–170.
22. Vasiladiotis, M.; Cherix, N.; Rufer, A. Impact of grid asymmetries on the operation and capacitive energy storage design of modular multilevel converters. *IEEE Transactions on Industrial Electronics* **2015**, *62*, 6697–6707.
23. Teodorescu, R.; Liserre, M.; Rodriguez, P. *Grid converters for photovoltaic and wind power systems*; Vol. 29, John Wiley & Sons, 2011.

Sample Availability: Samples of the compounds ..... are available from the authors.

Machine Learning based Operating Region Extension of Modular Multilevel Converters under Unbalanced Grid Faults

Songda Wang, Tomislav Dragicevic, *Senior Member, IEEE,* Yuan Gao, *Student Member, IEEE*, Sanjay K Chaudhary, *Senior Member, IEEE,* and Remus Teodorescu, *Fellow, IEEE*

***Abstract*— The capacitor voltage ripples of the modular multilevel converter (MMC) are increased under unbalanced grid fault conditions. Since high capacitor voltage ripples deteriorate their lifetimes and may even cause tripping of the MMC system, it is important to restrict them. To this end, it is well known that injecting double fundamental frequency circulating currents can reduce the capacitor voltage ripples. However, finding a proper circulating current reference to achieve desired ripples analytically is complicated. This paper proposes an alternative method to quickly calculate the proper circulating current references without analytical computations, which is achieved by an artificial neural network (ANN) trained to approximate the relationship between circulating current references and capacitor voltage ripples. The training data is firstly extracted from a detailed simulation model of the MMC. Afterwards, the ANN is trained by the input-output data to obtain the mapping relationship, which is then used to derive the desired circulating current references. Both the simulation and the experimental results verify the practicability of the proposed method, where the operating region can be extended 30% at a minimum in all testing conditions.**

***Index Terms*— Modular multilevel converter (MMC), artificial neural network (ANN), operating region extension, capacitor voltage ripple reduction, machine learning.**

I. INTRODUCTION

THE modular multilevel converter (MMC) is one of the most attractive topologies for voltage source converter-based high voltage direct current (HVDC) systems due to MMC's advanced merits: modularity, scalability, lower harmonics, and small (or no) harmonic filter requirements [1].

Unbalanced grid conditions during asymmetric faults affect the charging of the MMC submodule (SM) capacitors. As a result, the capacitor voltage ripples will be unbalanced and will present higher amplitudes [2]. High SM capacitor voltages will cause tripping of the MMC system immediately if they exceed the safe voltage limit [3]. Therefore, the safe operating region of the MMC is limited during such faults [4]. Moreover, the SM capacitors will deteriorate more quickly through the aging process if they are subjected to high voltage operation [5]. Aging gradually reduces their capacitance, and with aging the capacitor voltage will get even higher under unbalanced grid fault conditions.

Several approaches have been proposed to address operation region extension by reducing SM capacitor voltage ripples under different grid conditions. In [4], the operating region is extended by injecting the second-order harmonic circulating current under single phase grid fault condition. However, in this paper the amplitude of injected AC circulating current is fixed, which means that different three-phase unbalanced grid fault conditions have not been addressed. Therefore, this method cannot flexibly control the voltage according to different fault conditions. In [6], the second-order harmonic circulating current injection method is combined with the optimized zero-sequence voltage to extend the operation region. Still, the method in [6] is only designed for balanced grid condition. In [7], AC circulating current reference is derived from the instantaneous capacitance with the upper and lower arm under single-phase grid. Then the SM capacitor voltage ripple can be reduced. This instantaneous method is also applied under unbalanced grid condition in [8], and the results showed that this method can also reduce the SM capacitor voltage ripple under unbalanced grid conditions. However, these papers applied the method of injecting circulating currents regardless of whether SM voltages of these phases exceed the safe limit or not. If so, unnecessary power losses will occur in the phase that does not exceed the safe voltage limit. In [9]–[11], analytical equations are introduced to model submodule voltage ripple under balanced grid condition. However, these ripple equations do not consider the influence of unbalanced grid condition, since deriving the equations for the unbalance-grid-condition case would be very complicated and time-consuming because of the extra negative-sequence current/voltage. Their derivation also requires strong control and domain expertise, which makes them difficult to reproduce and understand by practicing engineers. In [12]–[14], the components of the circulating current under unbalanced grid conditions are analyzed and a circulating current control is proposed in order to suppress all the AC components of circulating current. However,

Manuscript received August 15 2019, first revised November 5 2019, second revised December 24 2019, third revised February 06 2020, accepted February 28 2020. (Corresponding Author: Yuan Gao).

S. Wang, T. Dragicevic, S. K. Chaudhary, and R. Teodorescu are with the Department of Energy Technology, Aalborg University, Aalborg, Denmark. (email: sow@et.aau.dk; tdr@et.aau.dk; skc@et.aau.dk; ret@et.aau.dk).

Y. Gao is with the Department of Electrical and Electronic Engineering. University of Nottingham, Nottingham, UK. (email: Yuan.Gao@nottingham.ac.uk).

This article has been accepted for publication in a future issue of this journal, but has not been fully edited. Content may change prior to final publication. Citation information: DOI 10.1109/TIE.2020.2982109, IEEE Transactions on Industrial Electronics

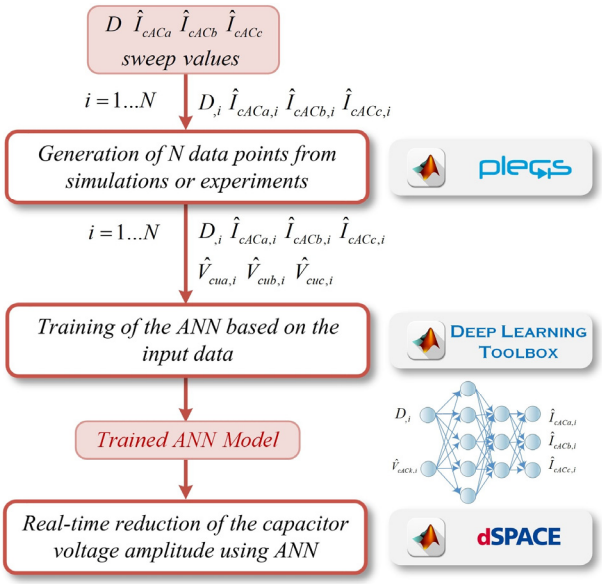

Fig. 1. Training steps for the ANN method.

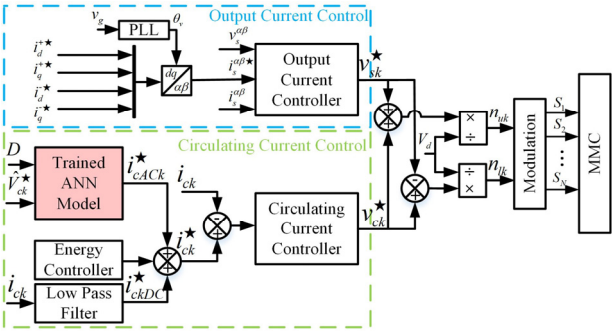

Fig. 2. The control block diagram of proposed MMC.

suppressing all the AC circulating currents will not guarantee that the voltage ripples in the submodule capacitors do not exceed the voltage limits. In [15], an analytical relationship between MMC arm power and circulating current references is derived. Then, the circulating current reference that reduces the submodule capacitor voltage ripple is calculated based on derived equations. However, [15] only analyzes the arm power of the MMC with different control techniques, whereas the accurate relation between submodule capacitor voltage ripples and circulating current references is not discussed. In other words, the theoretical foundation set in [15] is not sufficient to explicitly derive circulating current references for controlling three-phase SM submodule capacitor voltage ripples. In [3], an offset pulse-width modulation (OPWM) and zero sequence voltage injection method is proposed. The three-phase offsets added to the duty ratios to reduce the average SM capacitor voltages of the arms during unbalanced grid conditions [3]. However, this paper still does not address the accurate relation between submodule capacitor voltage ripples and circulating current references. In [16], a non-linear optimization method which can extend the operating region by on-line model predictive method is proposed. Moreover, this method is combined with frequency-domain models of MMC, which can eliminate the need for time-consuming simulations. However, in this paper, the overall control structure is different from the widely-use traditional MMC control structure because of the non-linear H-infinity output current controller and predictive control regulator. This new control structure with non-linear controller requires high knowledge level for implementation, which may make the practical application quite challenging.

Discussion above underlies the need of developing simple and easily generalizable control methods for compensation of SM capacitor voltage ripples under unbalanced grid conditions. This paper proposes a flexible and computationally light ripple-compensation technique based on trained artificial neural network (ANN) that acts as a fast surrogate model mapping the relationship between circulating-current references and SM capacitor voltage ripples. With the help of this ANN model, the injected circulating current references are calculated automatically according to different grid conditions. In addition, desired capacitor-voltage-ripple values, which are limited to some predefined operating range, can be obtained explicitly. The ANN is trained by the data collected from simulations, and the application of the proposed method has been experimentally demonstrated.

II. ANN Based Approach

A. Deployment of ANN

Several papers have used ANN to solve power electronics problems, from selecting weighting factors in model predictive control of power electronics converters [17] to automatically designing the power electronics system for reliability [18]. ANN is known to be a universal function approximator. In other words, it can in theory approximate any function with arbitrary precision, given that the number of layers and neurons has been appropriately chosen [19]. In practice, ANN structure is usually selected by trial-and-error.

The surrogate model in this paper is constructed by using a 3-layer ANN, where there are 9 neurons in the hidden layer. This surrogate model represents the relationship between circulating current, grid dip severity factor, and injected circulating current amplitude. In particular, this network represents the following relation:

$$y = F(\mathrm{x}) \Leftrightarrow (\hat{I}_{cACa}, \hat{I}_{cACb}, \hat{I}_{cACc}) = F(D, \hat{V}_{cua}, \hat{V}_{cub}, \hat{V}_{cuc}) \quad (1)$$

where $\hat{I}_{cACa}$, $\hat{I}_{cACb}$, $\hat{I}_{cACc}$ are circulating currents, $\hat{V}_{cua}$, $\hat{V}_{cub}$, $\hat{V}_{cuc}$ are capacitor voltages, and D is grid dip severity factor. The severity of two-phase-to-ground grid fault depends on D. The range of D is [0,1], where 1 means normal grid, and 0 means short circuit, more practices about D can be found in [20] and [21].

B. Design and Collection of Sample Data for ANN

ANN feedback is triggered when the unbalanced grid detector detects an unbalanced grid fault. After training, the ANN can give feasible circulating current references (i^*_{cACk}) to control the SM capacitor voltages in a desired way. This paper takes two-phase-to-ground grid fault as an example. The vector definition of the two-phase-to-ground grid fault can be described based on [20] as:

$$\hat{V}_{ga\_pu}=1,\hat{V}_{gb\_pu}=-\frac{1}{2}D-j\frac{\sqrt{3}}{2}D,\hat{V}_{gc\_pu}=-\frac{1}{2}D+j\frac{\sqrt{3}}{2}D \quad (2)$$

where $\hat{V}_{ga\_pu},\hat{V}_{gb\_pu},\hat{V}_{gc\_pu}$ are per unit values of the grid voltages in phase a, b, and c.

Circulating current circulates inside the MMC without affecting the AC output currents. It only influences the internal performance of the MMC system. In this paper, we define the circulating current as a parameter containing both DC and AC components:

$$i_{ck}=\frac{i_{uk}+i_{lk}}{2}=I_{ckDC}+\hat{I}_{cACk}\cos(2\omega t+\theta_{vk-}) \quad (3)$$

where k is phase number of three-phase system(0 for phase A, 1 for phase B, and 2 for phase C), i_{ck} is three-phase circulating currents, i_{uk} and i_{lk} are the upper and lower arm current respectively. I_{ckDC} is the DC component of circulating current, $\hat{I}_{cACk}\cos(2\omega t+\theta_{vk-})$ is AC component of three-phase circulating current, ω is fundamental angular frequency, and θ_{v-} is the phase angle of negative-sequence voltage. The injected AC circulating currents are double fundamental frequency, negative-sequence phases [0, -4/3*pi, -2/3*pi] with different amplitudes ($\hat{I}_{cACa}$, $\hat{I}_{cACb}$, $\hat{I}_{cACc}$). In this paper, we only consider AC circulating current components.

To clarify the training procedures, all the steps are shown in Fig. 1. Each step is further elaborated as follows.

1) Generation of N data samples from simulation to extract $\hat{V}_{cua}$, $\hat{V}_{cub}$, $\hat{V}_{cuc}$ for every combination of $\hat{I}_{cACa}$, $\hat{I}_{cACb}$, $\hat{I}_{cACc}$ and D.

The data can be extracted either from a detailed simulation or from an experimental setup. In this work, we collected data from simulations and verified the method both in a high voltage simulation model and in a low voltage experimental setup. In the simulation, the sweep values of input data are: grid dip severity D = [0.5, 0.6, 0.7, 0.8, 0.9]; three circulating currents $\hat{I}_{cACa,b,c}$ = [0, 50, 100, 150, 250, 300, 350, 400] for three phases *a, b, c*; the output data are three capacitor voltages $\hat{V}_{cua,b,c}$. The total number of data points is hence $5\times8\times8\times8=2560$. The paralleled simulations helped us to accelerate the simulation process. In particular, a workstation with a 24-core CPU was utilized for the data collection. Since the execution time was around 8 *sec* for one simulation, the overall simulation time for 2560 samples was approximately 14 *mins*. In the model that resembles the experimental setup, the sweep values of input data were: D = [0.5, 0.6, 0.7, 0.8, 0.9], $\hat{I}_{cACa,b,c}$ = [0.3, 0.5, 0.7, 0.9, 1.1, 1.3, 1.5]. The output data was the same $\hat{V}_{cua,b,c}$. The number of data points was 1715, and the overall data collection time for 1715 data was approximately 10 *mins*.

2) Reduction of the capacitor voltage amplitudes using ANN

The extracted data was used to train the desired surrogate model, which represents the relationship between $\hat{V}_{cu}$, D, and $\hat{I}_{cAC}$ under two-phase-to-ground faults conditions.

The trained ANN model was finally used to calculate the injected circulating current references for the MMC system under two-phase-to-ground grid faults. The inputs of the ANN model are the grid dip severity factor D and safe SM capacitor voltage limit, then the outputs of the ANN are the three-phase circulating current references. The trained ANN model was compiled to SIMULINK model. This model can both be applied in the PLECS Blockset software (for offline simulation) and in the dSPACE DS1006 platform (for real-time control).

III. RESULTS

The control block diagram of the proposed method is shown in Fig. 2. The MMC controller is divided into two main parts. 1). Proposed ANN and Circulating Current Controller: When two-phase-to-ground fault happens, the proposed ANN model will generate three-phase circulating current references based on desired capacitor voltages and detected *D*. Then, the circulating current controller enables the MMC to track its circulating current references. In this paper, the proportional resonant (PR) controller is used to track the AC circulating current [11]. The proposed ripple reduction method reduces the SM voltage ripple by injecting AC circulating current under unbalanced grid conditions. Energy controller ensures that the total amount of energy stored inside the converter is always controllable to stabilize the MMC system under unbalanced grid conditions. By energy controller, two types of energies are controlled. We refer to them as the "Sum" energy and the "Delta" energy. Sum energy is the sum of upper arm energy and lower arm energy; Delta energy is the difference between upper arm energy and lower arm energy. The detailed information about these two energy controllers can be found in [11] and [22]. The three-phase sum energies are controlled to a same level and the delta energies are controlled to zero. 2). Output Current Controller: PR controller is used in the output controller to control the output current of the MMC in grid-connected operation. This controller is conventional, and more details can be found in [11].

A. Simulation Results

The proposed ANN SM capacitor voltage ripple reduction method was first validated by PLECS simulation. The specifications of the simulation model are listed in Table I. The simulation results of MMC under balanced grid conditions are shown in Fig. 3. Fig. 3 (a1) shows the three-phase SM capacitor voltages under balanced grid condition. These voltages are balanced and within the safe voltage limit of around 10% of the nominal value. The average voltage ripple (peak to peak value of capacitor voltage) here is 38.72 kV. The unbalanced degree is 0.046%, unbalanced degree (*UD)* is defined in (4) as

$$UD=[\max(V_a,V_b,V_c)-\min(V_a,V_b,V_c)]/V_{avg}+(V_a+V_b+V_c)/3 \quad (4)$$

Fig. 3 (b1) - (b3) show the SM capacitor voltages under two-phase-to-ground grid faults. The capacitor voltages are unbalanced and exceed the safe voltage limit. The average ripple increases to 46.03 kV, and the *UD* increases to 1.48%.

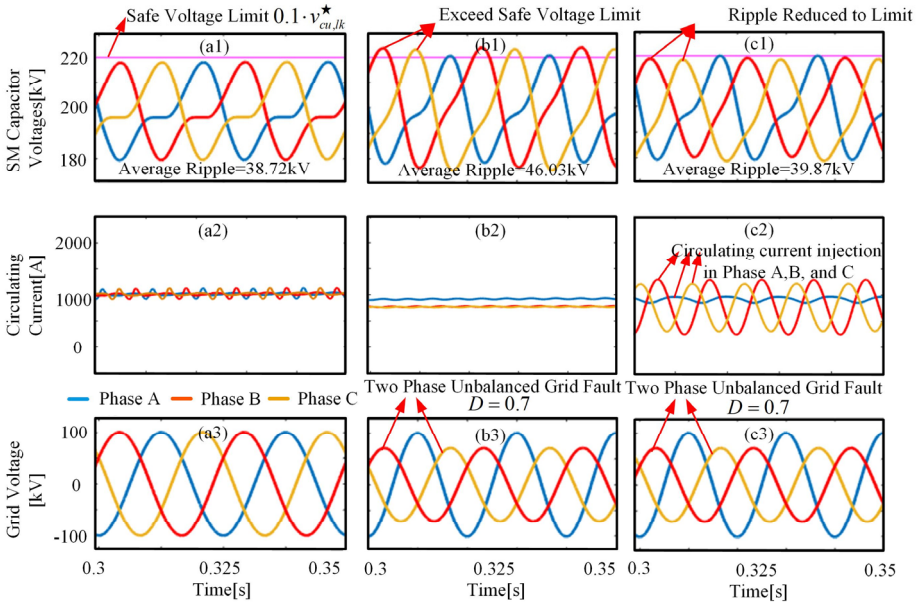

Fig. 3. Simulation results: (a) normal grid condition; (b) unbalanced grid condition without proposed method; (c) unbalanced grid condition with proposed method.

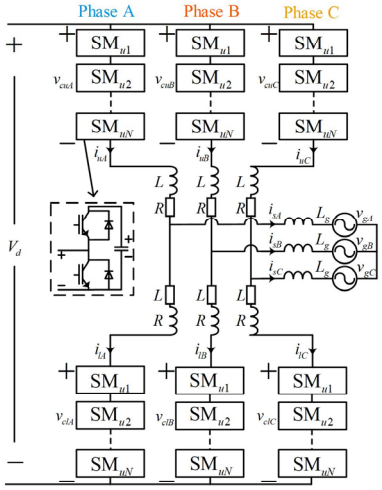

Fig. 4. Grid connected MMC diagram.

The results of the proposed method are presented in Fig. 3 (c1) - (c3). The circulating current components are injected into the MMC system. Injected AC circulating currents are calculated by the ANN model, the amplitudes of them are $\hat{I}_{cACa} = 60.53$ A, $\hat{I}_{cACb} = 551$ A, $\hat{I}_{cACc} = 480.8$ A respectively. It can be noticed that the three-phase injected circulating currents are not symmetrical. In this way, the losses of the MMC are lower because the root mean square current in phase a is low. The capacitor voltages of the proposed method are within the safe limit, as shown in Fig. 3 (c1). The average ripple is reduced to 39.87 kV, and this voltage is reduced to the same level of capacitor voltage under balanced grid conditions. The *UD* here is reduced to 0.64%. In this case, the operating region is extended 30% because the proposed ANN method prevents MMC capacitor overvoltage trip when D=0.7.

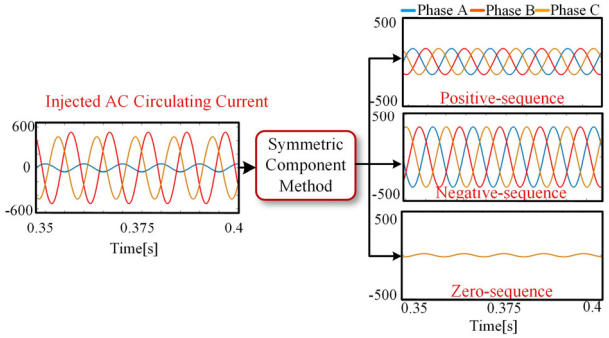

Fig. 5 Injected circulating current components

TABLE I
MMC PARAMETERS IN SIMULATION AND EXPERIMENT

	Simulation	Experiment
Number of SMs per arm (N)	100	4
Rated DC voltage (v_d)	200 kV	200 V
Rated active power	150 MW	1 kW
Nominal SM capacitance (C)	3.75 mF	2000 μF
Nominal SM capacitor voltage (v_c)	2 kV	50 V
Rated frequency (f)	50 Hz	50 Hz
Arm inductance (L)	50.9 mH	10 mH
Sample frequency	10 kHz	10 kHz
Grid voltage magnitude	100 kV	83 V
Dip severity grid factor in two-phase-to ground fault (D)	0.7	0.5

In this paper, the injected AC circulating current components are flexible, which means the amplitudes of injected AC circulating current can be varied. Therefore, the three-phase components with different amplitudes usually contain positive-, negative- and zero-sequence components. The injected circulating current components are shown in Fig. 5.

B. Experimental Results

The proposed ANN capacitor voltage reduction method is also demonstrated in an experimental setup. The experiment is carried out in a scaled-down three-phase grid-connected MMC setup with 4 half-bridge SMs per arm. The MMC controller is implemented in DS1006 from dSPACE. The specifications of the experimental setup are also listed in Table I. The data points for experiments were collected from a detailed simulation model using the same parameters with the lab setup. In this way, the data extraction time was greatly saved.

Similar to the simulation results, three-phase capacitor voltages are balanced under balanced grid. In addition, the voltage is within the safe limit, as shown in Fig. 6 (a1). The average ripple is 6.5 V, and the *UD* is 0.18%.

The capacitor voltages become unbalanced under two-phase-to-ground faults. Moreover, the capacitor voltage amplitudes exceed the limit, which is shown in Fig. 6 (b1). The average ripple increases to 7.3 V. The *UD* increases to 1.112%.

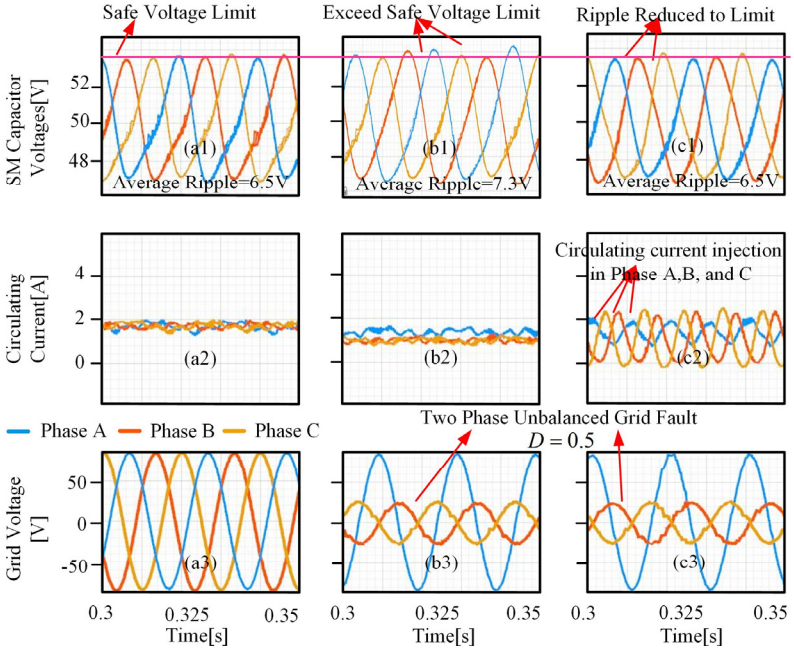

Fig. 6. Experimental results: (a) normal grid condition; (b) unbalanced grid condition without proposed method; (c) unbalanced grid condition with proposed method.

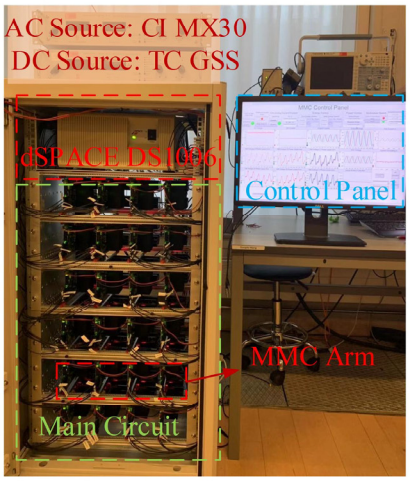

Fig. 7. MMC setup.

The proposed method can also reduce the capacitor voltages to a safe voltage limit in the experiment as shown in Fig. 6 (c1). The amplitudes of injected AC circulating current components are $\hat{I}_{cACa} = 0.51$ A, $\hat{I}_{cACb} = 1.13$ A , and $\hat{I}_{cACc} = 1.29$ A respectively. The average ripple here is 6.5 V, and the *UD* is reduced to 0.5%. With the proposed method, MMC capacitor overvoltage trip is prevented when *D*=0.5.

C. Extension of the Proposed Method to Other Unbalanced Grid Conditions

TABLE II
VECTOR DEFINITION OF DIFFERENT UNBALANCED GRID CONDITIONS

Fault Types	Vector Definitions
Two-phase-to-ground fault	$\begin{cases}\hat{V}_{ga\_pu}=1\\ \hat{V}_{gb\_pu}=-\frac{1}{2}D-j\frac{\sqrt{3}}{2}D\\ \hat{V}_{gc\_pu}=-\frac{1}{2}D+j\frac{\sqrt{3}}{2}D\end{cases}$
Three-phase-to-ground fault	$\begin{cases}\hat{V}_{ga\_pu}=D\\ \hat{V}_{gb\_pu}=-\frac{1}{2}D-j\frac{\sqrt{3}}{2}D\\ \hat{V}_{gc\_pu}=-\frac{1}{2}D+j\frac{\sqrt{3}}{2}D\end{cases}$
Phase-to-phase short-circuit fault	$\begin{cases}\hat{V}_{ga\_pu}=1\\ \hat{V}_{gb\_pu}=-\frac{1}{2}-j\frac{\sqrt{3}}{2}D\\ \hat{V}_{gc\_pu}=-\frac{1}{2}+j\frac{\sqrt{3}}{2}D\end{cases}$
Single-phase-to-ground fault	$\begin{cases}\hat{V}_{ga\_pu}=D\\ \hat{V}_{gb\_pu}=-\frac{1}{2}-j\frac{\sqrt{3}}{2}\\ \hat{V}_{gc\_pu}=-\frac{1}{2}+j\frac{\sqrt{3}}{2}\end{cases}$

This paper thus far only discussed the two-phase-to-ground grid condition as an example. Here we elaborate how this proposed method can be easily extended to other unbalanced grid conditions:

There are 4 types of unbalanced grid conditions [19], [20]: Two-phase-to-ground fault, three-phase-to-ground fault, single-phase-to-ground fault, and phase-to-phase short circuit fault. In this paper, the vector definition of grid under two-phase-to-ground fault is expressed as equation (3). The vector definitions of other unbalanced grid conditions are shown in Table II (see below). From the vector definitions we can see that grid dip severity factor *D* defines the severity of the unbalanced grid, where the range of *D* is [0, 1]. Here, 1 means normal grid, while 0 means short circuit. By the type of unbalanced grid condition and changing *D* from [0, 1], we can cover all possible fault scenarios by doing numerous parallel simulations and extracting corresponding data. This process can be significantly accelerated by paralleling the tasks using a computer cluster that contains many CPU cores. Therefore, the only limitation to extend our method to any other fault is computational capacity. If we have enough computational power, the data for other unbalanced fault conditions can be quickly collected. Then, new artificial intelligence neural network can be trained by the collected data and the circulating current reference for different unbalanced grid conditions can be calculated easily.

D. Comparison of Different MMC Operation Extension Methods

To clearly elaborate the advantages and disadvantages of the proposed machine learning method in this paper, a comparison of analytical frequency-domain based methods [4], [6]-[7], the MPC oriented method [16], and the proposed machine learning method is listed in Table III.

TABLE III
COMPARISON OF DIFFERENT MMC OPERATION EXTENSION METHODS

	Analytical Frequency-Domain Methods [4, 6, 7]	MPC Oriented Method [16]	Proposed Method
Need of Analytical Derivation?	Yes	Yes	No
Frequency Domain Model	Yes	Yes	No
Computation Burden	Low	Medium	Low
Easy to Implement to Experiment	Easy	Difficult	Easy

The Table III shows that the analytical frequency-domain based methods have a low computation burden as well as a good operation region extension performance because injecting method is proven to be effective for operation region extension. However, the main drawback of these methods is that engineers need to derive the complicated analytical equations to get the desired circulating current components. The MPC oriented method is proposed in [16] to build a model predictive control to extend the operation, in this way the parallel simulation for data collect can be eliminated. However, the non-linear controller in this method increases the difficulty for engineers not familiar with advanced control theory to implement this method in the real MMC project.

The proposed method does not need to derive any analytical equations to get the reference of circulating current. Also, the proposed method is suitable for both balanced and unbalanced grid conditions: The proposed method uses the data from parallel simulation then trains a ML model offline to get the parameters for the desired ANN model (biases, weights). In this way we can achieve a very low computation burden in real microprocessor such as DSP, dSPACE. Moreover, as this ML method is just an additional simple block for the traditional MMC controller (shown in Fig. 2), there is no need for engineers to build a non-linear MMC controller from the scratch.

IV. CONCLUSION

This paper proposed a fast method to reduce the capacitor voltage oscillations under two-phase-to-ground grid faults. This is achieved by training an artificial neural network, which explicitly maps the relationships between circulating current references and capacitor voltages. The operating region is extended by 30% with the proposed method at a minimum in all testing conditions. Therefore, the paper provides a solution to handle the non-parametric optimization of the complex internal characteristics of MMC. This method has been validated for two-phase-to-ground grid faults but can also be extended to other unbalanced grid conditions. In future work, the application of this proposed ANN method to DC circulating current components optimization will be expanded.

REFERENCES

[1] A. Lesnicar and R. Marquardt, "An innovative modular multilevel converter topology suitable for a wide power range," *in Proc. IEEE Power Tech Conf., vol. 3, Bologna, Italy, Jun. pp. 272–277, 2003.*

[2] M. Guan and Z. Xu, "Modeling and control of a modular multilevel converter-based HVDC system under unbalanced grid conditions," *IEEE Trans. Power Electron.*, vol. 27, no. 12, pp. 4858–4867, 2012.

[3] J. Li, G. Konstantinou, H. R. Wickramasinghe, C. D. Townsend, and J. Pou, "Capacitor Voltage Reduction in Modular Multilevel Converters under Grid Voltages Unbalances," *IEEE Trans. Power Deliv.*, vol. 35, no. 1, pp. 160-170, 2020.

[4] H. Kim, S. Kim, Y. H. Chung, D. W. Yoo, C. K. Kim, and K. Hur, "Operating Region of Modular Multilevel Converter for HVDC with Controlled Second-Order Harmonic Circulating Current: Elaborating P-Q Capability," *IEEE Trans. Power Deliv.*, vol. 31, no. 2, pp. 493–502, 2016.

[5] D. Ronanki and S. S. Williamson, "Failure Prediction of Submodule Capacitors in Modular Multilevel Converter by Monitoring the Intrinsic Capacitor Voltage Fluctuations," *IEEE Trans. Ind. Electron.*, vol. 67, no. 4, pp. 2585-2594, 2020.

[6] S. Norrga, L. Ängquist and K. Ilves, "Operating region extension for multilevel converters in HVDC applications by optimisation methods," *10th IET International Conference on AC and DC Power Transmission (ACDC 2012)*, Birmingham, pp. 1-6, 2012.

[7] J. Pou, S. Ceballos, G. Konstantinou, V. G. Agelidis, R. Picas, and J. Zaragoza, "Circulating current injection methods based on instantaneous information for the modular multilevel converter," *IEEE Trans. Ind. Electron.*, vol. 62, no. 2, pp. 777–788, 2015.

[8] J. Li, G. Konstantinou, H. R. Wickramasinghe, J. Pou, X. Wu, and X. Jin, "Investigation of MMC-HVDC operating region by circulating current control under grid imbalances," *Electr. Power Syst. Res.*, vol. 152, pp. 211–222, 2017.

[9] K. Ilves, A. Antonopoulos, L. Harnefors, S. Norrga, L. Ängquist, and H. P. Nee, "Capacitor voltage ripple shaping in modular multilevel converters allowing for operating region extension," *in Proc. Industrial Electron*, pp. 4403–4408, 2011.

[10] B. Li, Y. Zhang, G. Wang, W. Sun, D. Xu, and W. Wang, "A Modified Modular Multilevel Converter with Reduced Capacitor Voltage Fluctuation," *IEEE Trans. Ind. Electron.*, vol. 62, no. 10, pp. 6108–6119, 2015.

[11] K. Sharifabadi, L. Harnefors, H.-P. Nee, S. Norrga, and R. Teodorescu, *Design, Control and Application of Modular Multilevel Converters for HVDC Transmission Systems*. 2016. New York, NY, USA: Wiley, 2016.

[12] J. Moon, S. Member, J. Park, and D. Kang, "A Control Method of HVDC-Modular Multilevel Converter Based on Arm Current Under the Unbalanced Voltage Condition," *IEEE Trans. Power Deliv.*, vol. 30, no. 2, pp. 1–8, 2014.

[13] X. Shi, Z. Wang, B. Liu, Y. Li, L. M. Tolbert, and F. Wang, "Steady-State Modeling of Modular Multilevel Converter under Unbalanced Grid Conditions," *IEEE Trans. Power Electron.*, vol. 32, no. 9, pp. 7306–7324, 2017.

[14] J. W. Moon, C. S. Kim, J. W. Park, D. W. Kang, and J. M. Kim, "Circulating current control in MMC under the unbalanced voltage," *IEEE Trans. Power Deliv.*, vol. 28, no. 3, pp. 1952–1959, 2013.

[15] M. Vasiladiotis, N. Cherix, and A. Rufer, "Impact of Grid Asymmetries on the Operation and Capacitive Energy Storage Design of Modular Multilevel Converters," *IEEE Trans. Ind. Electron.*, vol. 62, no. 11, pp. 6697–6707, 2015.

[16] J. M. Rodriguez-Bernuz and A. Junyent-Ferre, "Operating Region Extension of a Modular Multilevel Converter using Model Predictive Control: a Single Phase Analysis," *IEEE Trans. Power Deliv.* Early Access.

[17] T. Dragicevic and M. Novak, "Weighting Factor Design in Model Predictive Control of Power Electronic Converters: An Artificial Neural Network Approach," *IEEE Trans. Ind. Electron.*, vol. 66, no. 11, pp. 8870-8880, 2019.

[18] T. Dragicevic, P. Wheeler, and F. Blaabjerg, "Artificial Intelligence Aided Automated Design for Reliability of Power Electronic Systems," *IEEE Trans. Power Electron.*, vol. 34, no. 8, pp. 7161–7171, 2019.

[19] K. Hornik, M. Stinchcombe, and H. White, "Multilayer feedforward networks are universal approximators" *Neural Networks* vol. 2, pp.

359–366, 1989.

[20] M. H. Bollen, Understanding Power Quality Problems. New York, NY, USA: Wiley, 2000.

[21] T. Tanaka, K. Ma, and S. Member, "Asymmetrical Reactive Power Capability of Modular Multilevel Cascade Converter (MMCC) based STATCOMs for Offshore Wind Farm," *IEEE Trans. Power Electron.,* vol. 34, no. 6, pp. 5147-5164, 2019.

[22] A. Antonopoulos, L. Ängquist, L. Harnefors, K. Ilves, and H. P. Nee, "Global asymptotic stability of modular multilevel converters," *IEEE Trans. Ind. Electron*., vol. 61, no. 2, pp. 603–612, 2014.

Machine Learning Emulation of Model Predictive Control for Modular Multilevel Converters

***Abstract*—This paper proposes a machine learning (ML) based emulation of model predictive control (MPC) for modular multilevel converters (MMCs). In particular, the artificial neural network model, trained offline by the data collected from the traditional fast MPC method, is used to control the MMCs with high accuracy. With this offline training, the majority of computational burden is transferred from online to offline. Therefore, the proposed ML MPC can replace the role of the traditional MPC. The experimental results show that the proposed ML based MPC has the same performance as the conventional MPC but a significantly computationally efficient structure. The finding from the letter provides ground for many other applications for ML based emulation of complex controllers in power electronic systems.**

***Index Terms* — Modular multilevel converter, machine learning, model predictive control, computational burden.**

I. Introduction

With the large-scale development of renewable power transmission, Modular Multilevel Converter (MMC) is the most dominant topology in voltage source - high voltage direct current (VSC-HVDC) application. Because of the modular nature of MMC, MMC has good expandability and redundancy fault tolerance. And the MMC output current harmonics are very small, making it possible to use a small (or even no) filter [1]. However, the complicated structure of series-connected submodules needs to be controlled properly.

Traditional proportional-integral (PI) /proportional resonance (PR) based controllers rely heavily on the careful design of individual controller parameters (output current controller and circulating current controller), and the bandwidths of controllers need to be carefully designed according to the actual situations. Model predictive control is a mathematical model-based multi-input-multi-output (MIMO) control algorithm, which was proved to have a good dynamic response even under significant parameter variations [2]. Paper [3] first proposed the MPC controller in the MMC system, from the results, the output currents and the circulating current are well controlled by the MPC controller. However, since each bridge arm of the MMC has many sub-modules, the MPC imposes a high computational cost in order to balance the capacitive voltages of these sub-modules, which is a major disadvantage of the MPC MMC. Many papers proposed computational efficient methods for MPC based MMC [5]–[7]. However, those solutions cannot change the MPC's key trait:

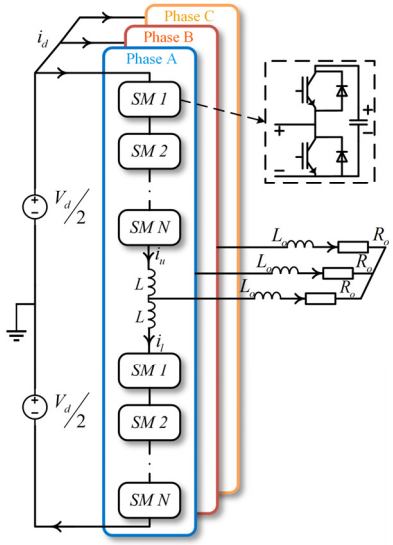

Fig. 1. Three-phase MMC circuit diagram.

The model predict controller evaluates all possible switching signals at each control cycle and selects the best set of control signals to minimize the cost function. This online exhaustive approach can lead to a heavy controller computational cost.

In this letter, a machine learning emulation of the model predictive control is proposed to significantly reduce the computational cost but while maintaining excellent dynamic response. ML technology is widely applied in power electronics applications, for example, a short-term memory recurrent neural network based power fluctuations identification method is proposed to maintain the power system frequency in [10]. In [9], an artificial neural network (ANN) based power electronics design method by including the reliability is proposed to achieve a better comprehensive performance of power electronics systems.

The machine learning models can be trained by data get non-parameter models to represent the real-world input-input relationships [8], [9]. The ANN is a subset of machine learning technology which is applied in this letter. The machine learning network can be trained offline and then the trained network can be applied in the offline simulation or implemented in a real-time microprocessor system such as DSP and dSPACE controller. And also, this letter shows the computational cost of the proposed method is significantly lower than the MPC controller and also perfectly emulates the MPC controller.

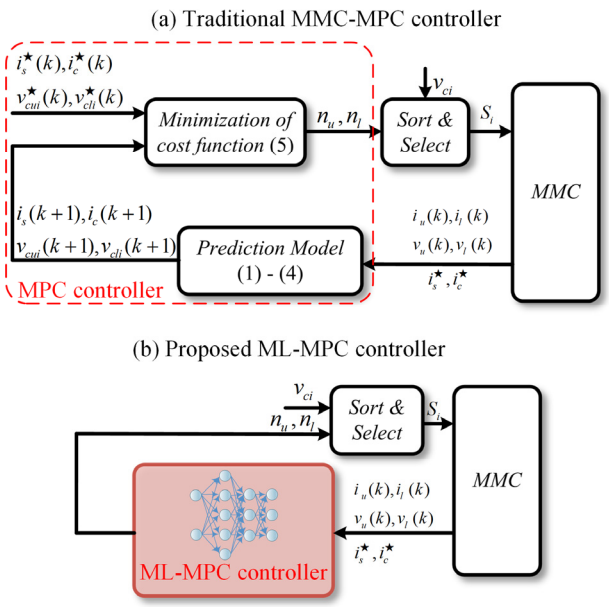

Fig. 2. (a). Traditional MPC for MMCs; (b) The proposed ML based controller for MMCs.

II. MPC FOR MMCS

To train the ML MPC controller, the traditional MPC need to be established first to collect the input/output data.

A. The model predictive control for MMCs

Fig. 2(a) presents the MPC based MMC system, and the controller structure comparison between MPC and the proposed ML based controller is also shown. The implementation of the MPC in MMC is described step by step. The comprehensive introduction of the MPC MMC implementation is in [7].

1) The MMC sensors measure the variables: upper/lower arm currents, upper/lower arm voltages, output current, and internal circulating current;
2) The MPC algorithms predict the all the possible output variable values in next sampling interval for all the possible switching signals;
3) The MPC algorithms create the MPC cost function regarding the output/circulating current.
4) The MPC algorithms selected the optimized switching signal which can track the control references, i.e. achieve the lowest cost function;
5) The optimized switching signals are used to control the MMC.

The discrete-domain dynamics of output variables are [8]:

$$i_s(k+1) = \mathrm{A}[(n_l(k)\cdot v_{cl}(k+1) - n_u(k)\cdot v_{cu}(k+1))/N] + \mathrm{B}i_s(k)$$
$$\mathrm{A} = 2T_s/(L_{arm}+2L_s), \mathrm{B} = 1-2T_sR_s/(L_{arm}+2L_s) \quad (1)$$

$$i_c(k+1) = \mathrm{C}[V_d - (n_l(k)\cdot v_{cl}(k+1) + n_u(k)\cdot v_{cu}(k+1))/N] + i_c(k)$$
$$\mathrm{C} = T_s/(2L_s) \quad (2)$$

$$v_{cu}(k+1) = \frac{n_u(k)\cdot T_s}{C_{SM}} i_u(k) + v_{cu}(k) \quad (3)$$

$$v_{cl}(k+1) = \frac{n_l(k)\cdot T_s}{C_{SM}} i_l(k) + v_{cl}(k) \quad (4)$$

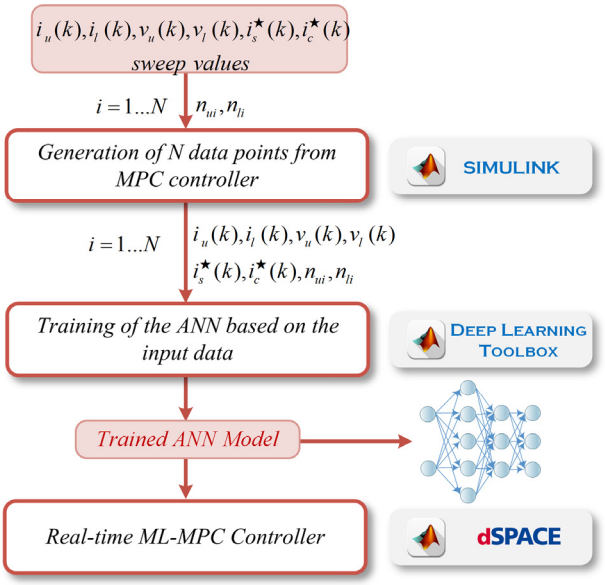

Fig. 3. The training and implementation procedures of ML MPC

where v_{cu}, v_{cl} / i_u, i_l are upper/lower arm voltages/currents respectively, n_u, n_l are upper/lower submodule inserted numbers, respectively, T_s is digital sampling interval, L_{arm} is arm inductance, L_s, R_s are load inductance and resistance, respectively, V_d is DC voltage, C_{SM} is the capacitance of the submodule capacitor, $x(k+1)$, $x(k)$ are the values of the variables at sampling moment k+1 and k.

The cost function (CF) for the MMC control is:

$$g = w_1 \cdot |i_s^\star(k) - i_s(k+1)| + w_2 \cdot |i_c^\star(k) - i_c(k+1)| \quad (5)$$

where w_1 is the output current weighting factor w_2 is the circulating current weighing factor. $i_s^\star$ is the output current reference and $i_c^\star$ is the circulating current reference. In this letter, $w_1 = w_2 = 1$.

In the real-time experiment, the delay of the digital controller is compensated by the method which in introduced in [11]. This letter applied this delay compensation approach.

B. Deterministic input-output relationship of MPC

The deterministic relationship between input variables and output variables of MPC is the key feature that allows the ML based controller to accurately emulate the behavior of the MPC controller. This deterministic relationship is: all the possible output currents and circulating currents are predicted by the MPC controller by considering all possible switching configurations with a set of measured input variables. Then the best switching signal is selected to minimize the cost function. That is to say, the output variables (inserted number of MMC arm) will always be unchanged when the cost function and the measured input variables are unchanged. However, MPC has a heavy computational burden because the MPC controller has to search exhaustively for all the possible switching signals to find the suitable switching signal in every controller time interval. On the other hand, when this deterministic feature is represented by a more computationally light structure (i.e.

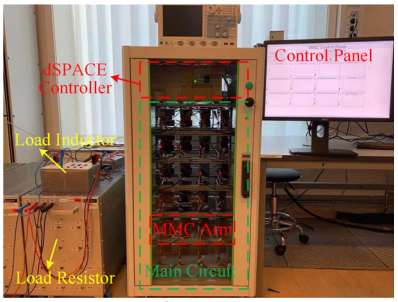

Fig. 4. The picture of the experimental prototype

neural network in our paper), an essentially the same control effect is achieved, but with a far lower online computational cost. In the next sections, a ML based controller is used to represent this deterministic feature of MPC.

II. Machine Learning Based Model Predictive Controller for MMCs

A. Machine learning based MPC for MMCs

Fig. 2 illustrates the comparison of the traditional MPC method and the proposed ML based MPC method. The only difference of these two methods is that ANN model replaces the MPC block. In next section, we will introduce the data collection steps for training the ANN model.

B. Data Acquisition and Model Training

The following describes how to get data from the MPC controller and use this data to train a machine learning model. The general steps are presented in Fig. 3.

1) *The Training Data Sampling:* To train the ML controller, the training data should be collected from the MPC controller first. The data collection algorithm will sample the variables within a certain range. The arm voltages v_{cu}, v_{cl} are sampled from a range [0,350], with a 10V step, then 36 values are sampled from upper/lower arm voltage. We use [0:10:350] to represent this sample operation. Similarly, upper/lower arm currents i_u, i_l, the output current reference $i_s^\star$, and the circulating current reference $i_c^\star$ are sampled as follows respectively: [-6:1:6], [-6:1:6], and [0:0.2:2]. It only takes 76 seconds to collect this data. In order to make sure the training performance is good, we recommend each input variable should be sampled at least 10 points for the whole variable range. What is more, it is important to consider the whole range of the input variable, otherwise the tracking performance is worse compared to traditional controller.
2) *ML Network Structure Selection:* Firstly, the ANN is selected because it is extremely simple. Although ANN is simple, it is still useful to deal with the problem that the data may consist of a completely different set of features, such as table data [13]. Secondly, we selected the hidden layer number of the network, the universal approximation theorem [14] states that an ANN with a single hidden layer, containing a finite number of neurons, can approximate any continuous function with mild assumptions on the activation function [15]. In this letter, one hidden layer structure is applied. The neuron number selection is based on a rule of thumb. To achieve a better training performance, a high neuron number is recommended to select within the range of the min/max neuron numbers
Minimum neuron number:
$$0.5(N_i + N_o) = 4 \quad (N_i = 6, N_o = 2) \tag{6}$$
Maximum neuron number:
$$2N_i = 12 \tag{7}$$
where N_i is the input unit number $N_i = 6$, N_{out} is the output unit number $N_{out} = 2$.
In this letter, we select the neuron number as 9.
3) *ML Model Training:* The data was used to train the proposed ML MPC network, i.e. a feedforward neural network, which represents the relationship between input variables and output variables. The trained ML model is used to calculate the upper and lower arm inserted number of MMC. With the changing of the insert numbers, the output variables can be controlled to track their references. The ANN contains three layers: input layer, hidden layer, and output layer. The hidden layer contains 9 neurons. The network training is implemented in MATLAB.

TABLE I
MMC PARAMETERS IN EXPERIMENT

	Experiment
Number of SMs per arm (N)	4
Rated DC voltage (v_d)	200 V
Nominal SM capacitance (C_{SM})	2000 μF
Nominal SM capacitor voltage (v_c)	50 V
Rated frequency (f)	50 Hz
Arm inductance (L_{arm})	10 mH
Sample frequency	10 kHz
Load inductance (L_s)	1.8mH
Load resistance (R_s)	10.8Ω

III. Experimental Results

The proposed ML MPC controller is verified in the lab prototype. A 24-submodule, three-phase MMC experimental platform is used to verify the proposed method. The digital controller is based on the dSPACE real-time control platform, the controller model is DS1006. The parameter of the experimental platform is presented in Table. I. The prototype picture is presented in Fig. 4.

A. Steady State Performance

Fig. 5 presents the steady state performance of proposed ML MPC and the traditional MPC. From Fig. 5 (a1) and (b1), the output currents of the MMC are controlled to the references: AC currents with 4A amplitudes. The total harmonic distortion (THD) of the ML control output current is 0.023%. The THD of the MPC control output current is 0.021%. The circulating

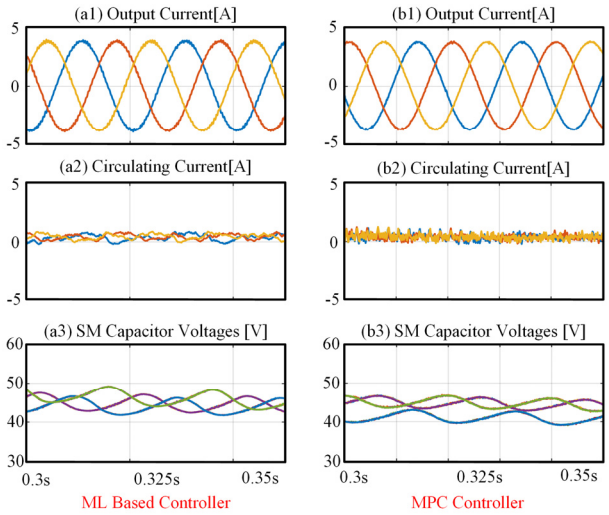

Fig. 5. The experimental results of ML MPC and traditional MPC

currents are suppressed by both control methods which are shown in Fig. 5 (a2) and (b2). The capacitor voltages are shown in Fig. 5 (a3) and (b3), the capacitors are sorted and balanced by the sort & select algorithm [12].

B. Dynamic Performance

Fig. 6 shows the dynamic performance when the reference amplitudes are suddenly increased and decreased. In Fig. 6 (a1), the output current references are suddenly stepped from 2A to 4A, the proposed ML controller can accurately follow the changed references in a short period of time. The output currents are suddenly decreased from 4A to 2A, which is shown in Fig. 6 (a2).

Fig. 7 shows the dynamic performance when the frequency of output current is changed. In Fig. 7 (a1), the frequency of output current is suddenly decreased from 50Hz to 20Hz. In Fig. 7 (a2), the frequency is increased from 20Hz to 40Hz. The results verify that the proposed controller can control the output current in different frequencies, which is an advantage

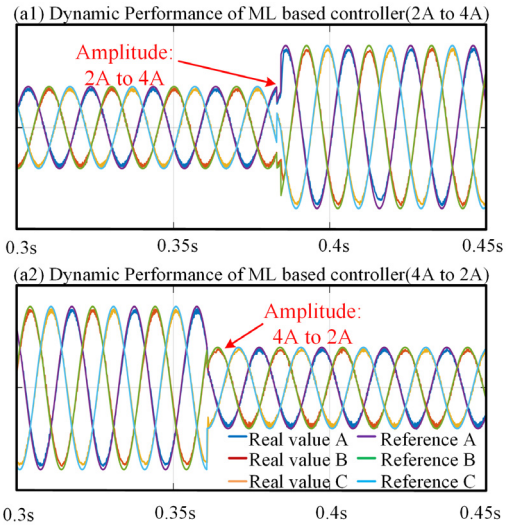

Fig. 6. Output Current dynamic.

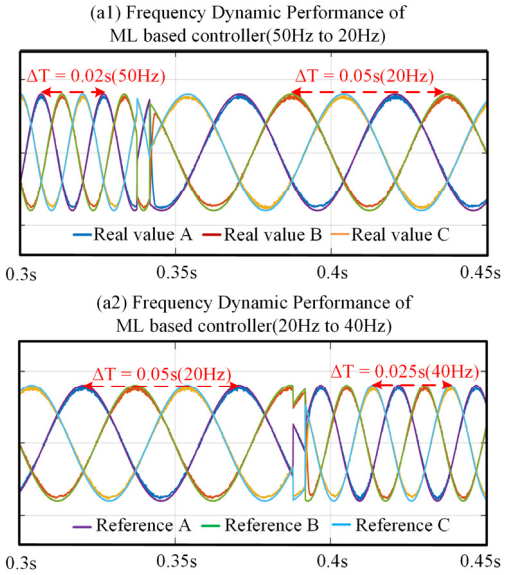

Fig. 7. Output Current frequency dynamic.

TABLE II
TRAINING PERFORMANCE

Number of Neurons	Training Time	MSE
4	2:15:56	0.302
6	2:52:58	0.199
9	3:26:54	0.177

TABLE III
COMPUTATIONAL BURDEN

	ML	Fast MPC	MPC
Mean Turnaround Time (μs)	1.123	1.615	9.790
Max Turnaround Time (μs)	1.252	1.788	9.690
Min Turnaround Time (μs)	1.070	1.561	9.947

comparing to traditional PI/PR controller because PI/PR controller need to set a specific working frequency or to extract the dq components from PLL [16], [17].

C. Performance with different neuron numbers.

The influence of the neuron numbers of the trained networks is introduced in this subsection. Table II shows the training performance of the trained networks with different neuron numbers. MSE is the mean squared error, a lower MSE means a better training performance. When the neuron number is 9, the best performance is achieved (lowest MSE).

Fig. 8 shows the experimental results of the trained networks with different neuron numbers. Those three networks all can achieve good performance, the experimental results show that this ML controller is not under a specific structure that a good control effect can be achieved

D. Performance with different data size

The size of the training data influences the control performance of the proposed controller. Fig. 9 shows the output current results and the tracking errors of the trained networks. The definition of the testing error is as below:

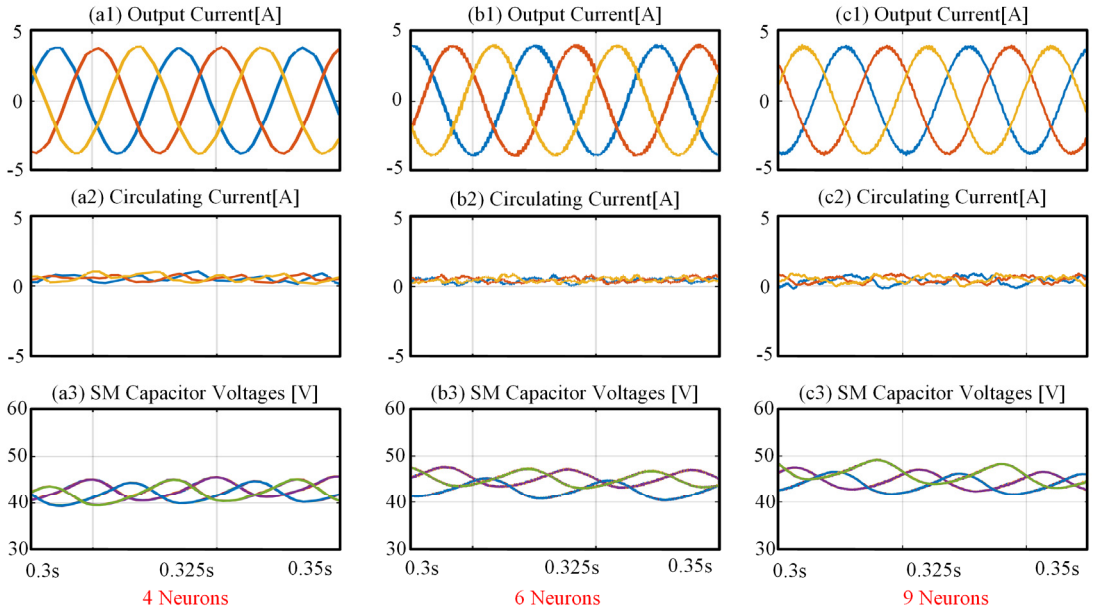

Fig. 8. Experimental Results of ML controller with different neuron numbers.

$$TrackingError = (1 - \frac{V_{ispp}}{V_{isrefpp}}) \times 100\% \quad (8)$$

where V_{ispp} is the peak to peak value of the output current, $V_{isrefpp}$ is the peak to peak value of the output current reference.

In Fig. 9, when the data size is low (4860 and 22500), the tracking errors are unacceptable (11.18% and 13.46% respectively). When the data size is increased to 249018, the tracking error is reduced to 2.61%. When the data size is further increased to 4889808, the tracking error is further reduced to 1.97%. Finally, when the data number is 31320432, the tracking error is below 1%. So in this letter, we recommend each input variable should be sampled at least 10 points for the whole variable range, and the recommended training error should below 1%.

E. Computational Burden

The computational burden can be estimated by the calculation number of the controllers [19]. The calculation number of traditional MPC in [18] is $C_8^4 = 70$ because the this MPC algorithm will select 4 out of 8 submodules to be inserted. All those insertion conditions need to be calculated and predicted by the MPC [4]. The calculation number of the fast MPC with experimental delay compensation algorithm in [7] is $4^2 = 16$ because it has 2 loops, each loop has 4 vectors to predict. And the calculation number of the proposed ML based controller is 9 because it has 9 neurons in the hidden layer [19]. Thus, the traditional MPC's calculation number is almost 8 times the ML based controller's calculation number, and the calculation number of MPC controller is 43.75% higher than the ML controller' s calculation number.

The computational cost of the proposed ML based controller is very small because the pre-trained ANN structure. Thus this method can be easily implemented in DSP or dSPACE controller. The computation cost of the MMC controllers can be measured by the dSPACE Profiler. Table III shows the computational burden in dSPACE platform of the proposed ML controller, the fast MPC method in [7], and the traditional MPC method in [18]. From Table III, the mean turnaround time of the traditional MPC is 9.790 μs which is almost 8 times the mean turnaround time of the proposed ML controller (1.123μs). And also, the mean turnaround time of the computational efficient MPC is 1.615μs which is still 49.2% higher than the proposed ML-based controller.

F. ML Based Method VS Lookup Table

Since the ANN is to emulate the deterministic relationship of MPC, lookup table is another opinion to represent this deterministic relationship. In this section, we discuss the advantages of ML based compare to lookup table method.

Once the network with suitable structure is trained, its evaluation is computationally light as it takes only around 1.1 μsec to generate the output signals. Interestingly, if the same amount of data as in the ANN training set is used to try and create a look-up table, the system runs out of memory. For instance, the data size we used as a training set is 31320432, and the system was not able compile such a huge amount data. Therefore, it can be concluded that due to large data size, ML methods are suitable for use for fast real time applications as opposed to lookup tables.

G. Performance of Unseen Input data

The ML network is trained by the data with a given range. In this subsection, the performance of the unseen input data performance is discussed. In this letter, the training range of the output current reference is [-6A, 6A]. When the output current reference exceeds [-6A, 6A], this reference is unseen data. We tested 2 unseen output current references: 7A and 9A

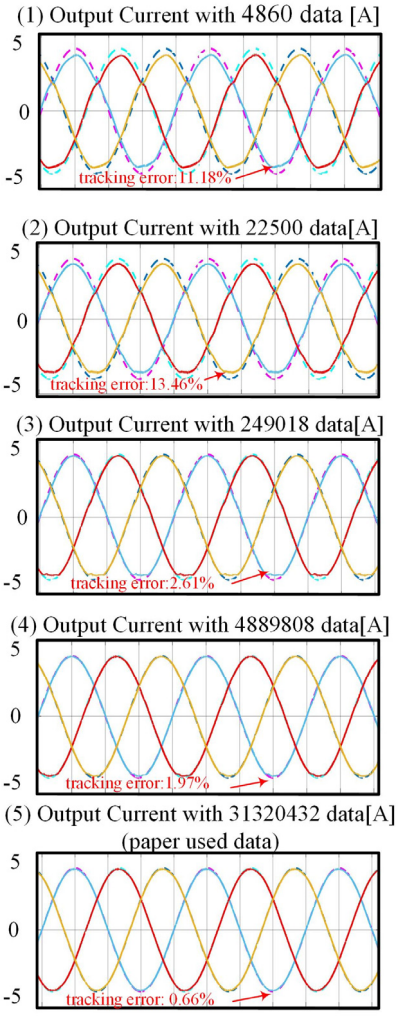

Fig. 9. Results of ML controller with different size of data

amplitudes of the output current. The results are shown in Fig. 10.

From Fig. 10, two unseen output current references results are shown. In Fig. 10(a), the output current reference amplitude is 7A, which is 1A above the training range [-6A, 6A]. Both the MPC and ML based controller can track the reference precisely. These results prove the ML network has the ability to work properly even under the unseen data, which is slightly beyond the training range.

However, when the unseen output reference is 9A, which is 50% above the training range, Fig. 10 (b) shows the ML based controller cannot track the reference precisely. To prevent this problem, we suggest the original range should be at least 30% higher than the rated condition.

IV. Conclusion

This paper proposes a machine learning based MPC controller for MMCs. The artificial neural network is offline trained by the data extracted from the traditional MPC algorithm. The experimental results show that this artificial neural network can control the MMCs with a good steady state and fast dynamic performance, but at the same time with a low computational burden. In future, this method can simulate more complex model predictive control algorithms and reduce further the computational burden.

References

[1] L. Harnefors, A. Antonopoulos, S. Norrga, L. Angquist, and H. P. Nee, "Dynamic analysis of modular multilevel converters," *IEEE Trans. Ind. Electron.*, vol. 60, no. 7, pp. 2526–2537, 2013.

[2] S. Vazquez et al., "Model predictive control: A review of its applications in power electronics," *IEEE Ind. Electron. Mag.*, vol. 8, no. 1, pp. 16–31, Mar. 2014.

[3] J. Böcker, B. Freudenberg, A. The and S. Dieckerhoff, "Experimental Comparison of Model Predictive Control and Cascaded Control of the Modular Multilevel Converter," in *IEEE Trans. Ind. Electron*,

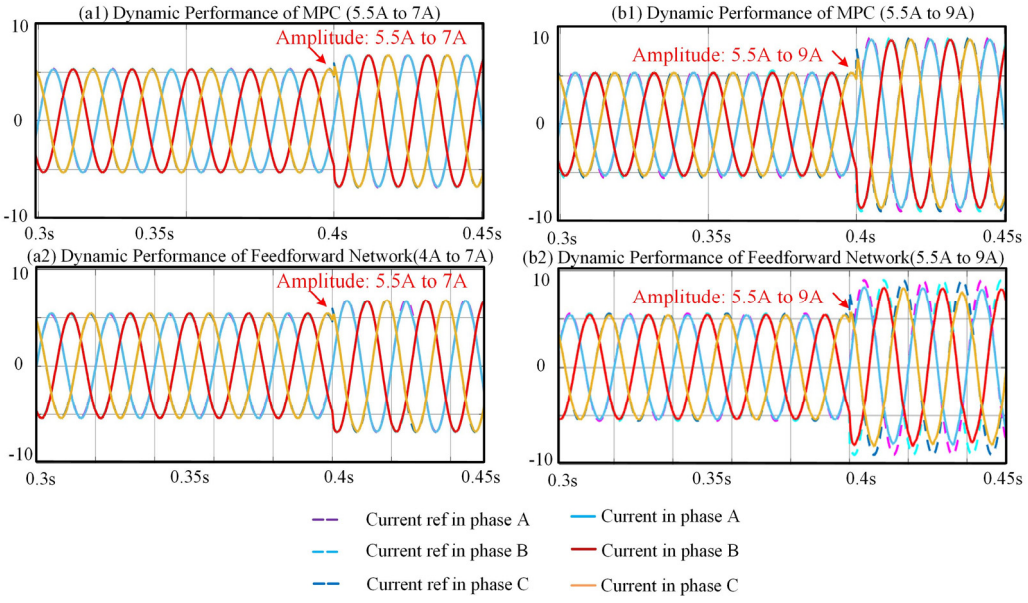

Fig. 10 The results when the output current references exceed the training range.

vol. 30, no. 1, pp. 422-430, Jan. 2015。

[4] A. Dekka, B. Wu, V. Yaramasu, R. L. Fuentes, and N. R. Zargari, “Model Predictive Control of High-Power Modular Multilevel Converters-An Overview,” *IEEE J. Emerg. Sel. Top. Power Electron.*, vol. 7, no. 1, pp. 168-183, March 2019.

[5] Z. Li, R. Lizana, A. V. Peterchev and S. M. Goetz, "Distributed balancing control for modular multilevel series/parallel converter with capability of sensorless operation," in Proc. IEEE Energy Convers. Congr. Expo. (ECCE), Sep 2017, pp. 1787-1793.

[6] X. Liu et al., "A Fast Finite-Level-State Model Predictive Control Strategy for Sensorless Modular Multilevel Converter," *IEEE J. Emerg. Sel. Topics Power Electron,* Early Access.

[7] Z. Gong, P. Dai, X. Yuan, X. Wu, and G. Guo, “Design and Experimental Evaluation of Fast Model Predictive Control for Modular Multilevel Converters,” *IEEE Trans. Ind. Electron.*, vol. 63, no. 6, pp. 3845–3856, 2016.

[8] Bishop C M. Pattern recognition and machine learning. springer, 2006.

[9] T. Dragicevic, P. Wheeler, and F. Blaabjerg, “Artificial Intelligence Aided Automated Design for Reliability of Power Electronic Systems,” *IEEE Trans. Power Electron.*, vol. 34, no. 8, pp. 7161–7171, 2019.

[10] S. Wen, Y. Wang, Y. Tang, Y. Xu, P. Li and T. Zhao, "Real-Time Identification of Power Fluctuations Based on LSTM Recurrent Neural Network: A Case Study on Singapore Power System," *IEEE Trans. Ind Inform*, vol. 15, no. 9, pp. 5266-5275, 2019.

[11] P. Cortes, J. Rodriguez, C. Silva, and A. Flores, “Delay Compensation in Model Predictive Current Control of a Three-Phase Inverter,” *IEEE Trans. Ind. Electron.*, vol. 59, no. 2, pp. 1323–1325, 2012.

[12] Siemaszko D. “Fast sorting method for balancing capacitor voltages in modular multilevel converters.“ IEEE Trans. Power Electron., vol. 30, no. 1, pp. 463-470, 2014.

[13] YY. Chen, YH. Lin, CC. Kung, MH. Chung, and I Yen . "Design and implementation of cloud analytics-assisted smart power meters considering advanced artificial intelligence as edge analytics in demand-side management for smart homes.", in *Sensors*, vol 19, no 9, 2019.

[14] C. George. "Approximations by superpositions of a sigmoidal function." Mathematics of Control, in *Signals and Systems* vol. 2, pp. 183-192, 1989.

[15] K. Hornik, "Approximation capabilities of multilayer feedforward networks." in *Neural networks*, vol. 4, no. 2, pp.251-257, 1991.

[16] J. Pou, S. Ceballos, G. Konstantinou, V. G. Agelidis, R. Picas, and J. Zaragoza, “Circulating current injection methods based on instantaneous information for the modular multilevel converter,” *IEEE Trans. Ind. Electron.*, vol. 62, no. 2, pp. 777–788, 2015.

[17] K. Sharifabadi, L. Harnefors, H. Nee, S. Norrga, and R. Teodorescu, "Dynamics and Control," in *Design, Control, and Application of Modular Multilevel Converters for HVDC Transmission Systems* , IEEE, 2016, pp.133-213.

[18] J. Qin and M. Saeedifard, “Predictive control of a modular multilevel converter for a back-to-back HVDC system,” *IEEE Trans. Power Deliv.*, vol. 27, no. 3, pp. 1538–1547, 2012.

[19] Novak M, Dragicevic T. "Supervised imitation learning of finite set model predictive control systems for power electronics." *IEEE Trans. Ind. Electron*, 2020, early access.

Neural Network based Model Predictive Controllers for Modular Multilevel Converters

Songda Wang, *Student Member*, Tomislav Dragicevic, *Senior Member, IEEE,* Yuan Gao, *Student Member, IEEE,* and Remus Teodorescu, *Fellow, IEEE*

***Abstract*--Modular multilevel converter (MMC) has attracted much attention for years due to its good performance in harmonics reduction and efficiency improvement. Model predictive control (MPC) based controllers are widely adopted for MMC because the control design is straightforward and different control objectives can be simply implemented in a cost function. However, the computational burden of MPC imposes limitations in the control implementation of MMC because of many possible switching states. To solve this, we design machine learning (ML) based controllers for MMC based on the data collection from the MPC algorithm. The ML models are trained to emulate the MPC controllers which can effectively reduce the computation burden of real-time control since the trained models are built with simple math functions that are not correlated with the complexity of the MPC algorithm. The ML method applied in this study is a neural network (NN) and there are two types of establishing ML controllers: NN regression and NN pattern recognition. Both are trained using the sampled data and tested in a real-time MMC system. A comparison of experimental results shows that NN regression has a much better control performance and lower computation burden than the NN pattern recognition.**

***Index Terms*--Modular multilevel converter (MMC), Model predictive control (MPC), control design, neural network (NN), pattern recognition**

I. Introduction

MODULAR multilevel converter (MMC) is one of the most attractive topologies for high voltage direct current (HVDC) applications due to its merits: low harmonics, high efficiency, and good fault tolerance ability [1-4]. However, the complicated structure of the MMC makes it challenging to control effectively.

In order to control the MMC to achieve its merits, a lot of different control methods have been proposed, from the conventional proportional-integral controller (PI) [5] / proportional-resonant (PR) control [6] to non-linear sliding mode control [7], and to model predictive control (MPC) [8], [9]. Out of different control methods, the model predictive control (MPC) is widely accepted by power electronics engineers because of its merits: simplicity, fast dynamic response, easy inclusion of nonlinearities, and others [10].

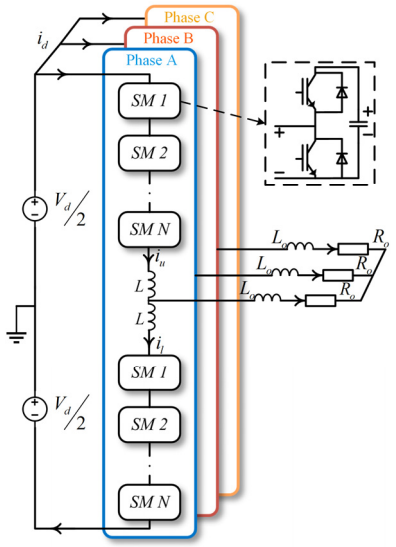

Fig. 1. MMC diagram.

Many earlier papers have studied the MPC based MMC controllers [11], [12]. MPC is a discrete model-based control method for multi-input-multi-output (MIMO) system based on the cost functions, established based on the predicted behavior of the system in accordance with its discrete dynamic model. For MMC in particular, by minimizing the cost function in every sampling step, the output current and circulating current can be controlled and the submodule voltages can also be balanced at the same time [9]. However, the main drawback of the MPC MMC is the heavy computational burden, which becomes particularly limiting when the number of submodules is high [8]. Namely, the MPC algorithm should manage to evaluate all the possible capacitor voltage combinations in one sampling period. However, as the number of modules rises, the amount of calculations rises rapidly in three-phase optimal switching state method in [13], and also in three-phase optimal switching vector method in [14]. In order to reduce this burden, researchers have proposed many modifications to the conventional MPC algorithms [15-17]. However, all these methods did not change the core feature of the MPC: the MPC algorithm exhaustively evaluates the switching signals online to

Manuscript received May 5, 2020; revised July 22, 2020; accepted August 28, 2020. (Corresponding author: Yuan Gao.)
S. Wang, and R. Teodorescu are with the Department of Energy Technology, Aalborg University, Aalborg, Denmark. (email: sow@et.aau.dk; ret@et.aau.dk).
Y. Gao is with the Department of Electrical and Electronic Engineering. University of Nottingham, Nottingham, UK. (email: Yuan.Gao@nottingham.ac.uk).
T. Dragicevic is with the Department of Electrical Engineering, Technical University of Denmark, Copenhagen, Denmark. (email: tomdr@elektro.dtu.dk)

This article has been accepted for publication in a future issue of this journal, but has not been fully edited. Content may change prior to final publication. Citation information: DOI 10.1109/TEC.2020.3021022, IEEE Transactions on Energy Conversion

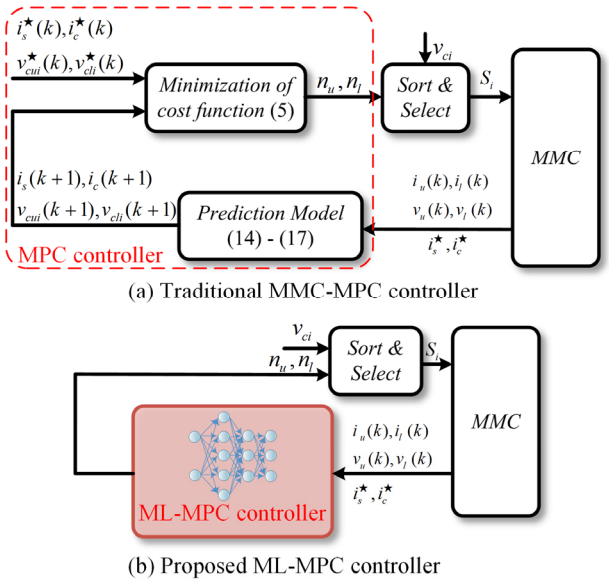

Fig. 2. The comparison of ML MPC and traditional MPC.

find the one that minimizes some predefined cost function. This online optimization method leads to a high computational burden when the number of possible switching signals is high. And such computational burden reduction methods are very complex to implement and require very high-level math expertise [18].

Applying machine learning (ML) to emulate the MPC can help to reduce the computational burden. In [19], a supervised learning framework is proposed to emulate an MPC with reduced computational complexity. This article introduces the methodology of using machine learning models to simulate MPC. Paper [20] also introduces the same idea. Paper [21] extends this method to control the three-phase inverter with an output LC filter. By this method, a lower THD and a better steady and dynamic performance are achieved. In [22], a lower computational burden is achieved by machine learning based controller in a two-level converter, the performance is the same as the performance with model predictive control. However, such techniques have thus far mainly been proposed for robotic systems and very simple power converters. To best of our knowledge, an MPC-based machine learning imitator has not yet been developed nor experimentally tested for the MMC.

ML is a cutting-edge technology that has been widely used for establishing non-parametric models of various complicated power electronic processes using solely the process data. Several papers have used neural network (NN) to solve power electronics problems, e.g. identifying power system's active power fluctuations in real-time [23]; automatically designing the power electronics system for reliability [24]; online weighting factor adjustment for predictive torque control of induction machines fed by 3L-NPC converters [25]. ML is a technology which can learn from the sample data, also known as "training data", which could be from the real world or a software. ML can change its memory based on different settings. All machine learning technologies build desired math models based on the training data in order to make predictions or decisions without being explicitly programmed. Therefore, the training and prediction performance of ML is highly related to the quality of the data. For now, the data that ML can process is getting larger because the computing power of modern computers is getting stronger with the development of computing technology [26].

There are different algorithms in machine learning, such as regression, decision tree, NN, and support vector machine. In this paper, we only use neural network but focus on two different types, regression [22] and pattern recognition [27]. This category is due to their output types: outputs of NN regression are usually continuous but NN pattern recognition only has two or more features as the output. Initially, NNs were proposed to simulate the structure of human brain. NN could have one or several hidden layers, where each layer has several neurons. Every neuron is a node that determines the input-output relationship of the signal. NN can be trained to a nonlinear model using a proper data set. Such a general nonlinear model can approximate any given input-output function with arbitrary precision [24], [28].

In this paper, two ML-based emulations of the MPC algorithm are designed to control the MMC with much lower computational burden compared to the original MPC and, one emulation (NN regression) achieves excellent control performance. The ML models are trained offline and such trained models can either be used offline or implemented in a digital microprocessor for online operation. In fact, we show in this paper that the computational burden of the NN regression model, that perfectly emulates the MPC controller, is much lower than the MPC itself.

II. System Model

In this section, the structure and working principle of MMC will be introduced. The topology of half bridge MMC will be explained briefly and the large signal model of MMC will be derived.

A. MMC Introduction

Fig. 1 shows the topology of a half-bridge submodule MMC. Normally, an MMC consists of three phases, where each phase has two arms: upper and lower arm. Each arm is comprised of N series-connected half bridge submodules, and an arm inductance L_{arm}[29]. The submodule capacitor voltage is kept close to the rated dc voltage by the MMC controller. In this way, the single submodule can be controlled as a voltage source by inserting or bypassing the submodule. The MMC output AC voltage can be controlled by changing the number of inserted submodules [30].

B. Dynamics of MMC

The direction of the upper arm current and lower arm current is shown in Fig. 1. By applying the Kirchhoff's voltage law to the MMC circuit, the MMC dynamic equations can be derived as follows:

$$\frac{V_d(t)}{2} - v_{cuk}(t) - L_{arm}\frac{di_{uk}(t)}{dt} = R_s i_{sk}(t) + L_s\frac{di_{sk}(t)}{dt} \qquad (1)$$

$$\frac{V_d(t)}{2}-v_{clk}(t)-L_{arm}\frac{di_{lk}(t)}{dt}=-R_s i_{sk}(t)-L_s\frac{di_{sk}(t)}{dt} \tag{2}$$

where V_d is DC line voltage, v_{cuk} and v_{clk} are the upper and lower arm voltage in phase *k* respectively, i_{uk} and i_{lk} are the upper and lower arm current in phase *k* respectively. *k* means the phase number, *k=0, 1, 2* (0 for phase a, 1 and 2 for b and c respectively); R_s and L_s are the output resistance and inductance respectively; i_{sk} is output current.

We define the output current i_{sk} and circulating current i_{ck}:

$$i_{sk}(t)=i_{lk}(t)-i_{uk}(t) \tag{3}$$

$$i_{ck}(t)=\frac{1}{2}\left[i_{uk}(t)+i_{uk}(t)\right]-\frac{1}{3}i_d(t) \tag{4}$$

The dynamic equations of the output ac current and circulating current can be derived from (1)-(4):

$$\frac{di_{sk}(t)}{dt}=\frac{1}{L+2L_0}[v_{clk}(t)-v_{cuk}(t)-2R_0 i_{sk}(t)] \tag{5}$$

$$\frac{di_{ck}(t)}{dt}=\frac{1}{2L}[v_d(t)-v_{clk}(t)-v_{cuk}(t)] \tag{6}$$

When the submodule is in on state, the dynamic of submodule capacitor voltage can be expressed by the relation of capacitance and the arm current:

$$\frac{du_{cuki}(t)}{dt}=\frac{i_{uki}}{C_{SM}} \qquad \frac{du_{clki}(t)}{dt}=\frac{i_{lk}}{C_{SM}} \tag{7}$$

where u_{cuki} and u_{clki} are the *i*th upper and lower submodule capacitor voltages respectively (*i=1…N*); C_{SM} is submodule capacitance.

III. Model Predictive Control of MMCs

In this section, the working principle of MPC for MMCs is introduced by using the dynamic equations in Section II. This MPC model will be used to collect the input/output sample data for training the NN-based controllers in Section IV.

A. MMC Control Scheme

Taking one-phase MMC as an example, the conventional MPC for MMCs can be introduced step by step as follows, where the detailed information of this MPC method is described in [17]. The control scheme of MPC MMC is shown in Fig.2 (a), and is executed in the following sequence:

1) Measurement of MPC input variables;
2) Prediction of the output current and circulating current for the next sampling period for every possible inserted submodule number;
3) Creation of the cost function including the information of circulating current and output current;
4) Selection of the best upper/lower arm inserted submodule number that minimizes the cost function;
5) Application of the optimized upper/lower arm inserted submodule number.

B. MMC Model Predictive Control Model

Based on the Euler forward equation in (8), the dynamic equations of MMCs can be transferred to the discrete mathematical model [17] :

$$\frac{dx(t)}{dt}\approx\frac{x(k+1)-x(k)}{T_s} \tag{8}$$

where $x(k+1)$ and $x(k)$ are the variable of at time instant *k+1* and *k* respectively; T_s is the sampling interval.

The dynamic equations (5)-(8) can be transferred to a discrete model by (8)

$$\begin{cases} i_s(k+1)=\mathbf{A}[(n_l(k)\cdot v_{cl}(k+1)-n_u(k)\cdot v_{cu}(k+1))/N]+\mathbf{B}i_s(k) \\ \mathbf{A}=2T_s/(L_{arm}+2L_s),\mathbf{B}=1-2T_sR_s/(L_{arm}+2L_s) \end{cases} \tag{9}$$

$$\begin{cases} i_c(k+1)=\mathbf{C}[V_d-(n_l(k)\cdot v_{cl}(k+1)+n_u(k)\cdot v_{cu}(k+1))/N]+i_c(k) \\ \mathbf{C}=T_s/(2L_s) \end{cases} \tag{10}$$

$$v_{cu}(k+1)=\frac{n_u(k)\cdot T_s}{C_{SM}}i_u(k)+v_{cu}(k) \tag{11}$$

$$v_{cl}(k+1)=\frac{n_l(k)\cdot T_s}{C_{SM}}i_l(k)+v_{cl}(k) \tag{12}$$

In order to reduce the computation burden of MPC, the sorting and selecting of submodule capacitor voltages are achieved by independent sorting and balancing block, which is outside of the MPC algorithm. Fig. 2 shows this block. The sorting and balancing method of MMC capacitor voltages is introduced in [2] and [30].

The cost function used in this case is:

$$g=w_1\cdot|i_s^{\star}(k)-i_s(k+1)|+w_2\cdot|i_c^{\star}(k)-i_c(k+1)| \tag{13}$$

where w_1, w_2 are weighing factors for i_s and i_c respectively. $i_s^{\star}$, $i_c^{\star}$ are the references of output current and circulating current, respectively. In this paper, $w_1=w_2=1$.

C. Delay Compensation

In order to compensate the delay in the experimental setup, the delay compensation method described in [31] is applied. The key idea is to estimate the controlled variables (circulating current and output current) in time instant *k+1* by considering the applied control signals and then predict the variables in time instant *k+2* for all the impossible control signals. In this way, the cost function is minimized by applying the best switching signals in time *k+2*. The new discrete mathematical equations are introduced in (14)-(17):

$$\begin{cases} i_s(k+2)=\mathbf{A}[(n_l(k+1)\cdot v_{cl}(k+2)-n_u(k+1)\cdot v_{cu}(k+2))/N] \\ \qquad +\mathbf{B}i_s(k+1) \\ \mathbf{A}=2T_s/(L_{arm}+2L_s),\mathbf{B}=1-2T_sR_s/(L_{arm}+2L_s) \end{cases} \tag{14}$$

$$\begin{cases} i_c(k+2)=\mathbf{C}[V_d-(n_l(k+1)\cdot v_{cl}(k+2)+n_u(k+1)\cdot v_{cu}(k+2))/N] \\ \qquad +i_c(k+1) \\ \mathbf{C}=T_s/(2L_s) \end{cases} \tag{15}$$

This article has been accepted for publication in a future issue of this journal, but has not been fully edited. Content may change prior to final publication. Citation information: DOI 10.1109/TEC.2020.3021022, IEEE Transactions on Energy Conversion

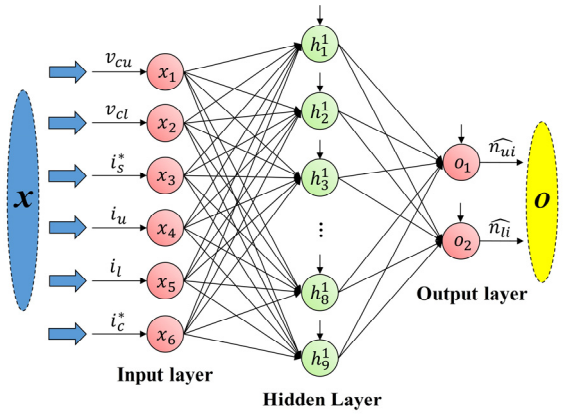

(a) NN regression controller.

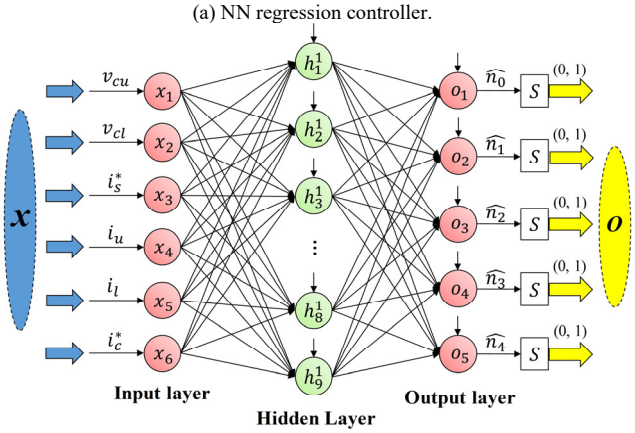

(b) NN pattern recognition controller

Fig. 3. Deployment of the proposed two NN-based controllers. Both have 3 layers with 9 neurons in the hidden layer. Weights and biases are omitted for simplicity.

$$v_{cu}(k+2)=\frac{n_u(k+1)\cdot T_s}{C_{SM}}i_u(k+1)+v_{cu}(k+1) \tag{16}$$

$$v_{cl}(k+2)=\frac{n_l(k+1)\cdot T_s}{C_{SM}}i_l(k+1)+v_{cl}(k+1) \tag{17}$$

D. Deterministic input-output relationship of MPC

Let us consider one digital sampling interval (T_s) of MPC as an example. During this interval, set of measured input variables are transferred to the MPC algorithm that accordingly predicts the output currents and circulating currents for all possible switching signals and applies the one that minimizes the cost function. An important observation is that this process is completely deterministic, i.e. for the same set of input variables (i.e. measurements) and a given cost function, the outputs (inserted submodules) will always be the same. In this context, while the conventional MPC uses exhaustive search in every time instant to identify the optimal actuation, this is not necessary. On the contrary, it should be possible to represent the deterministic input-output relationship with more computationally efficient structure. Then, we could achieve the same control effect as the MPC, but with a lower online computational burden. This is indeed a key idea of this paper.

In the following parts, we will introduce two offline NN models to represent the deterministic relationship between inputs and outputs in the MPC algorithm.

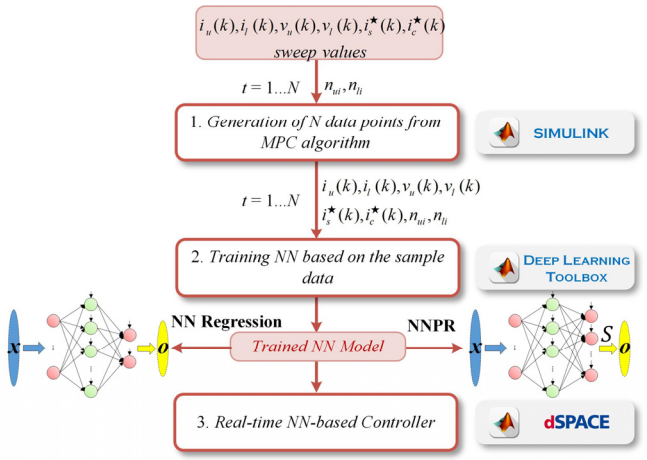

Fig. 4. Implement procedure of the proposed NN-based controller.

IV. Neural Network Based Controllers for MMCs

A. Introduction of the Neural Network Method

From Fig. 2, we can see the difference between the traditional MPC MMC and the NN controlled MMC. That is, the NN-based controller replaces the MPC controller block. The NN inputs include six elements: upper arm voltage v_{cu}, lower arm voltage v_{cl}, output current reference $i_s^\star$, upper arm current i_u, lower arm current i_l and circulating current reference $i_c^\star$. The upper arm insert number n_{ui} and lower arm insert number n_{li} are two outputs for the proposed NN controllers.

As mentioned, this paper represents two different neural networks: NN regression and Neural Network Pattern Recognition (NNPR). Though the training data collected from MPC algorithm (Section III) are the same for both networks, their data processing varies due to the different requires of NN outputs. NN regression has no limits for the output elements but NNPR requires the elements must be integer even can only be 0 or 1 in some applications. The following two subsections will introduce the two NN controllers in detail.

B. Proposed two Model Predictive Controllers for MMCs

For the NN regression controller, it is designed as a 3-layer NN whose inputs/outputs are directly using the same design with the training data (shown in Fig. 3(a)). Thus, this controller represents the following relation:

$$(n_{ui},n_{li})=F(v_{cu},v_{cl},i_s^\star,i_u,i_l,i_c^\star) \tag{18}$$

It is noted that the two outputs should be integer and their values could be 0, 1, 2, 3 or 4 in this study, thus the outputs of this controller should be rounded up and limited to these 5 features.

In contrast, NNPR controller is a novel design. As shown in Fig. 3(b), there are 5 elements in the NN output which corresponds to the 5 features instead of n_{ui},n_{li} in Fig. 3(a). The purpose of this design is to comprehensively explore the value space ([0, 4]) of n_{ui},n_{li} and to give an accurate prediction for MMC control. Based on that, according to the value of n_{ui},n_{li}, each element in output can be set 0 or 1 for NNPR training.

This article has been accepted for publication in a future issue of this journal, but has not been fully edited. Content may change prior to final publication. Citation information: DOI 10.1109/TEC.2020.3021022, IEEE Transactions on Energy Conversion

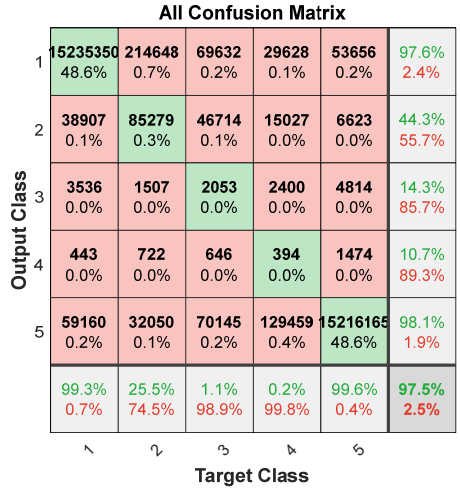

(a) NNPR training for n_{ui}

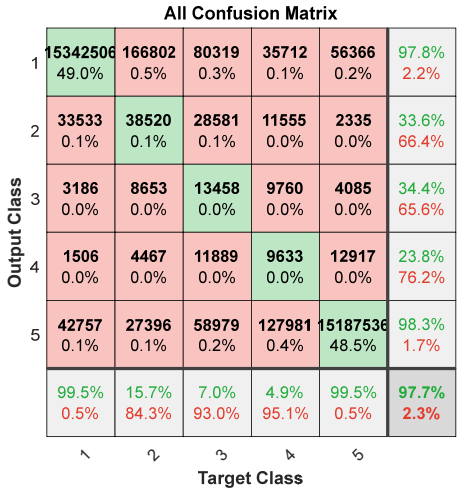

(b) NNPR training for n_{li}

Fig. 5. Confusion matrix of NNPR training.

Therefore, the NNPR controller represents this relation:

$$(n_0, n_1, n_2, n_3, n_4) = F(v_{cu}, v_{cl}, i_s^*, i_u, i_l, i_c^*) \quad (19)$$

where n_i $(i = 0,1,2,3,4)$ denotes the NNPR value that could quantify the probability of "insert number equals i" because NNPR training can limit all predictions into (0, 1) by the Softmax function [22]. Softmax function, also known as normalized exponential function, takes as input a vector (the output vector of NNPR in this case) and normalizes it into a (0, 1) probability distribution of each component in this vector. It is used in the final layer of the NNPR controller as a classifier.

As the NNPR generates the probabilities for 5 features, this controller for the studied MMC should use 2 networks, one for n_{ui} and the other for n_{li}.Besides, after getting the output vector $(n_0, n_1, n_2, n_3, n_4)$ in each network, 5 feature values should be compared and the largest one n_{j} determines that the final resulting insert number is j.

Then the neuron network structure should be selected. Firstly, we select one-hidden-layer structure thus we only need to select the neuron network number in the hidden layer. Rule of a thumb is used to determine the maximum and the minimum number of neurons [32], and then select a relatively high number of neurons to achieve better fitting performance within the recommended neuron number range:

Minimum neuron number:

$$0.5(N_{in} + N_{out}) = 4 \quad (N_{in} = 6, N_{out} = 2) \quad (6)$$

Maximum neuron number:

$$2N_{in} = 12 \quad (7)$$

where N_{in} is the input unit number $N_{in} = 6$, N_{out} is the output unit number $N_{out} = 2$.

In this paper, we selected 9 neurons in the hidden layer.

C. Collection and Training Steps

To clarify the training procedure, all the steps are shown in Fig. 4. Each step is further elaborated as follows.

1) Generation of N data samples from the MPC algorithm: The data can be extracted solely from the MPC algorithm block (only the MPC controller in MMC is used to generate the training data). The sweep values of input data are v_{cu}, v_{cl} : [0:10:350], which means the range of upper and lower arm voltages is from 0 to 350V with the gap of 10V, therefore each arm voltage has 36 data points; $i_s^\star$: [-6:1:6], 13 data points; i_u, i_l : [-6:1:6], 13 data points each; $i_c^\star$:[0:0.2:2], 11 data points. Therefore, the training data includes around 31.32 million samples but their collection time is only 76 *secs* based on the MPC algorithm.
2) NN Model Training: In order to train NN and set stop conditions, the samples were randomly divided into three data sets, i.e. the training set (70 % of data), the validation set (15 % of data), and the testing set (15 % of data). The extracted data was then used to train the desired NN controllers, which represent the afore-mentioned relationships between input variables and output variables. A workstation PC with Dual Intel Xeon Silver 4110 CPU is used to train the NN controllers, i.e. a regression NN and two pattern NNs. All networks have the same structure in the hidden layer and are trained for 800 iterations. Their training tool is the MATLAB Deeping Learning Toolbox.
3) After getting the trained NNs, they can be used to calculate n_{ui}, n_{li} of MMC in a real-time simulation or experiment. As discussed in the last subsection, the outputs of the two networks should be typically processed to give the final accurate n_{ui}, n_{li}, with which the output current and the circulating current can be controlled to track their

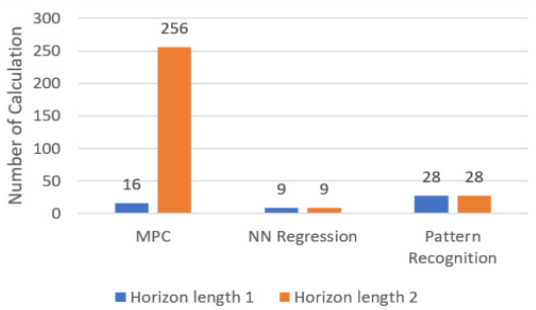

Fig. 6. Comparison of the number of calculations and the horizon length.

This article has been accepted for publication in a future issue of this journal, but has not been fully edited. Content may change prior to final publication. Citation information: DOI 10.1109/TEC.2020.3021022, IEEE Transactions on Energy Conversion

TABLE I MMC PARAMETERS IN EXPERIMENT

	Experiment
Number of SMs per arm (N)	4
Rated DC voltage (v_d)	200 V
Nominal SM capacitance (C_{SM})	2000 μF
Nominal SM capacitor voltage (v_c)	50 V
Rated frequency (f)	50 Hz
Arm inductance (L_{arm})	10 mH
Sample frequency	10 kHz
Load inductance (L_s)	1.8mH
Load resistance (R_s)	10.8Ω

references in MMC.

D. *Training performance of two NN controllers*

To clearly show the training performance of the proposed NN controller, Fig. 5 gives two confusion matrixes obtained from the NNPR training in MATLAB (one for n_{ui}, the other for n_{li}). As discussed, there are 5 features/classes in each NNPR controller and for every feature, it is a 1-0 classification problem. Each row in Fig. 5 corresponds to an output class (i.e. n_0, n_1, n_2, n_3, n_4), and the columns are the target classes which are from the sample data. The green cells in the diagonal of the matrix show the number and percentage of correctly classified data points (at the final training iteration), while all other red cells show the incorrect classifications. Therefore, nearly 98% of the predictions are matched with sample data in the NNPR training. On the other hand, five light-grey blocks in the last column and the other five light-grey blocks in the last row show the specific prediction accuracies for every class/feature. As shown in Fig. 5, the 3rd and 4th classes (n_2, n_3) have very low accuracies for both NNPR nets. Then, we may adjust the

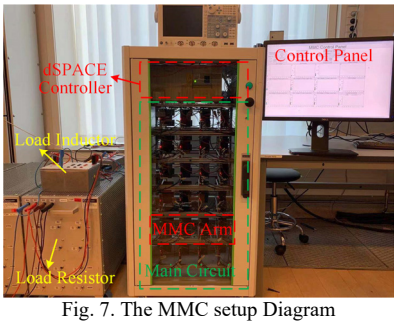

Fig. 7. The MMC setup Diagram

training data set of n_3 to pursue a better training performance. However, in this study, we did not further change the data of n_2, n_3 since all training data is obtained under certain conditions with sinusoidal references thus, it is very hard to manually determine which inputs can get n_2, n_3 data. In addition, amounts of n_2, n_3 data are relatively small (0.56% for n_{ui}, 0.62% for n_{li})). More importantly, the NNPR nets do not demonstrate good control performance in the experiment (see Section V) even though they both have excellent training performance. In contrast, the NN regression can reflect the MPC characteristic of n_{ui} and n_{li} properly because it trained n_{ui} and n_{li} in the same NN rather than two independent nets. Therefore, the confusion matrix can provide significant information for NN controller training analysis.

Regarding the trained NN regression controller, its performance needs to be additionally calculated based on the sample data because there are no classification results during the training process. Two outputs (Fig. 3(a)) should be rounded up into [0, 4] and then compared with the target classes of the sample. Then, we can also obtain the confusion matrixes for n_{ui} and n_{li}, their general accuracies are both around 93.2%, smaller

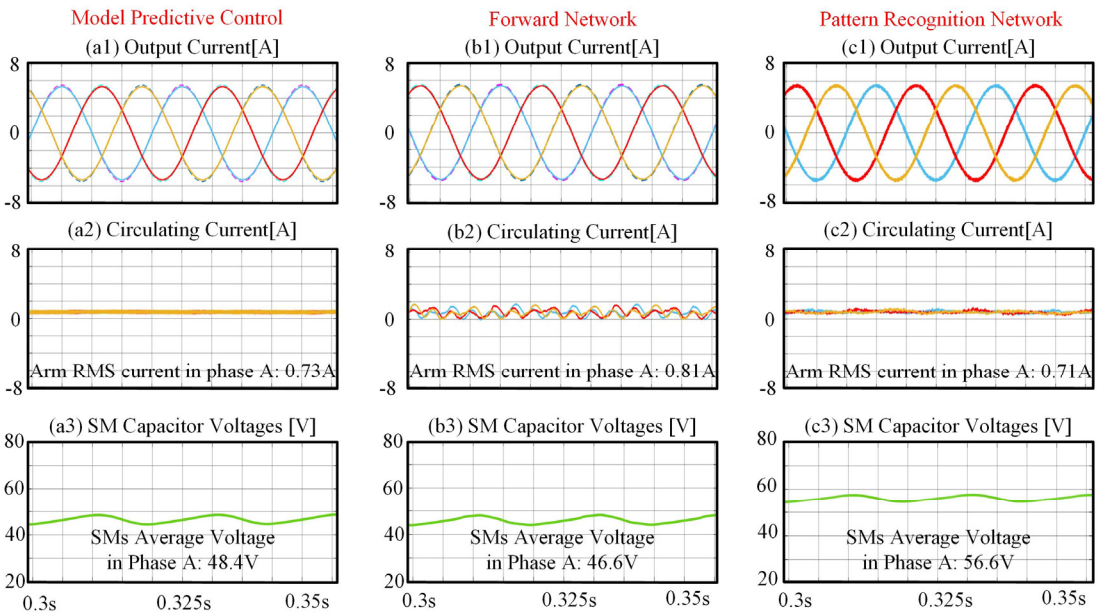

Fig. 8. Steady state performance of three controllers: (a) MPC controller, (b) NN regression controller, (c) NN pattern recognition controller.

This article has been accepted for publication in a future issue of this journal, but has not been fully edited. Content may change prior to final publication. Citation information: DOI 10.1109/TEC.2020.3021022, IEEE Transactions on Energy Conversion

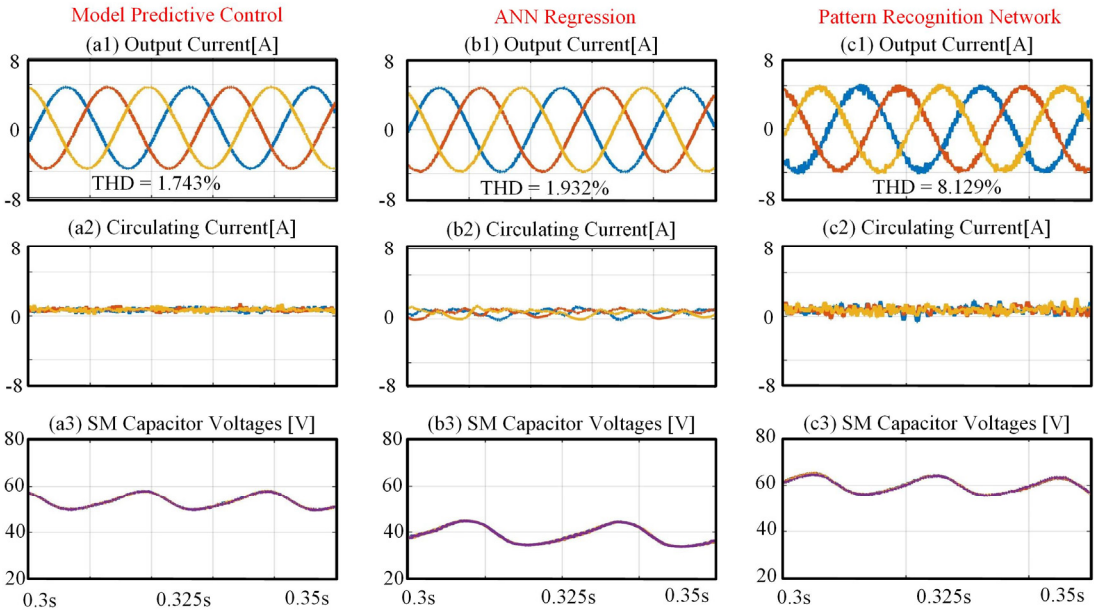

Fig. 9 Experimental Results of the 1). MPC, 2). NN Regression Network Method, and 3). Pattern Recognition Network

than NNPR. However, the prediction accuracy of n_2 using NN regression is 33.7% for n_{ui}, 34.9% for n_{li}, much higher than that of NNPR (1.1% for n_{ui}, 7.0% for n_{li}, see Fig. 5). The same phenomenon happens to n_1 and n_3: for example, the prediction accuracy of n_3 using regression is 27.3% for n_{ui}, 28.8% for n_{li} while, as shown in Fig. 5, we only got 0.2% for n_{ui}, 4.9% for n_{li} by using NNPR. Therefore, regarding the 2nd, 3rd and 4th classes, the prediction performance of NN regression is much better than NNPR. That is the main reason that NNPR performs very bad in the experimental regulation, see Section V.

In Fig. 6, the number of calculations and the horizon length results are shown, the number of calculations in conventional MPC control will significantly increase with horizon length. When the length is 1, the number of calculations is 16, however, the number of calculations increases to 256 when the length is 2. The NN based controllers have a small number of calculations no matter what the length is. Due to the different structure of different NN controllers, the number of calculations is different. The NN regression is 9, and NNPR is 14*2.

V. Verification Results

Two proposed NN controllers are verified in a real-time simulation model. The simulations and experiments are carried out in a three-phase MMC, with 4 half-bridge SMs per arm. The proposed controller is implemented in DS1006 from dSPACE. The experimental setup is shown in Fig. 7. The parameters of the simulation model and experimental setup are shown in TABLE I. The MMC block diagram is shown in Fig. 1 The controller structure is shown in Fig. 2(b). The input variables of the ML controller are: $v_{cu}, v_{cl}, i_u, i_l, i_s^\star, i_c^\star$. The output variables are the upper/lower arm inserted numbers of MMC. These inserted numbers are sent to the sort & select block for balancing the capacitor voltages. The detailed information about sort & select block is introduced in [2]. Setup Steady State Performance

Fig. 8 shows the simulation steady performance of the MPC controller, NN regression controller, and NN pattern recognition controller. From Fig. 8 (a1) to (a3), the three-phase output currents are controller to track their references: AC currents with 5.5A amplitudes. Regarding circulating current, the MPC and NNPR controller both have good circulating current reduction effect, but the NN regression controller has the worst results which are shown in Fig. 8 (b2). The RMS of circulating currents of MPC and NNPR are 0.71A and 0.73A respectively, the RMS of NN regression is 0.81A. Finally, the capacitor voltages are well balanced because of the common sort & select block, but the average voltage in pattern recognition controller is higher.

Fig. 9 shows the experimental results of the proposed methods. This figure clearly shows that even though NNPR can achieve good control performance in simulation, NNPR nets do not work well in the experiment (THD becomes larger than 8%). The main reason is that, as discussed in the last Section, the training performance of the 2nd class (n_1), 3rd class (n_2) and 4th class (n_3) are very poor (their loss rates are up to 84.3%, 98.9% and 99.8% respectively). The simulation results using NNPR are still acceptable because the simulated circuit and the environment in Simulink are relatively ideal without noise. But in experimental operation, the low-accuracy predictions of n_1, n_2 and n_3, practical noise and uncertainty in-circuit all affect the practical current control performance.

It is noted that features of training data and the decoupled training of n_{ui} and n_{li} determine the NNPR training performance (Fig. 5): on the one hand, the data amounts of n_2 and n_3 are both very small (smaller than 0.7%) thereby compromising their training accuracy to pursue higher holistic NN training accuracy; on the other hand, two NNs are trained separately thus only the error of one insert number (n_{ui} or n_{li})

This article has been accepted for publication in a future issue of this journal, but has not been fully edited. Content may change prior to final publication. Citation information: DOI 10.1109/TEC.2020.3021022, IEEE Transactions on Energy Conversion

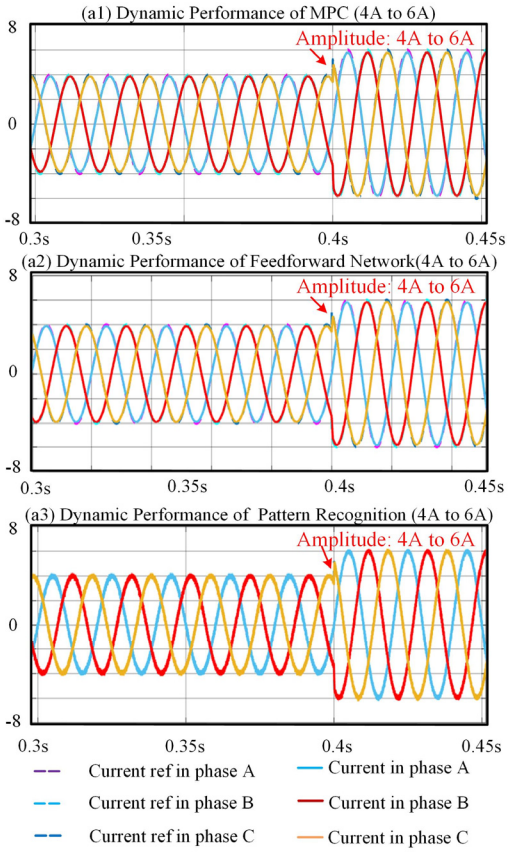

Fig .10. Dynamic performance within training range (a) NN regression controller, (b) NN pattern recognition controller.

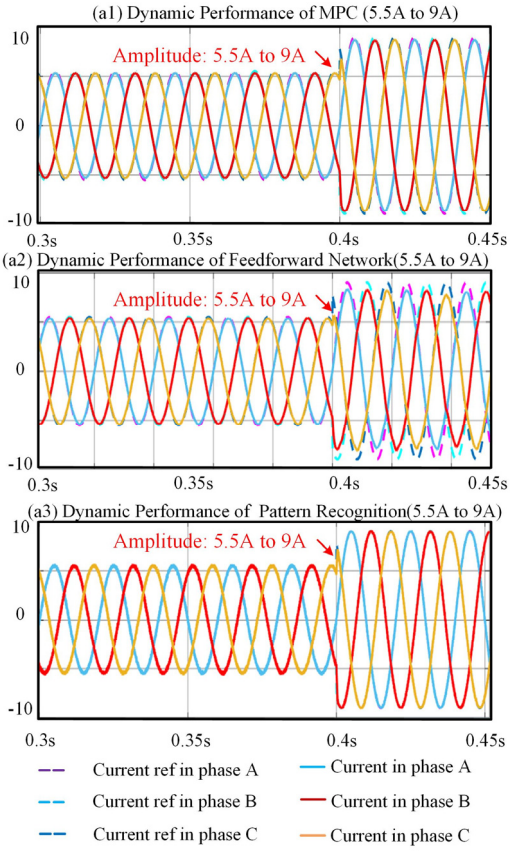

Fig .11. Dynamic performance out of training range (a) NN regression controller, (b) NN pattern recognition controller.

is set as the training goal without considering the other, even though the NNPR training can achieve high prediction accuracy, the trained NNPR nets cannot reflect the MPC characteristic of n_{ui} and n_{li} properly. In order to further verify this conclusion, we trained the decoupled two nets using NN regression for n_{ui} and n_{li} and found that, even though this two-net-regression method can achieve good general training accuracy (95.61% for n_{ui}, 95.12% for n_{li}) and acceptable simulation control, the experimental results show a poor control of MMC (THD is 8.129%)

In contrast, the NN from one-net regression training (Eq. (18)) has a similar control performance with the conventional MPC in experiment which demonstrates the fact it has learned the control characteristics of MPC very well. Therefore, this regression NN is finally chosen as the best NN approach for MMC predictive control.

A. Dynamic Performance in Simulation

Fig. 10 shows the dynamic frequency of two NN controllers when the output current references are suddenly changed. The output current reference is suddenly stepped from 4A to 6A. From the results, both NN controllers can track the stepped references easily in this range with a very fast dynamic response in this range. Dynamic Performance out of the Training Range

In this paper, the data range of $i_s^\star$ is from -6A to 6A (Section IV. C). We tested the dynamic performance of two proposed controllers when the range of $i_s^\star$ is larger than the NN training range (9A). In Fig. 11, the results show that, the NN pattern recognition controller can track the reference even out of training range. However, NN regression controller, cannot properly track the reference, thus the robustness of the NN pattern recognition is better.

B. Computational Burden in Experiment

The networks are trained by the collected data offline, where the bias and weights are obtained through the training. The computational burden of the NNs is very low due to its simple operation with bias and weights, thus NNs are very suitable to be implemented in a DSP or dSPACE controller for the sake of time saving. The computational performance was verified using the dSPACE Profiler software. The turnaround time (i.e. code execution time) obtained using this software is given in Table II.

From the experimental results, we can see that the NN regression has the lowest computational burden no matter what horizon length is. When the horizon length is high, the computational burden of MPC will increase significantly, but

TABLE II
TURNAROUND TIME

	NN Regression	NNPR	MPC
Mean Turnaround Time (horizon length 1)	1.123 µs	6.073 µs	1.615 µs
Mean Turnaround Time (horizon length 2)	1.104 µs	6.088 µs	16.102 µs

TABLE III
COMPARISON OF METHODS

	MPC	NN Regression	NNPR
Computational burden in horizon length 1	Low	Very Low	Medium
Computational burden in horizon length 2	High	Very Low	Medium
Output current THD performance	Low	Low	Medium
The ability to handle the input variables out of training range	Good	Medium	Good

the NN based controllers keep the same computational burden which is a big gain.

C. Comparison of different methods

The advantages and disadvantages of the proposed methods are summarized in Table III. Regarding the computation burden, the NN regression method has the lowest computation no matter what horizon length is. What is more, the computation burden keeps the same when the horizon length increased. This is the key advantage of the NN based method compared to the MPC method. Regarding the control performance, the THD of output current is almost the same between MPC and NN regression. The THD of the NNPR is the worst. However, NNPR has a better ability to handle the input variables which beyond the training data range.

VI. CONCLUSION

In this paper, two machine learning (ML) based modular multilevel converter controllers are designed to emulate the model predictive controller (MPC): neural networking regression controller and neural network pattern recognition controller. The data extracted from MPC is used to train the ML controllers. Using the proposed ML controller, the computation burden of the controller will be reduced compared to MPC with regards to horizon length.

VII. REFERENCES

[1] A. Lesnicar and R. Marquardt, "An innovative modular multilevel converter topology suitable for a wide power range," in *Proc. Int. Conf IEEE Bologna PowerTech*, 2003, vol. 3, pp. 272–277.

[2] P. Hu, R. Teodorescu, S. Wang, S. Li, and J. M. Guerrero, "A Currentless Sorting and Selection-Based Capacitor-Voltage-Balancing Method for Modular Multilevel Converters," *IEEE Trans. Power Electron.*, vol. 34, no. 2, pp. 1022–1025, 2019.

[3] H.-P. N. Antonios Antonopoulos, Lennart ¨ Angquist, "On Dynamics and Voltage Control of the Modular Multilevel Converter," pp. 4459–4466, 2009.

[4] M. A. Perez, J. Rodriguez, E. J. Fuentes, and F. Kammerer, "Predictive control of ac-ac modular multilevel converters," *IEEE Trans. Ind. Electron.*, vol. 59, no. 7, pp. 2832–2839, 2012.

[5] J. Moon, S. Member, J. Park, and D. Kang, "A Control Method of HVDC-Modular Multilevel Converter Based on Arm Current Under the Unbalanced Voltage Condition," *IEEE Trans. Power Deliv.*, vol. 30, no. 2, pp. 1–8, 2014.

[6] S. Li, X. Wang, Z. Yao, T. Li, and Z. Peng, "Circulating current suppressing strategy for MMC-HVDC based on nonideal proportional resonant controllers under unbalanced grid conditions," *IEEE Trans. Power Electron.*, vol. 30, no. 1, pp. 387–397, 2015.

[7] Q. Yang and M. Saeedifard, "Sliding mode control of the modular multilevel converter," *Conf. Proc. - IEEE Appl. Power Electron. Conf. Expo. - APEC*, vol. 2018–March, no. 1, pp. 1036–1043, 2018.

[8] A. Dekka, B. Wu, V. Yaramasu, R. L. Fuentes, and N. R. Zargari, "Model Predictive Control of High-Power Modular Multilevel Converters 2013; An Overview," *IEEE J. Emerg. Sel. Top. Power Electron.*, vol. PP, no. c, p. 1, 2018.

[9] Z. Zheng, Gong ; Xiaojie, Wu; Peng, Dai; Rongwu, "Modulated Model Predictive Control for MMC-Based Active Front-End Rectifiers Under Unbalanced Grid Conditions," *IEEE Trans. Power Electron.*, vol. 66, no. 3, pp. 2398–2409, 2019.

[10] J. W. Moon, J. S. Gwon, J. W. Park, D. W. Kang, and J. M. Kim, "Model Predictive Control with a Reduced Number of Considered States in a Modular Multilevel Converter for HVDC System," *IEEE Trans. Power Deliv.*, vol. 30, no. 2, pp. 608–617, 2015.

[11] J. Qin and M. Saeedifard, "Predictive control of a three-phase DC-AC Modular Multilevel Converter," *2012 IEEE Energy Convers. Congr. Expo. ECCE 2012*, pp. 3500–3505, 2012.

[12] J. Qin and M. Saeedifard, "Predictive control of a modular multilevel converter for a back-to-back HVDC system," *IEEE Trans. Power Deliv.*, vol. 27, no. 3, pp. 1538–1547, 2012.

[13] A. Dekka, B. Wu, and N. R. Zargari, "Minimization of DC-Bus Current Ripple in Modular Multilevel Converter Under Unbalanced Conditions," *IEEE Trans. Power Electron.*, vol. 32, no. 6, pp. 4125–4131, 2017.

[14] A. Dekka, B. Wu, V. Yaramasu, and N. R. Zargari, "Integrated model predictive control with reduced switching frequency for modular multilevel converters," *IEE Electr. Power Appl.*, vol. 11, pp. 857–863, 2017.

[15] B. Yang, F. Guo, Z. Wang, and X. Tong, "Priority Sorting Approach for Modular Multilevel Converter Based on Simplified Model," *IEEE Trans. Ind. Electron.*, vol. 65, no. 6, pp. 4819–4830, 2018.

[16] Y. Wang, W. Cong, M. Li, N. Li, M. Cao, and W. Lei, "Model Predictive Control of Modular Multilevel Converter with Reduced Computational Load," *2014 IEEE Appl. Power Electron. Conf. Expo. - APEC 2014*, pp. 1776–1779, 2014.

[17] Z. Gong, P. Dai, X. Yuan, X. Wu, and G. Guo, "Design and Experimental Evaluation of Fast Model Predictive Control for Modular Multilevel Converters," *IEEE Trans. Ind. Electron.*, vol. 63, no. 6, pp. 3845–3856, 2016.

[18] T. Geyer and D. E. Quevedo, "Performance of Multistep Finite Control Set Model Predictive Control for Power Electronics," in *IEEE Trans. Power Electron.*, vol. 30, no. 3, pp. 1633-1644, 2015.

[19] M. Hertneck, J. Köhler, S. Trimpe and F. Allgöwer, "Learning an Approximate Model Predictive Controller With Guarantees," in *IEEE Control Systems Letters*, vol. 2, no. 3, pp. 543-548, 2018.

[20] D. Georges, "A Simple Machine Learning Technique for Model Predictive Control," *2019 27th Mediterranean Conference on Control and Automation (MED)*, Akko, Israel, 2019, pp. 69-74.

[21] I. S. Mohamed, S. Rovetta, T. D. Do, T. Dragicević and A. A. Z. Diab, "A Neural-Network-Based Model Predictive Control of Three-Phase Inverter With an Output LC Filter," in *IEEE Access*, vol. 7, pp. 124737-124749, 2019.

[22] M. Novak and T. Dragičević, "Supervised Imitation Learning of Finite Set Model Predictive Control Systems for Power Electronics," *IEEE Trans. Ind. Electron.*, vol. Early Acce, Jan. 2020.

[23] T. Dragicevic and M. Novak, "Weighting Factor Design in Model Predictive Control of Power Electronic Converters: An Artificial Neural Network Approach," *IEEE Trans. Ind. Electron.*, vol. PP, no. c, p. 1, 2018.

[24] T. Dragicevic, P. Wheeler, and F. Blaabjerg, "Artificial Intelligence Aided Automated Design for Reliability of Power Electronic Systems," *IEEE Trans. Power Electron.*, vol. 34, no. 8, pp. 7161–7171, 2019.

[25] P. Michael, and P. Thomas, *MATLAB Machine Learning Recipes: A Problem-solution Approac*h. Apress, 2019.

[26] B. Christopher M. *Pattern Recognition and Machine Learning.* Springer, 2006.

[27] K. Hornik, M. Stinchcombe, and H. White, "' Multilayer feedforward networks are universal approximators ' Theoretical properties of multilayer feedforward networks," vol. 2, pp. 359–366, 1989.

[28] L. Bessegato, S. Member, K. Ilves, L. Harnefors, and S. Norrga, "Effects of Control on the AC-Side Admittance of a Modular Multilevel Converter," *IEEE Trans. Power Electron.*, vol. PP, no. c, p. 1, 2018.

[29] K. Ilves, S. Norrga, L. Harnefors, and H. P. Nee, "On energy storage requirements in modular multilevel converters," *IEEE Trans. Power*

Electron., vol. 29, no. 1, pp. 77–88, 2014.

[30] K. Sharifabadi, L. Harnefors, H.-P. Nee, S. Norrga, and R. Teodorescu, *Design, Control and Application of Modular Multilevel Converters for HVDC Transmission Systems*. 2016.

[31] P. Cortes, J. Rodriguez, C. Silva, and A. Flores, "of a Three-Phase Inverter," *IEEE Trans. Ind. Electron.*, vol. 59, no. 2, pp. 1323–1325, 2012.

[32] *Hinton, G. E.; Osindero, S.*; Teh, Y. W. (2006). "A Fast Learning Algorithm for Deep Belief Nets" Neural Computation. 18 (7): 1527–1554.

Capacitor Voltage Ripple Reduction Methods of Modular Multilevel Converter under Unbalanced Fault Conditions: A Comparison

Songda Wang
Department of Energy Technology
Aalborg University
Aalborg, Denmark
sow@et.aau.dk

Remus Teodorescu
Department of Energy Technology
Aalborg University
Aalborg, Denmark
ret@et.aau.dk

Sanjay K Chaudhary
Department of Energy Technology
Aalborg University
Aalborg, Denmark
skc@et.aau.dk

***Abstract*—Modular Multilevel Converter (MMC) is one of the most promising converter topology in medium/high-voltage applications. Reduction of capacitor voltage ripple during unbalanced grid conditions is very important for stable operation. A comparison of capacitor voltage ripple suppression methods under unbalanced conditions is presented in this paper. Three methods are explained and compared in simulation: circulating current specific sequence elimination method (CCSSE), instantaneous circulating current optimization method (ICCO), and arm current control method (ACC). The simulation model of these three methods are achieved in PLECS, the results show that the ICCO has best submodules capacitors voltage ripple reduction effect, but it will increase the peak arm current and DC line current ripple. CCSSE and ACC methods balance three phase energy in different perspectives, but the essence of these two methods are same.**

Keywords— modular multilevel converter, unbalanced fault conditions, voltage ripple of submodule capacitor, circulating current.

I. INTRODUCTION

Voltage source converter (VSC) based high voltage dc (HVDC) transmission is an attractive technique for large offshore wind power plants[1]. In 2003, a new type of multilevel converter, modular multilevel converter (MMC) was proposed. Due to its modularity, scalability, high efficiency and low harmonic distortion in addition to all other merits of voltage source converters, MMC has earned increasing attention in these years. Industry and academia generally agree that MMC is the most promising topology for medium/high-voltage applications, particularly in the field of high-voltage direct current power transmission for offshore wind power plants.

The MMC control strategies are much more complex than traditional 2 or 3 levels converters' because of the large number of submodules (SMs). Energy is stored in SM capacitors, and each SM capacitor stores a small amount of energy. Capacitors voltage depends on the capacitors stored energy and capacitance. The SMs capacitors voltage ripple will affect the stability and cost of MMC system largely. The SMs capacitor voltage ripple is influenced by different MMC internal control strategies because internal control can change the SMs internal energy. It is meaningful to research advanced internal control strategies to reduce the SM voltage ripple.

Unbalanced fault condition is common fault in grid-connected converter operation, two main targets should be achieved, one is to control the AC power(AC output current), the other is to stable the DC side active power[2]. Besides, it is also very important that to optimize the internal performance such as SMs capacitors ripple and loss. Most of conventional control methods consider that the operating status of each phase is symmetrical, however, the energy and power of three phase are asymmetry under unbalanced grid conditions. SMs voltage ripple in some phase easily get higher than normal conditions.

Paper [3] proposed a SMs voltage ripple reduction method by injecting the instantaneous circulating current but this paper did not consider three phase unbalanced grid conditions. The circulating current controller of MMC under unbalanced grid conditions was proposed in [4] and [5], but the SMs voltage ripple is not analyzed in detail. Paper [6] proposed an energy based control method which can improve the internal performance of MMC under unbalanced grid conditions, but this method contains so many control loops which make the controller hard to tune.

This paper is outlined as follows. The introduction of MMC is introduced in Section II. Then, the circulating current specific sequence elimination method (CCSSE) is analyzed in Section III. Section IV describes the working principle of the instantaneous circulating current optimization method (ICCO). The arm current control method (ACC) is introduced in Section V. The simulation results and analysis are presented in Section VI. Finally, Section VII concludes this paper.

978-1-5386-6054-6/18/$31.00 ©2018 European Union

II. INTRODUCTION OF MODULAR MULTILEVEL CONVERTER

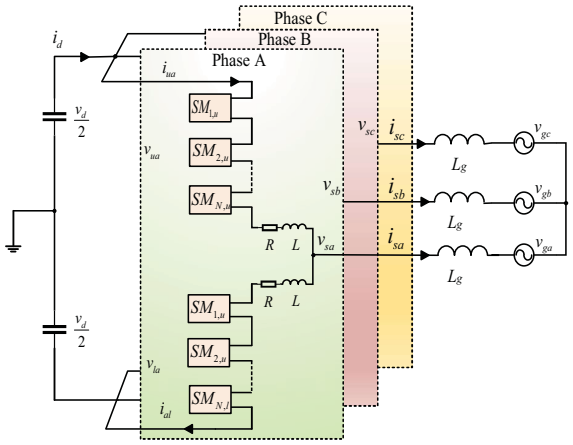

Fig. 1. Basic structure of modular multilevel converter

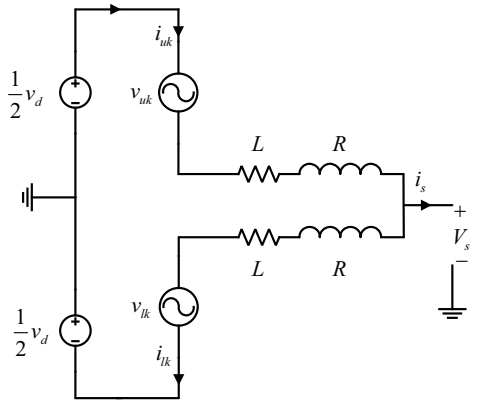

Fig. 2. Single phase equivalent circuit of MMC

Fig. 1 is the basic diagram of MMC. Each phase has two sets of SMs in series. Each SM has a half bridge converter which can generate two DC voltage: v_c and 0, where v_c is the voltage of SM capacitor. By changing the inserting status of SMs, the desired output voltage is obtained.

The output current and circulating current is defined as

$$i_{sk} = i_{uk} - i_{lk} \qquad i_{ck} = i_{uk} + i_{lk} \tag{1}$$

where i_{sk} is output current; i_{ck} is circulating current; i_{uk} and i_{lk} is upper and lower arm current respectively; k is phase a, b, and c.

By adding and subtracting of i_{sk} and i_{ck}, the upper and lower arm current i_{uk} and i_{lk} are obtained.

$$i_{uk} = \frac{1}{2}i_{sk} + i_{ck} \qquad i_{lk} = -\frac{1}{2}i_{sk} + i_{ck} \tag{2}$$

The output voltage and internal voltage are defined,

$$v_{sk} = \frac{v_{uk} - v_{lk}}{2} \qquad v_{ck} = \frac{v_{uk} + v_{lk}}{2} \tag{3}$$

where v_{ck} is internal voltage which drives the circulating current i_{ck}; v_{sk} is output voltage; v_{uk} and v_{lk} are inserted upper and lower arm voltage respectively.

Fig. 2 shows the single phase equivalent circuit of MMC. Circulating current is caused by the difference of DC source voltage and total SMs voltage of each phase. Circulating current equation of this circuit can be obtained by means of Kirchhoff's law,

$$v_{ck} = L\frac{di_{ck}}{dt} + Ri_{ck} = \frac{1}{2}[v_d - (v_{uk} + v_{lk})] \tag{4}$$

where L and R are, respectively, the value of arm inductor and capacitor; v_d is the voltage of DC source.

Circulating current contains two parts: DC part and AC part. The circulating current is defined by (5),

$$i_{ck} = \frac{i_{uk} + i_{lk}}{2} = i_{cdck} + i_{cack} = \frac{i_d}{3} + i_{cack} \tag{5}$$

where i_{cdck} is the DC component of circulating current; i_{cack} is the unbalanced AC component of circulating current; i_d is the current of DC line.

SMs capacitors are charged by arm current, (2) show that circulating current influence the arm current, then the SMs voltages are influenced by circulating current.

III. CIRCULATING CURRENT SPECIFIC SEQUENCE ELIMINATION METHOD (CCSSE)

This method based on suppression of all ac components in circulating current. All AC components of circulating current are suppressed by proportional resonance (PR) controller. Sum and Delta energy controller are used to rebalance the MMC are energy. Then SMs voltage ripple can be reduced.

The output voltage and current of MMC contains positive and negative components under unbalanced grid condition:

$$v_{sk} = V_m^+ \cos(\omega t + \delta_k^+ + \theta_k^+) + V_m^- \cos(\omega t + \delta_k^- + \theta_k^-) \tag{6}$$

$$i_{sk} = I_m^+ \cos(\omega t + \delta_k^+ + \varphi_k^+) - I_m^- \cos(\omega t + \delta_k^- + \varphi_k^-) \tag{7}$$

where V_m^+ and V_m^- are the amplitude of positive and negative output voltage respectively; I_m^+ and I_m^- are the amplitude of positive and negative output current respectively; $\theta_k^{+/-}$ and $\varphi_k^{+/-}$ are the phase angle of output voltage and current respectively; $\delta_k^+ = [\delta_a^+, \delta_b^+, \delta_c^+]^T = [0, -2/3\pi, -4/3\pi]^T$ and $\delta_k^- = [\delta_a^-, \delta_b^-, \delta_c^-]^T = [0, -4/3\pi, -2/3\pi]^T$ represent positive and negative sequence phase angle.

Ideally, the instantaneous AC power equals to the DC power

$$v_{sk} i_{sk} = \frac{1}{2} v_d i_{ck} \tag{8}$$

Form (5)-(8), the circulating current of MMC under unbalanced conditions is obtained

$$\begin{aligned} i_{ck} &= I_{dck} + I_{ck}^{+2\omega} \cos(2\omega t + \theta_k^- + \varphi_k^-) \\ &+ I_{ck}^{-2\omega} \cos(2\omega t + \theta_k^+ + \varphi_k^+) \\ &+ I_{ck}^{zero\_2\omega} \cos(2\omega t + \theta_k^+ + \varphi_k^-) \\ &+ I_{ck}^{zero\_2\omega} \cos(2\omega t + \theta_k^- + \varphi_k^+) \end{aligned} \tag{9}$$

where I_{dck} is the DC component of circulating current; $I_{ck}^{+2\omega}$, $I_{ck}^{-2\omega}$, and $I_{ck}^{zero\_2\omega}$ are the positive, negative, and zero sequence component of circulating current at double line-frequency respectively[7]. DC component of circulating current will not be equal under unbalanced grid conditions; the positive and negative sequence component at double line-frequency will not flow into DC side but the loss of MMC will be increased. The zero sequence component will flow into DC side, then, DC line voltage ripple will be higher [7].

The CCSSE method is described comprehensively in [8]. The right part of Fig. 3 is the circulating current controller of CCSSE, the proportional resonance (PR) controller is used to eliminate all the ac undesired circulating current components.

Sum and delta energy controller the total energy to a constant and the imbalance energy to zero. The unequal SMs ripple can be reduced by energy controllers under unbalanced grid conditions. Sum and delta arm energy dynamics are[8]

$$\frac{dW_{\Sigma k}}{dt} = 2v_{ck}^{\star} i_{ck} - v_{sk}^{\star} i_{sk} \qquad \frac{dW_{\Delta k}}{dt} = 2v_{ck}^{\star} i_{sk} - v_{sk}^{\star} i_{ck} \tag{10}$$

where $W_{\Sigma k}$ is total arm energy; $W_{\Delta k}$ is imbalance arm energy; $v_{sk}^{\star}$ is the reference of output voltage.

The circulating current transfers the energy between the upper and lower arm. By control the total energy, a transient DC component will be added in circulating current i_{ck}. By control the imbalance energy, an extra AC component will be added in circulating current i_{ck}.

The left part of Fig. 3 is sum and delta energy controller. Proportional controller is chosen to control the energy.

IV. INSTANTANEOUS CIRCULATING CURRENT OPTIMIZATION METHOD (ICCO)

In ICCO method, an instantaneous circulating current is injected in arm current, it can change the sharing of the current between the upper and lower. ICCO method is based on an assumption that higher capacitance will help to reduce the capacitor ripple when capacitor current rises or falls quickly. The inserted arm equivalent capacitance of MMC will change according to the insert/bypass of SMs. If fewer capacitors in series (i.e. higher arm capacitance) carry more arm current, the SMs voltage ripple can be reduced. The sum and imbalance arm energy controller introduced in Section III is applied to control MMC arm energy under unbalanced grid conditions.

In [3], the equivalent capacitance of arm SMs capacitors is defined by two new methods due to the characteristics of MMC SMs capacitors. The duty cycle of every SM in one arm can be considered as same because of the switching frequency is high enough. Assuming that all the SMs capacitors inserted for a short time to generate the arm capacitors. Then, all the SMs capacitors will have a same of charging/discharging time.

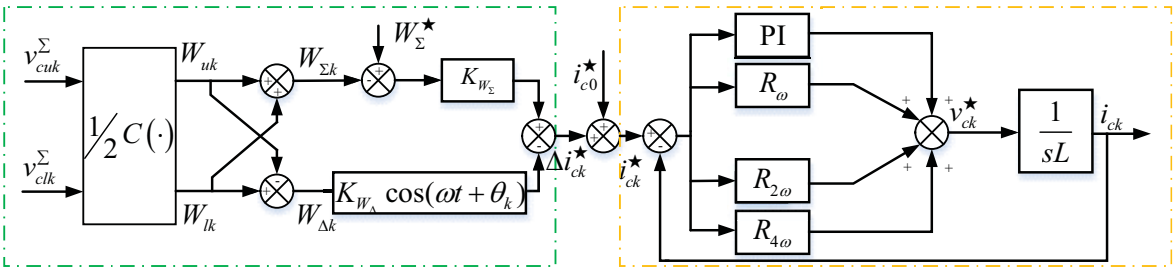

Fig. 3. The control diagram of circulating current specific sequence elimination(CCSSE) method

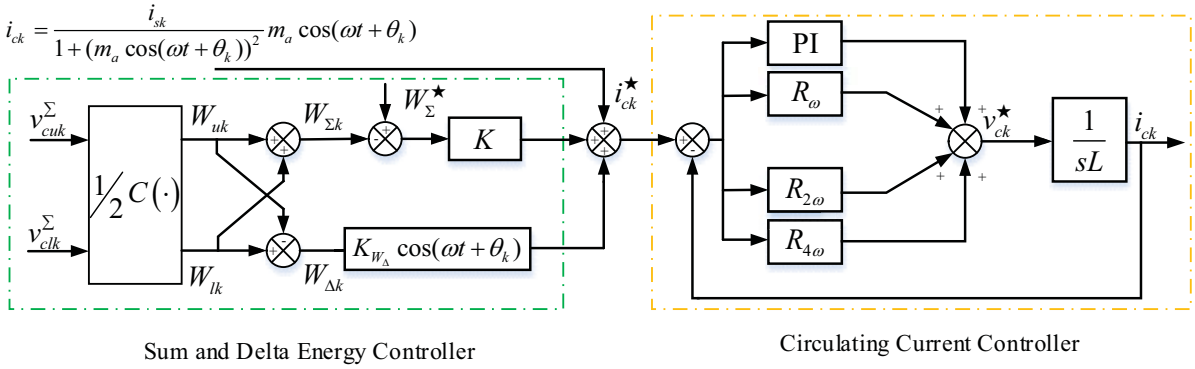

Fig. 4. The control diagram of instantaneous circulating current optimization(ICCO) method

The equivalent capacitance can be derived by considering the total energy variation of an arm,

$$\Delta E_{cu} = E_{cut1} - E_{cut0} = N\frac{1}{2}C(v_{c1}^2 - v_{c0}^2) \tag{11}$$

where ΔE_{cu} is the energy variation of an arm between time t0 and t1; E_{cut1} and E_{cut0} are the total energy of SMs capacitors in time t0 and t1 respectively. N and C are the number and the capacitance of SMs in an arm. v_{c0} and v_{c1} is the voltage of SMs capacitors.

The energy variation can also be expressed by the new definition of SMs capacitance:

$$\Delta E_{cu} = E_{cut1} - E_{cut0} = N_u\frac{1}{2}C'(v_{c1}^2 - v_{c0}^2) \tag{12}$$

where N_u is the inserted number of upper arm SMs, C' is the new equivalent capacitance of capacitor.

Equivalent capacitance is calculated from (11) and (12),

$$C' = \frac{N}{N_u}C \qquad C' = \frac{N}{N_l}C \tag{13}$$

where N_l is the inserted number of lower arm SMs.

Each arm has N_u or N_l inserted SMs, so the capacitance of arm are

$$C_{u_{eq}} = \frac{C'}{N_u} = \frac{N}{N_u^2}C \qquad C_{l_{eq}} = \frac{C'}{N_l} = \frac{N}{N_u^2}C \tag{14}$$

The current sharing of upper and lower arm are

$$i_u = \frac{C_{u_{eq}}}{C_{u_{eq}} + C_{l_{eq}}}i_s = \frac{N_l^2}{N_u^2 + N_l^2}i_s \tag{15}$$

$$i_l = \frac{C_{l_{eq}}}{C_{u_{eq}} + C_{l_{eq}}}i_s = \frac{N_u^2}{N_u^2 + N_l^2}i_s \tag{16}$$

The inserted number are

$$N_u = N\frac{1 - m_a\cos(\omega t)}{2} \tag{17}$$

$$N_l = N\frac{1 + m_a\cos(\omega t)}{2} \tag{18}$$

The circulating current is repeated in here.

$$i_{ck} = \frac{1}{2}(i_{uk} + i_{lk}) \tag{19}$$

From (15)-(19), the instantaneous reference of circulating current is obtained.

$$i_{ck} = \frac{i_{sk}}{1 + (m_a\cos(\omega t + \theta_k))^2}m_a\cos(\omega t + \theta_k) \tag{20}$$

where θ_k is the phase angle of phase a, b, and c.

The block diagram of ICCO is shown in Fig. 4. Like CCSSE method, the sum and delta arm energy are controlled by the PI and P controller. The instantaneous reference of circulating current is determined by (20).

V. Arm Current Control Method (ACC)

In [9], the capacitor voltages are controlled directly to generate the arm current reference. In this way, the active powers between ac side and dc bus is balancing naturally. The DC components reference of circulating current reference are not equal due to the average capacitor voltage controller. Then, the energy of three phase is changed and the SMs voltage ripple is reduced.

From (1) and (2), the upper and lower arm current contains the information of output current and circulating current. Therefore, the output current and circulating current can be controlled by one controller instead of conventional two separate controller. Besides, the arm current controller is applied instead of circulating current controller and output current controller, P controller is used to track the arm current reference avoiding complex control parameters tuning process.

Fig.5 is the control structure of arm current controller. $i_{uk}^{\star}$ and $i_{lk}^{\star}$ are the upper/lower arm current reference respectively. n_{uk} and n_{lk} are the insert index of upper and lower respectively.

D_{uk} and D_{lk} is the steady-state feedforward PWM duty to increase the dynamics response. The n_{uk}^{Δ} and n_{lk}^{Δ} are the output of arm current controller. The insert index are

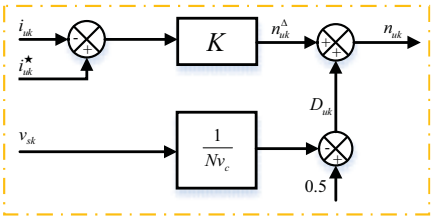

Upper Arm Current Controller

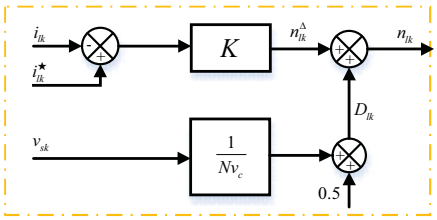

Lower Arm Current Controller

Fig. 5. The control diagram of arm current controller

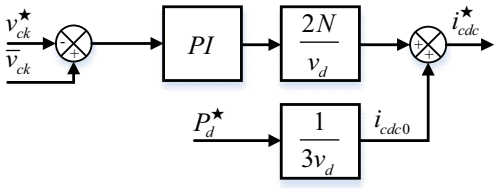

Fig. 6. The control diagram of average phase capacitor voltage controller

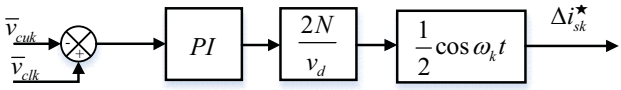

Fig. 7. The control diagram of delta arm capacitor voltage controller

$$n_{uk} = D_{uk} + n_{uk}^{\Delta} \qquad n_{lk} = D_{lk} + n_{lk}^{\Delta} \tag{21}$$

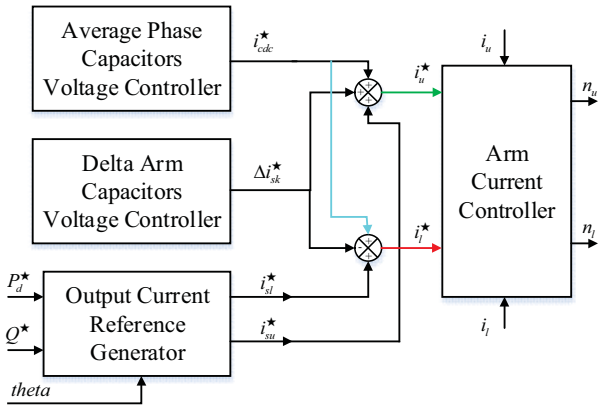

Fig. 8. The overall control diagram of arm current controller (ACC)

The SMs capacitor voltage controller has two parts: one is average phase capacitors voltage controller, another is delta arm capacitors voltage controller.

To control the average phase SMs voltage, using PI controller to control the average voltage to a rated value. Fig. 6 is the control structure of the average phase capacitor voltages controller. The output of this controller is the DC component reference of circulating current $i_{cdc}^{\star}$. $v_{ck}^{\star}$ is the reference of SM capacitor voltage. $P_d^{\star}$ is the rated active power of MMC. i_{cdc0} is the DC feedforward component.

To eliminate the difference of upper and lower arm capacitor voltages, using PI controller to achieve this goal. Fig. 7 is the control structure of the delta arm capacitor voltages controller. $\overline{v}_{cuk}$ and $\overline{v}_{clk}$ are the average value of upper and lower arm SMs capacitor voltages.

The overall control diagram of arm current controller is shown in Fig. 8. When MMC works in inverter mode, the reference is obtained by the output current reference block, detailed information reference calculation is shown in [2].

VI. Simulation Resrults

A simulation model of MMC with the parameters shown in Table. I has been built in PLECS to verify the effectiveness of these two methods under unbalanced conditions. The effect of the voltage ripple reduction methods are presented in Fig. 8, Fig. 9, and Fig. 10. Table. II shows controller parameters of MMC simulation model. The model of submodules is the submodule-level switched model, which is introduced in [8].

In order to compare the effects on voltage ripple, The components of grid fault are: $v_g^p = 0.8v_g$, $v_g^n = 0.2v_g$. The unbalanced fault is enabled at 0.25s, the fault duration is 0.25s.

TABLE I. The Parameters of MMC Plant Model

Parameters	Notation	Value
P(MW)	Active Power	150
N_{arm}	Submodules/arm	12
V_{dc}(kV)	Direct voltage	200
C_{sm}(mF)	Capacitance	0.0454
L_{arm}(mH)	Arm Inductance	5.09
V_g(kV)rms	Alternating voltage	100
f(Hz)	Rated frequency	50

TABLE II. Control Parameters

CCSSE		ICCO		ACC	
$K_{P\_i_s}$	57	$K_{P\_i_s}$	57	K	0.0033953
$K_{I\_i_s}$	5730	$K_{I\_i_s}$	5730	K_{P_avg}	100
$K_{R\_i_c}$	2	$K_{P\_i_c}$	20	K_{I_avg}	50
$K_{R_a\_i_c}$	20	$K_{R\_\omega_1}$	8000	K_{P_del}	100
$K_{I\_i_c}$	40	$K_{R\_2\omega_1}$	8000	K_{I_del}	70
$K_{R\_\omega_1}$, K_{W_Σ}	400	K_{W_Σ}	0.002		
$K_{R\_2\omega_1}$, K_{W_Δ}	400	K_{W_Δ}	0.001		

It is shown in Fig. 8(b), Fig. 9(b), and Fig. 10(b) that the output AC component only contain positive component. The circulating current in CCSSE and ACC method which are shown in Fig. 8(c) and Fig. 9(c) are injected a DC component to balance the energy control in CCSSE, voltage control in ACC, the AC components of circulating current are also eliminated. The instantaneous component is added into circulating current by means of ICCO so the AC amplitude is much bigger than the other two methods', the RMS circulating current of phase a ,b, and c in ICCO are 381A, 325A, and 325A respectively. Correspondingly, the RMS of circulating current in ACC are 303A, 221A, and 215A respectively, the RMS of circualting current are 315A, 232A, and 221A respectively. Higher RMS increases the loss of MMC. An excellent ripple reduction waveform (ripple ≈ 3100V) is shown in Fig. 9(d), (e) under both operating conditions. As shown in Fig. 8(d), (e) and Fig. 9(d).(e), the ripple of CCSSE and ACCO are 3800V and 5000V respectively. The reason why these simlar methods have different results is, compared to the CCSSE method, there is only P controller to track arm current. Arm current reference definitely contains DC and AC

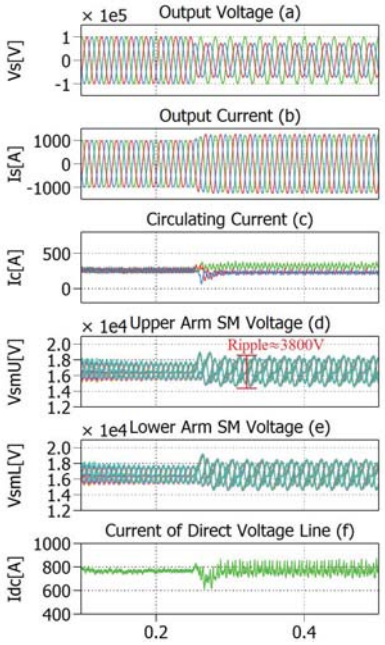

Fig. 8. Simulation Waveforms for CCSSE. (a) Output Voltage, (b) Output Current, (c) Circulating Current, (d) Upper Arm SMs Voltage, (e) Lower Arm SMs Voltage, (f) Current of Direct Voltage Line.

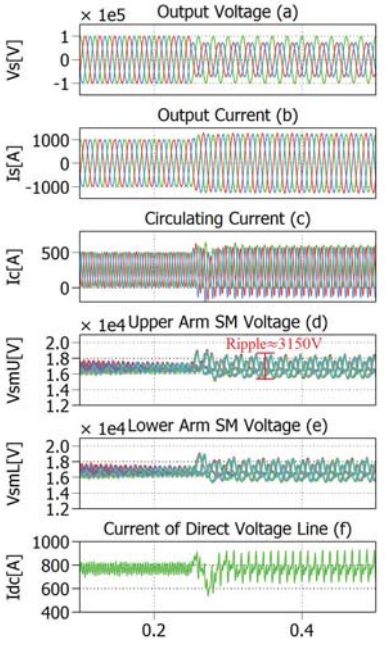

Fig. 9. Simulation Waveforms for ICCO. (a) Output Voltage, (b) Output Current, (c) Circulating Current, (d) Upper Arm SMs Voltage, (e) Lower Arm SMs Voltage, (f) Current of Direct Voltage Line.

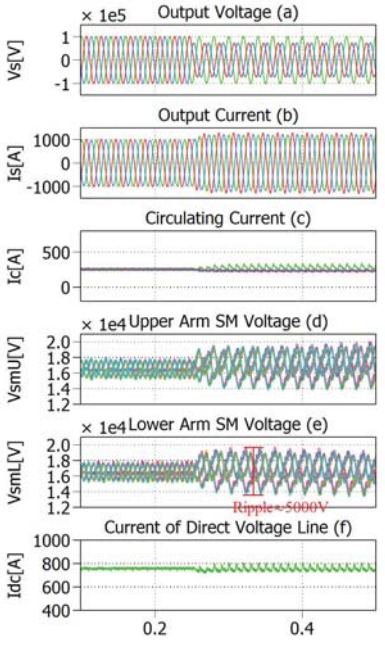

Fig. 10. Simulation Waveforms for ACC. (a) Output Voltage, (b) Output Current, (c) Circulating Current, (d) Upper Arm SMs Voltage, (e) Lower Arm SMs Voltage, (f) Current of Direct Voltage Line.

components, P controller is not capable of accurately tracking mission. The zero -sequence component of circulating current will flow into DC side, then the DC current oscillations will increase. Fig. 9(f) shows that the DC current oscillations of ICCO method are biggest compared to other two methods.

VII. CONSLUSIONS

This paper compared three capacitor voltage ripple reduction methods. ICCO method can increase equivalent arm capacitance of SMs capacitors and then the ripple is smaller. Essentially, the CCSSE and ACC methods are same because the arm energy control and SMs capacitors control are the same from the physical point of view. The simulation result shows that the voltage ripple is smaller when the ICCO method is enabled, the ripple of ICCO smallest compared to the CCSSE and ACC methods. However, the RMS of circulating current in ICCO method is much higher, the loss of MMC will increase.

REFERENCES

[1] S. K. Chaudhary, R. Teodorescu, P. Rodriguez, and P. C. Kjaer, "Control and operation of wind turbine converters during faults in an offshore wind power plant grid with VSC-HVDC connection," *IEEE Power Energy Soc. Gen. Meet.*, pp. 1–8, 2011.

[2] A. Yazdani and R. Iravani, "A unified dynamic model and control for the voltage-sourced converter under unbalanced grid conditions," *IEEE Trans. Power Deliv.*, vol. 21, no. 3, pp. 1620–1629, 2006.

[3] J. Pou, S. Ceballos, G. Konstantinou, V. G. Agelidis, R. Picas, and J. Zaragoza, "Circulating current injection methods based on instantaneous information for the modular multilevel converter," *IEEE Trans. Ind. Electron.*, vol. 62, no. 2, pp. 777–788, 2015.

[4] Y. Zhou, D. Jiang, J. Guo, P. Hu, and Y. Liang, "Analysis and control of modular multilevel converters under unbalanced conditions," *IEEE Trans. Power Deliv.*, vol. 28, no. 4, pp. 1986–1995, 2013.

[5] J. W. Moon, C. S. Kim, J. W. Park, D. W. Kang, and J. M. Kim, "Circulating current control in MMC under the unbalanced voltage," *IEEE Trans. Power Deliv.*, vol. 28, no. 3, pp. 1952–1959, 2013.

[6] A. E. Leon and S. J. Amodeo, "Energy Balancing Improvement of Modular Multilevel Converters under Unbalanced Grid Conditions," *IEEE Trans. Power Electron.*, vol. 32, no. 8, pp. 6628–6637, 2017.

[7] S. Li, X. Wang, Z. Yao, T. Li, and Z. Peng, "Circulating current suppressing strategy for MMC-HVDC based on nonideal proportional resonant controllers under unbalanced grid conditions," *IEEE Trans. Power Electron.*, vol. 30, no. 1, pp. 387–397, 2015.

[8] K. Sharifabadi, L. Harnefors, H.-P. Nee, S. Norrga, and R. Teodorescu, *Design, Control and Application of Modular Multilevel Converters for HVDC Transmission Systems*. 2016.

[9] Z. Ou and G. Wang, "Modular Multilevel Converter Control Strategy Based on Arm Current Control under Unbalanced Grid Condition," *IEEE Trans. Power Electron.*, vol. 8993, no. c, pp. 1–1, 2017.

Learning Based Capacitor Voltage Ripple Reduction of Modular Multilevel Converters under Unbalanced Grid Conditions with Different Power Factors

Songda Wang
Department of Energy Technology
Aalborg University
Aalborg, Denmark
sow@et.aau.dk

Tomislav Dragicevic
Department of Electrical Engineering
Technical University of Denmark
Lyngby, Denmark
tomdr@elektro.dtu.dk

Remus Teodorescu
Department of Energy Technology
Aalborg University
Aalborg, Denmark
ret@et.aau.dk

***Abstract*— A fast and non-parameter-dependent grid-current-control method to ride through dangerous unbalanced gird condition is proposed in this paper. The grid-current references are calculated from an artificial intelligence (AI) surrogate model in order to keep the capacitor voltage at a safe level under a two phases short circuit to ground condition. And also, the circulating current reference are determined when the power factor is different when the grid fault is not serious. This machine learning network represents the relation between grid-current references and submodule capacitor voltages. The results show that this method prevents capacitor-overvoltage trips under completely short-circuited grid.**

Keywords—Modular Multilevel Converters, submodule capacitor voltage, machine learning, grid current control.

I. INTRODUCTION

Submodule (SM) capacitor voltages of modular multilevel converter (MMC) will be higher and unbalanced under two phases short circuit to ground condition (Two Phase SC) [1]. This submodule overvoltage fault is one of the most dangerous faults in the MMC-HVDC application. Then high capacitor voltages may cause SM capacitor overvoltage trip [2] [3]. Thus, it is important to reduce and limit the increased voltage ripples, under completely short circuit two phases SC grid fault.

In MMC, the analytical capacitor voltage equations can be derived by considering the grid voltages, circulating currents, and grid currents [4]. In normal grid condition, grid voltages are balanced, circulating currents are suppressed to pure DC components, and grid currents are controlled to meet the grid code, then the SM capacitor voltages are within the safe voltage limit. However, when two phase SC fault occurs, the submodule voltages will be higher because the grid voltages become unbalanced and, thus, new current components flow through the SM capacitors. The usual solution is to inject circulating current components to suppress the submodule ripple [5]. However, when the grid fault is serious, the capacitor voltage will be much higher, and only injecting AC circulating current cannot make sure that the capacitor voltage will be within its safe limits. At this time, we need to find a new control variable to reduce the capacitor voltages, we choose to control the grid currents in order to suppress the submodule voltages under serious two phases SC fault.

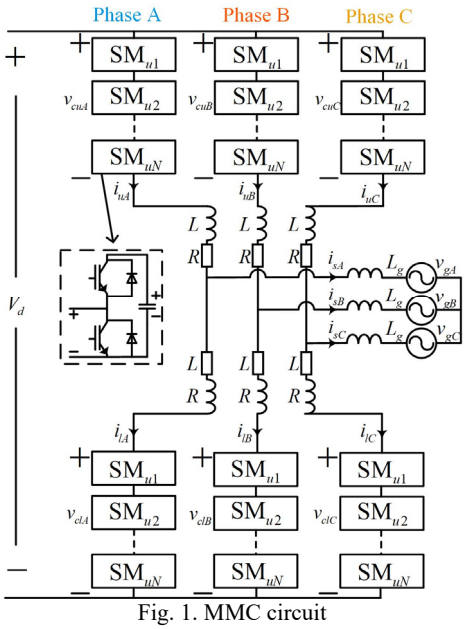

Fig. 1. MMC circuit

Because there are many factors which can influence the submodule voltage when the grid is in unbalanced two phases SC to ground fault such as: circulating currents, output currents, and the grid voltages. Taking a three-phase MMC as an example, three-phase submodule voltages, three-phase circulating currents, three-phase grid voltages, and three-phase output current. It is very difficult to figure out this relationship by analytical equations.

Machine learning network is a solution to help us to represent the complex coupling relationship of those factors. Machine learning network is able to represent the nonlinear relationship of a fixed input output relationship. It is computation light, easy to train, and simple structure [6]. In [6],

978-1-7281-6990-3/20/$31.00 ©2020 IEEE

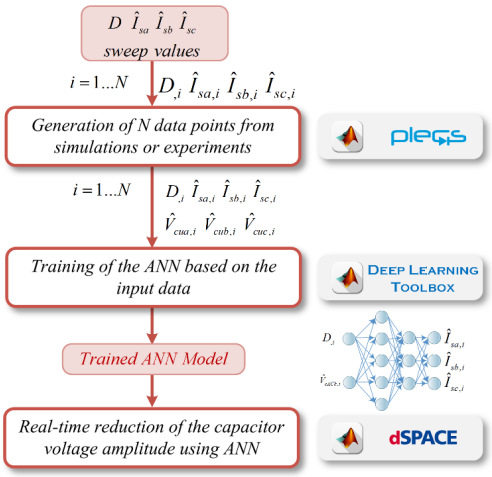

Fig. 2. Training steps for machine learning model.

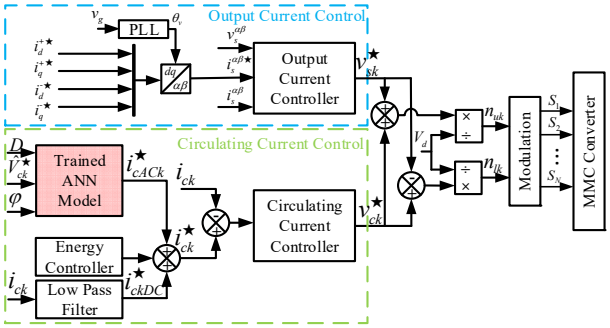

Fig. 3. Control block diagram of method when the power factor changes under a not serious grid fault

the artificial neural network (ANN) is used to solve one important problem of the model predictive control: weighting factor selection. The ANN will select the best weighting factor under different operation scenarios with the low computational burden. In [7], an ANN network is trained to repeat the behavior of the finite set MPC, the computational burden of the controller is much reduced by applying the ANN, and also good steady and dynamic performance. In [8], the machine learning based method is applied to design system with high reliability. The relationship between system parameter and the reliability is represented by the ANN_1, and this ANN_1 is used to generate the data of design parameter into lifetime consumption to train the ANN_2, this network will help to design the optimal balance between the reliability and the filter size. In [9], a machine based network is used to extend the MMC operating region under unbalanced grid condition. The AC circulating current reference is calculate by the machine learning network. Then the submodule voltage will also below the alarm voltage value.

This paper proposes a fast and non-parameter-dependent method to keep the capacitor voltage at a safe level under a two phases SC to ground grid fault. A machine learning network mapping grid current and the submodule voltages is got by training. Therefore, this model can help to calculate the proper three-phase grid current references to make sure the submodule capacitor voltage is always within the acceptable voltage range. What is more, when the grid fault is not serious, only injecting the circulating current by machine learning model under different power factor is also proposed in this paper. The machine learning network training data is extracted from Simulink, and the proposed machine learning based controller is verified by simulation in this paper.

II. THE PROPOSED ML METHOD

In this section, the proposed artificial intelligence grid current control (AI-GCC) method to suppress the submodule voltages under two phases SC to ground conditions is introduced. The proposed method depends on the machine learning model which presents the gird currents and SM capacitor voltages relationship. This machine learning network is trained by the parallel simulation data. The procedure the ML method is presented in Fig. 1. The introduction of the training is introduced as follows step by step:

First, we collect the training data points from simulation. The training data contains the information of grid currents, grid

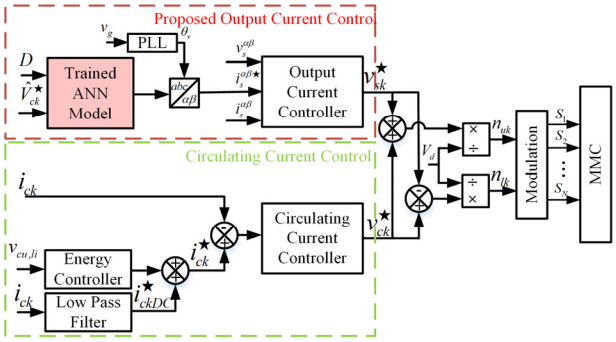

Fig. 3. Control block diagram of when the grid fault is serious

voltages (represented by the fault severity number D), and the submodule voltage. In order to describe the factor clearly, the vector definition of two phases SC fault is listed as follows:

$$\begin{aligned}\hat{V}_{ga\_pu} &= 1\\ \hat{V}_{gb\_pu} &= -\tfrac{1}{2}D - j\tfrac{\sqrt{3}}{2}D\\ \hat{V}_{gc\_pu} &= -\tfrac{1}{2}D + j\tfrac{\sqrt{3}}{2}D\end{aligned} \tag{1}$$

where $\hat{V}_{ga\_pu}, \hat{V}_{gb\_pu}, \hat{V}_{gc\_pu}$ are grid PU value in a, b, and c respectively. D is the

fault severity number, the range is [0,1], where 0 means completely short circuit, 1 means normal grid condition. This vector definition describes two phases SC to ground grid analytically. By sweeping severity factor from 0 to 1, we can cover all the two phases SC to ground grid conditions.

Grid currents are introduced in (2):

$$\begin{aligned}i_{sa} &= \hat{I}_{sa}\cos(\omega t + \varphi)\\ i_{sb} &= \hat{I}_{sb}\cos(\omega t - \tfrac{2}{3}\pi + \varphi)\\ i_{sc} &= \hat{I}_{sc}\cos(\omega t - \tfrac{4}{3}\pi + \varphi)\end{aligned} \tag{2}$$

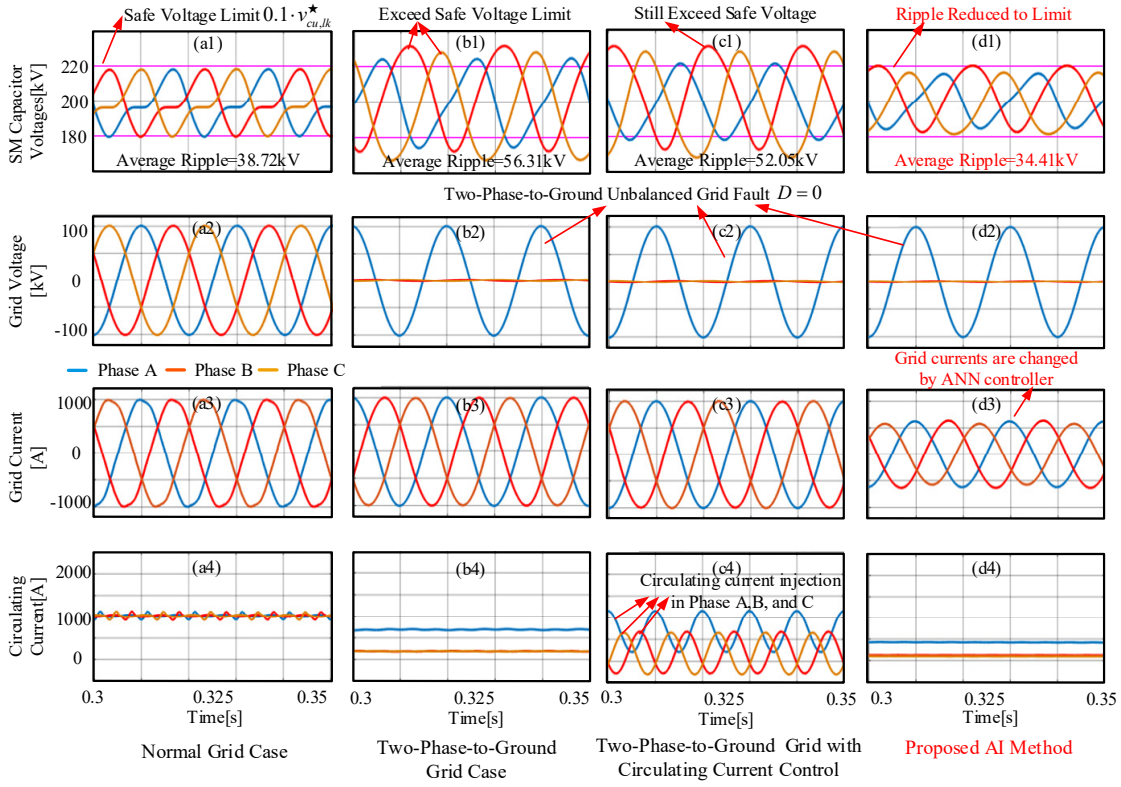

Fig. 4. Results: (a) normal grid condition; (b) two phases SC to ground grid condition without proposed method; (c) two phases SC to ground grid condition with circulating current injection; (d) proposed AI method.

where i_{sa}, i_{sb}, i_{sc} are the output currents of three phases, $\hat{I}_{sa}, \hat{I}_{sb}, \hat{I}_{sc}$ are the amplitudes of output current of three phases. By sweeping the amplitudes of gird currents, we can create a combination of all the possible grid currents.

The ANN model represents the relation between grid current and SM capacitor voltage as follows:

$$y = F(\mathrm{x}) \Leftrightarrow (\hat{I}_{sa}, \hat{I}_{sb}, \hat{I}_{sc}) = F(D, \hat{V}_{cua}, \hat{V}_{cub}, \hat{V}_{cuc}) \tag{3}$$

where $\hat{V}_{cua}, \hat{V}_{cub}, \hat{V}_{cuc}$ are capacitor voltage amplitude of phase a, b, and c. By this relationship, if we input D and ideal capacitor voltage amplitude $\hat{V}_{cua}, \hat{V}_{cub}, \hat{V}_{cuc}$, the grid current references can be calculated. The MMC controllers will track these grid current references then suppress the submodule voltages under two phases SC conditions.

In this paper, the sweep input values are grip dip severity factor D = [0, 0.1, 0.2, 0.3, 0.4, 0.5, 0.6, 0.7], and the three-phase grid current amplitudes are: $\hat{I}_{sa,b,c}$ = [600, 700, 800, 900, 1000]; By sweeping the input data variables in simulation model, the simulation model will generate the data of SM capacitor voltage amplitude with different sweep input values. The parameter of MMC system is listed in Table I. The data collection process is accelerated by parallel simulation, with 24 core CPU we can carry out 24 simulations at the same time. In this case, the data size is 1000, and the data collection period is 5.5 mins. The extracted data is used to train the machine learning network, the network is a 3 layers feedforward neural network: 1 input, 1 output, and 1 hidden. MATLAB Deep Learning Toolbox helps the training with an easy and fast way. After training the machine learning network model, we can use this model to determine the output current references for the controller.

The case when the grid dip severity is not low than 0.6, that is to say the two phases SC faults are not serious, the capacitor voltage ripple will also be high and dangerous. The different power factor will influence the charging the submodule capacitor so in this case the injected circulating current need to be considered when the power factor changes. In this case, the sweep input values are grip dip severity factor D = [0, 0.1, 0.2, 0.3, 0.4, 0.5, 0.6, 0.7], and the three-phase circulating current amplitudes are: $\hat{I}_{ca,b,c}$ = [0, 100, 200, 300, 400, 500,600, 700, 800, 900, 1000], and the power factor φ = [-1, -0.5, 0, 0.5, 1], the number of data is 31944, and the overall simulation time is 273 mins.

III. RESULTS

The machine learning based controller is implemented in simulations. The block diagram of MMC controller is in Fig. 3. The controller has two parallel sections: proposed output current

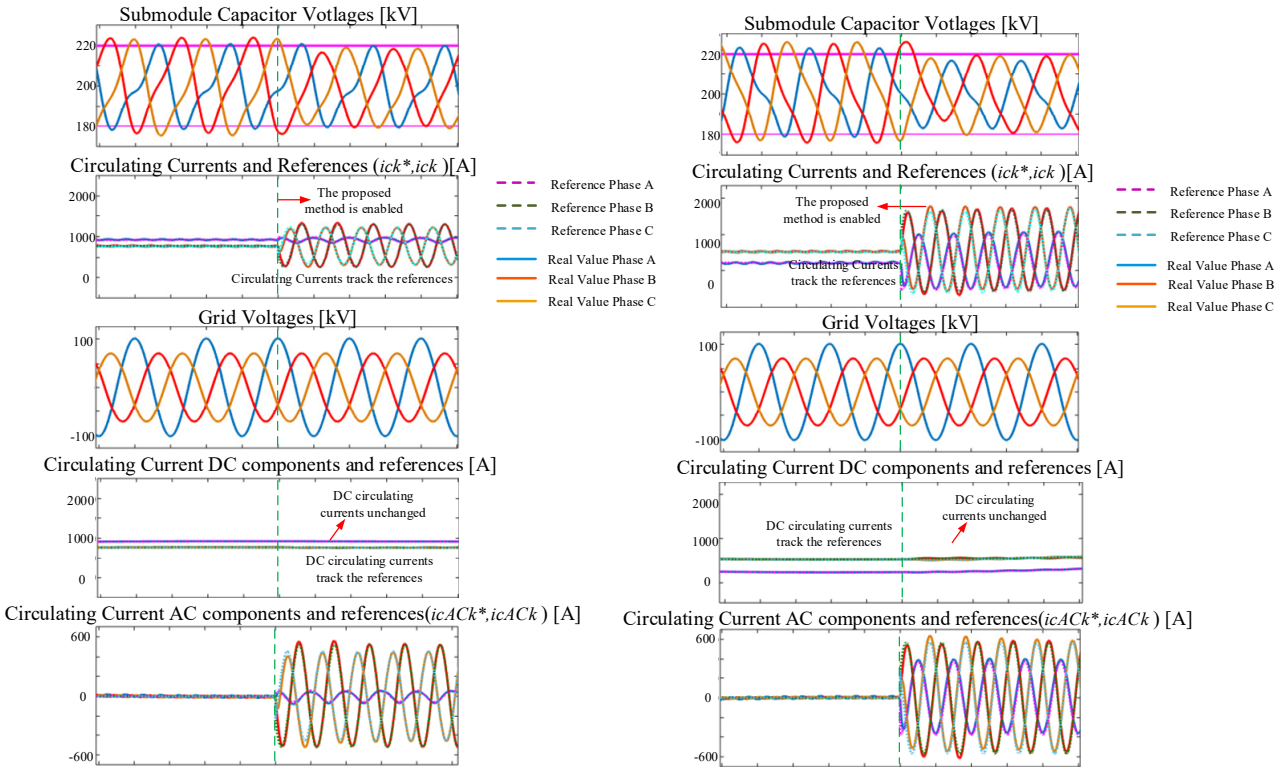

Fig. 5. Simulation results: (a) power factor = 1, (b) power factor = -1.

controller and circulating current controller (CCC): Proposed machine learning model determines the output grid current references and the output current controller tracks these references and CCC helps the MMC to suppress the AC circulating current components, then the MMC efficiency is improved. The detailed information of these two controllers is introduced in [4].

The simulation results are verified in Fig. 4. In Fig. 4 (a1) - (a4), the submodule voltages, circulating current values, and the grid values are displayed, the three-phase submodule voltages have the same amplitudes and smaller than the 10% of DC voltage safe peak value, which is shown in Fig. 4 (a1). And all the AC circulating currents are suppressed by circulating current controller (Fig. 4 (a4)). The average value of the submodule voltage here is 38.72kV.

The results under fault gird are shown in Fig. 4 (b), (c), and (d). Phase b and c are completely short circuited which are shown in Fig. 4 (b2), (c2), and (d2). In Fig. 4 (b3), the grid currents are same as the normal grid case. Then, the three-phase SM capacitor voltages exceed the safe voltage limit which will cause MMC system trip (Fig. 4 (b1)). And also, the three-phase AC circulating currents are suppressed by circulating current controller. The average capacitor voltage ripple here increases to 56.31kV.

Fig. 4 (c1) – (c2) show the results of the submodule capacitor voltage ripple reduction method by injecting AC circulating current. This method is introduced in [5]. By this method, the three-phase AC circulating currents are injected into MMC to suppress the submodule votage. The submodule voltages here are reduced to 52.05kV as Fig. 4 (c1) shows. However, the three-phase capacitor voltages still higher than the safe submodule voltage limit value.

The results of the machine learning based method are shown in Fig. 4 (d1) –(d4). In Fig. 4 (d1), the three-phase capacitor voltages are reduced to the safe limit by changing the grid currents. The grid currents are changed by the proposed ANN method which is displayed in Fig. 4 (d3). The average submodule voltage here is further suppressed to 34.41kV which is within the safe voltage limit.

The simulation results of the proposed method when the power factor is 1 are presented in Fig. 5. In Fig. 5 (a), the grid voltages are unbalanced with two phases SC grid with power factor 1, the dip severity factor is 0.7. During this fault, the capacitor voltages are high and unbalanced. And then, the proposed ML controller is enabled, the three-phase AC circulating currents are injected to the MMC system. Then the capacitor voltages are reduced to the safe voltage level (10% percentage of the rated DC voltage).

Also, the similar capacitor voltage reduction effect can be seen in the case when power factor is -1. In Fig. 5 (b), the grid voltages are unbalanced with two phases SC grid with power factor -1, the dip severity factor is 0.7. During this fault, the capacitor voltages are high and unbalanced. And then, the proposed ML controller is enabled, the three-phase AC circulating currents are injected to the MMC system. Then the capacitor voltages are reduced to the safe voltage level (10% percentage of the rated DC voltage).

TABLE I: MMC Parameters in Simulations

	Simulation
Number of SMs per arm (N)	100
Rated DC voltage (v_d)	200 kV
Rated active power	150 MW
Nominal SM capacitance (C)	3.75 mF
Nominal SM capacitor voltage (v_c)	2 kV
Rated frequency (f)	50 Hz
Arm inductance (L)	50.9 mH
Sample frequency	10 kHz
Grid voltage magnitude	100 kV

IV. Conclusion

In this paper, an artificial intelligence output current control and circulating current method to suppress the submodule voltages when the grid is two phases SC fault condition is introduced. By this method, the submodule voltage can be reduced considerably to prevent system capacitor overvoltage trip.

References

[1] Ilves, K., Norrga, S., Harnefors, L., Nee, H.P.: 'On energy storage requirements in modular multilevel converters' *in IEEE Trans. Power Electron*., 2014, Vol. 29, (1), pp. 77–88.

[2] Shi, X., Wang, Z., Liu, B., Li, Y., Tolbert, L.M., Wang, F.: 'Steady-State Modeling of Modular Multilevel Converter under Unbalanced Grid Conditions' in *IEEE Trans. Power Electron*., 2017, Vol. 32, (9), pp. 7306–7324.

[3] Ou, Z., Wang, G., Zhang, L.: 'Modular multilevel converter control strategy based on arm current control under unbalanced grid condition' in *IEEE Trans. Power Electron*., 2018, Vol. 33, (5), pp. 3826–3836.

[4] Sharifabadi, K., Harnefors, L., Nee, H.-P., Norrga, S., Teodorescu, R.: 'Design, Control and Application of Modular Multilevel Converters for HVDC Transmission Systems' Wiley Press, 2016

[5] Moon, J., Member, S., Park, J., Kang, D.: 'A Control Method of HVDC-Modular Multilevel Converter Based on Arm Current Under the Unbalanced Voltage Condition' in *IEEE Trans. Power Deliv*., 2014, Vol. 30, (2), pp. 1–8.

[6] Novak, Mateja, et al. "Optimal Cost Function Parameter Design in Predictive Torque Control (PTC) Using Artificial Neural Networks (ANN)." *IEEE Transactions on Industrial Electronics* (2020).

[7] Novak M, Dragicevic T. Supervised imitation learning of finite set model predictive control systems for power electronics[J]. *IEEE Transactions on Industrial Electronics*, 2020.

[8] Dragičević T, Wheeler P, Blaabjerg F. Artificial intelligence aided automated design for reliability of power electronic systems[J]. *IEEE Transactions on Power Electronics*, 2018, 34(8): 7161-7171.

[9] S. Wang, T. Dragicevic, Y. Gao, S. K. Chaudhary and R. Teodorescu, "Machine Learning based Operating Region Extension of Modular Multilevel Converters under Unbalanced Grid Faults," in *IEEE Transactions on Industrial Electronics*, doi: 10.1109/TIE.2020.2982109.

ISSN (online): 2446-1636
ISBN (online): 978-87-7210-828-5 AALBORG UNIVERSITY PRESS